UNIVERSITÉ DE NEUCHÂTEL

INVESTIGATIONS OF CANDIDATE PLASTOGLOBULE PROTEINS

Characterization of chloroplast NON-INTRINSIC ABC PROTEINS 13 and -14 in *Arabidopsis thaliana*

&

Constitutive expression of CAROTENOID CLEAVAGE DIOXYGENASE 4 leads to a reduced level of photosynthesis-related carotenoids during senescence

A dissertation submitted to the
UNIVERSITY OF NEUCHATEL
For the degree of
Doctor of Philosophy in Biological Sciences

Presented by
Sarah ROTTET
Laboratory of Plant Physiology, Institute of Biology

Accepted on the recommendation of
Prof. Felix Kessler, thesis director
Dr. Didier Schaefer
PD Dr. Markus Geisler

April 8th, 2016

UNIVERSITÉ DE NEUCHÂTEL

Faculté des sciences
Secrétariat-décanat de Faculté
Rue Emile-Argand 11
2000 Neuchâtel - Suisse
Tél: + 41 (0)32 718 2100
E-mail: secretariat.sciences@unine.ch

IMPRIMATUR POUR THESE DE DOCTORAT

La Faculté des sciences de l'Université de Neuchâtel autorise l'impression de la présente thèse soutenue par

Madame Sarah ROTTET

Titre:

“Investigations of candidate plastoglobule proteins”

sur le rapport des membres du jury composé comme suit:

- Prof. Felix Kessler, directeur de thèse, Université de Neuchâtel, Suisse
- Dr Didier Schaefer, Université de Neuchâtel, Suisse
- PD Dr Markus Geisler, Université de Fribourg, Suisse

Neuchâtel, le 3 mai 2016

Le Doyen, Prof. B. Colbois

Keywords: Chloroplasts, plastoglobules, lipids, albino phenotype, ABC transporter, carotenoid cleavage

Mot-clés: Chloroplastes, plastoglobules, lipides, phénotype albinos, transporteur ABC, clivage des caroténoïdes

Table of contents

Abstract

Photosynthesis is the key bioenergetic process taking place in the chloroplast. The components of the photosynthetic machinery are embedded in a highly dynamic matrix, the thylakoid membrane. The galactolipids are the major polar lipid components of the thylakoid membrane conferring bilayer properties, while neutral thylakoid lipids such as the prenyllipids and carotenoids contribute to essential functions such as electron transport and photoprotection. Despite a large number of studies, the intriguing processes of thylakoid membrane biogenesis and dynamics remain unsolved. Plastoglobules, thylakoid-associated lipid droplets, appear to actively participate in thylakoid function from biogenesis to senescence. Recruitment of specific proteins enables the plastoglobules to act in metabolite synthesis, repair and disposal under changing environmental conditions and developmental stages. In the first chapter of this thesis, we review plastoglobules as thylakoid membrane microdomains and discuss their involvement in lipid remodeling during stress and in the conversion from one plastid type to another.

The second chapter is dedicated to the characterization of NAP13 (ABCI10) and -14 (ABCI11). These two proteins belong to the large ABC family. Each member of the ABCI subfamily consists of only one of the typical domains of a full ABC transporter. *NAP13* and *-14* encode two predicted nucleotide-binding domains. Based on earlier results (Shimoni-Shor et al. 2010), our first hypothesis was that NAP14, possibly together with NAP13, are involved in lipid translocation between PG and thylakoids. However, this thesis demonstrates that NAP13 is extrinsically associated with the chloroplast inner envelope while NAP14 cofractionated with the thylakoid membrane. Both the *nap13* and *-14* mutants had albino phenotypes, emphasizing essential functions in the chloroplast. Interestingly, *nap13* and *-14* showed similar lipid profiles but distinct from three unrelated albino mutants. The most relevant observation was their reduced level of phosphatidylethanolamine 16:0/18:3. The striking similarities shared by *nap13* and *-14* suggest that they contribute to the same functional pathway. We hypothesize that this may be lipid transport at the envelope rather than between PG and thylakoids.

In the third chapter, we describe the characterization of CCD4, a carotenoid cleavage dioxygenase, and its physical and functional association with PG. Fluorescence-tagged CCD4 resulted in a punctate pattern inside chloroplasts typical for PG localization *in vivo*. To discover the function of CCD4, a comparative lipidomics study of Arabidopsis *ccd4* mutants and wild type was carried out under various conditions (light stress, senescence, *Pseudomonas syringae* infection). The results indicated that CCD4 is implicated in β-carotene and lutein degradation during leaf senescence. To further investigate the function of the enzyme, we engineered 35S:CCD4-YFP overexpressing lines. In conclusion, our findings indicate that β-carotene, lutein and violaxanthin are the principle substrates of CCD4 *in vivo* during chloroplast to gerontoplast differentiation.

Résumé

La photosynthèse est le processus clé se déroulant au sein du chloroplaste. La machinerie photosynthétique est intégrée à une matrice très dynamique, la membrane des thylakoïdes. Les galactolipides, les principaux lipides polaires de cette membrane, lui confèrent la propriété de bicouche alors que les lipides neutres tels que les prényllipides et les caroténoïdes contribuent à d'essentielles fonctions telles que le transport d'électrons et la photoprotection. Malgré de nombreuses études, la biogénèse et la dynamique des thylakoïdes restent irrésolus. Les plastoglobules (PG), des gouttelettes lipidiques associées aux thylakoïdes, participent activement aux fonctions des thylakoïdes. Sous un environnement changeant et lors des différents stades de développement, le recrutement d'enzymes spécifiques permet aux PG de participer à la synthèse, la réparation et l'élimination des métabolites. Dans le premier chapitre de cette thèse, nous passons en revue les PG en tant que microdomaines des thylakoïdes et discutons leur implication dans le remodelage lipidique lors de stress et lors de la conversion d'un type de plaste à l'autre.

Le chapitre II est dédié à la caractérisation de NAP13 (ABCI10) et -14 (ABCI11). Ces deux protéines appartiennent à la grande famille des ABC. Chaque membre de la sous-famille ABCI présente un seul des domaines typiques des transporteurs ABC. *NAP13* et *-14* codent deux domaines prédits pour la liaison des nucléotides. En se basant sur de précédents résultats (Shimoni-Shor et al. 2010), notre première hypothèse impliquait NAP14, éventuellement avec NAP13, dans un transport de lipides entre les PG et les thylakoïdes. Cependant, cette thèse démontre que NAP13 est extrinsèquement associée à l'enveloppe interne du chloroplaste, alors que NAP14 cofractionne avec les thylakoïdes. Les mutants *nap13* et *-14* ont un phénotype albinos, ce qui souligne une fonction essentielle au sein du chloroplaste. Notons que *nap13* et *-14* ont un profile lipidique similaire, bien que distinct de trois autres mutants albinos. L'observation la plus pertinente étant leur taux réduit de phosphatidyléthanolamine 16:0/18:3. Les similarités partagées par *nap13* et *-14* suggèrent que les protéines correspondantes contribuent à la même voie métabolique. D'après nos résultats, il s'agirait d'un transport de lipides au niveau de l'enveloppe.

Dans le chapitre III, nous décrivons la caractérisation de CCD4, une enzyme qui clive les caroténoïdes, et son association physique et fonctionnelle avec les PG. La fusion d'une protéine fluorescente avec CCD4 a donné lieu à un signal ponctué dans les chloroplastes typique d'une localisation aux PG *in vivo*. Pour élucider la fonction de CCD4, une étude de lipidomique comparative de mutants *ccd4* et de plantes sauvages a été effectuée sous diverses conditions. Les résultats indiquent que CCD4 est impliquée dans la dégradation du β-carotène et de la lutéine lors de la sénescence des feuilles. Pour approfondir, nous avons conçu des lignées de surexpresseurs 35S:CCD4-YFP. En conclusion, nos résultats indiquent que le β-carotène, la lutéine et la violaxanthine sont les principaux substrats de CCD4 *in vivo* durant la différenciation du chloroplaste en gérontoplaste.

List of abbreviations

% (v/v)	mL / 100mL
% (w/v)	g / 100 mL
35S	CaMV 35S promoter
6xHIS	hexahistidinyl-tag
A. thaliana	*Arabidopsis thaliana*
ABA	abscisic acid
ABC	ATP-binding cassette
ABC1K	activity of bc1 complex-like kinase
ABCISSE	ABC: information on sequence, structure and evolution
ACC	acetyl-coenzyme A carboxylase
ANOVA	analysis of variance
At	*Arabidopsis thaliana*
ATP	adenosine triphosphate
bp	base pairs
BP	substrate binding protein
CaMV	cauliflower mosaic virus
CBP	calmodulin binding peptide
CCD	carotenoid cleavage dioxygenase
Cd	cadmium
cDNA	complementary DNA
CFP	cyan fluorescent protein
CFU	colony-forming unit
Chl	chloroplast
Cit	*Citrus unshiu*
CLA1	CLOROPLASTOS ALTERADOS 1
clb5	*chloroplast biogenesis 5*
Cm	*Chrysanthemum morifolium* Ramat.
CoA	coenzyme A
CrtR-β	β-carotene β-hydroxylase
Cs	*Crocus sativus*
CTAB	cetyltrimethylammonium bromide
Ctrl	control
DAG	diacylglycerol
DAPI	4',6-diamidino-2-phenylindole
DGAT	diacylglycerol acyltransferase
DGDG	digalactosyldiacylglycerol
DMF	dimethylformamide
DMPBQ	2,3-dimethyl-6-phytyl-1,4-benzoquinone
DNA	deoxyribonucleic acid
dNTP	deoxy nucleotide triphosphate
dpi	dot per inch

DTT	1,4-dithio-DL-threitol
DXP	1-deoxyxylulose 5-phosphate
EDTA	ethylenediamine-N,N,N',N'-tetraacetic acid
Env.	envelopes
EtOH	ethanol
FA	fatty acid
FAPE	fatty acid phytyl ester
FAS	fatty acid synthase
FBN	fibrillin
Fd	ferredoxin
fmol	femtomole
For	forward
FW	fresh weight
gDNA	genomic DNA
GFP	green fluorescent protein
HA	human influenza hemagglutinin
HPLC	high performance liquid chromatography
HRP	horseradish peroxidase
IVT	*in vitro* translated
JA	jasmonic acid (jasmonate)
kb	kilo base pairs
kDa	kilo Dalton
LB	T-DNA left border or lysogeny broth
LD	lipid droplet
LHC	light harvesting complex
LHCBII	PSII light-harvesting chlorophyll a/b-binding protein 2
LP	left genomic primer
LSD	lignostilbene dioxygenases
LYC-β	Lycopene β-cyclase
MeOH	methanol
MEP	methylerythritol 4-phosphate
MES	2-morpholinoethanesulfonic acid
MGDG	monogalactosyldiacylglycerol
mRNA	messenger RNA
MS	Murashige and Skoog or mass spectrometry
NADPH	nicotinamide adenine dinucleotide phosphate
NAP	non-intrinsic ABC protein
NBD	nucleotide binding domain
NCED	9-cis-epoxycarotenoid dioxygenase
NDC1	NAD(P)H dehydrogenase C1
NDH	NADH dehydrogenase-like complex
NPQ	non-photochemical quenching
P.syringae	*Pseudomonas syringae*
PAC	pale cress

PC-8	plastochromanol
PCA	principal component analysis
PCR	polymerase chain reaction
PDHC	pyruvate dehydrogenase complex
PE	phosphatidylethanolamine
PES	phytyl ester synthase
PG	plastoglobules
PGL	plastoglobulin
PLB	(paracrystalline) prolamellar body
PLS-DA	partial least squares-discriminant analysis
PMSF	phenylmethylsulfonyl fluoride
pNAP13	precursor of NAP13
pNAP14	precursor of NAP14
PPH	pheophytin pheophorbide hydrolase
ppi2	*plastid protein import 2*
PQ	plastoquinone
PQH_2	plastoquinol
PSI	photosystem I
PSII	photosystem II
PSM	peptide spectral match
PSY	phytoene synthase
PYP	pale yellow petal
qRT-PCR	quantitative real-time PCR
RB	T-DNA right border
RBCL	RuBisCo large subunit
Rev	reverse
RNA	ribonucleic acid
ROS	reactive oxygen species
RP	right genomic primer
RT	room temperature or retention time
RT-PCR	reverse transcription-PCR
RuBisCo	ribulose-1,5-bisphosphate carboxylase/oxygenase
SD	standard deviation
SDS	sodium dodecyl sulfate
SDS-PAGE	SDS-polyacrylamide gel electrophoresis
SE	standard error
SSU	RuBisCo small subunit
TAG	triacylglycerol
TAIL-PCR	thermal asymmetric interlaced-PCR
TAP	tandem affinity purification
T-DNA	transfer DNA
TEM	transmission electron microscopy
TEV	tobacco etch virus nuclear inclusion A endopeptidase
TGD	trigalactosyldiacylglycerol

THF	tetrahydrofuran
Thyl.	thylakoids
TIC	translocon at the inner chloroplast membrane
TL	thermolysin
TM	transmembrane domain
TOC	translocon at the outer chloroplast membrane
Tricine	N-tris(hydroxymethyl)methylglycine
Tris	tris(hydroxymethyl)aminomethane
TX	triton X-100
UTR	untranslated region
VAR3	VARIEGATED 3
VitK	phylloquinone
VTE	vitamin E-deficient
Vv	*Vitis vinifera*
WT	wild type
YFP	yellow fluorescent protein
ZDS	ζ-carotene desaturase
α-T	α-tocopherol
α-TQH_2	α-tocopherol quinol
γ-T	γ-tocopherol

Upper case, italic	gene, WT allele (e.g. *NAP13*)
Lower case, italic	mutant allele (e.g. *nap13*)
Upper case	protein (e.g. NAP13)

Chapter I

General introduction[1]

1 Abstract

Photosynthesis is the key bioenergetic process taking place in the chloroplast. The components of the photosynthetic machinery are embedded in a highly dynamic matrix, the thylakoid membrane. This membrane has the capacity to adapt during developmental transitions and under stress conditions. The galactolipids are the major polar lipid components of the thylakoid membrane conferring bilayer properties, while neutral thylakoid lipids such as the prenyllipids and carotenoids contribute to essential functions such as electron transport and photoprotection. Despite a large number of studies, the intriguing processes of thylakoid membrane biogenesis and dynamics remain unsolved. Plastoglobules, thylakoid-associated lipid droplets, appear to actively participate in thylakoid function from biogenesis to senescence. Recruitment of specific proteins enables the plastoglobules to act in metabolite synthesis, repair and disposal under changing environmental conditions and developmental stages. In this introduction, we describe plastoglobules as thylakoid membrane microdomains and discuss their involvement in lipid remodeling during stress and in the conversion from one plastid type to another.

2 Plastids are malleable plant organelles

During the last 1.5 billion years, plastids evolved from cyanobacteria to become the most versatile organelle in plant cells (Timmis et al. 2004; Reyes-Prieto et al. 2007). In angiosperms, totipotent proplastids are maternally inherited (but exceptions exist) (Reboud and Zeyl 1994; Daniell et al. 2005; Hagemann 2010). They are able to differentiate into a large diversity of functional entities, from light harvesting photosynthetic factories to starch storage sites (Thomson and Whatley 1980). Depending on tissue, developmental stage and environmental conditions, proplastids morph into etioplasts, chloroplasts or leucoplasts, while chromoplasts and gerontoplasts are normally derived from chloroplasts (Vothknecht and Westhoff 2001). Even conversions of differentiated plastids into another plastid type are possible and require extensive ultrastructural reorganization (Li and Yuan 2013). Here, we will focus on chloroplasts and three developmentally related forms, namely etioplasts, chromoplasts and gerontoplasts.

Etioplasts occur in photosynthetic tissues in absence of light and represent the chlorophyll-less chloroplast precursor. Chromoplasts are found in reproductive tissues and lend attractiveness to pollinators and disseminators by storing colored carotenoids. Gerontoplasts represent senescent

[1] Adapted from Rottet et al. 2015

chloroplasts and appear during leaf senescence. Highly regulated catabolic activities take place in gerontoplasts, while resources are relocalized to seeds or perennial tissues.

Chloroplasts emerge upon illumination (photomorphogenesis) (Waters and Langdale 2009). Characterized by the presence of chlorophyll and a complex network of internal membranes, the thylakoids, chloroplasts allow plants to convert sunlight into chemical energy by photosynthesis. The light reactions of photosynthesis occur at the thylakoid membrane, a highly dynamic lipid matrix that must continuously adapt to changing environmental conditions and developmental cues.

3 Thylakoid membranes possess microdomains termed plastoglobules

The thylakoid bilayer is composed of four glycerolipids (Boudière et al. 2014). These include two galactolipids, monogalactosyldiacylglycerol (MGDG) and digalactosyldiacylglycerol (DGDG); one sulfolipid, sulfoquinovosyldiacylglycerol and one phospholipid, phosphatidylglycerol. Beside these polar lipids, the thylakoid membrane also contains neutral lipids. These play essential roles in electron transport between photosystem II (PSII) and cytochrome b_6f (plastoquinone, (Millner and Barber 1984)) and within PSI (phylloquinone), others act as photoprotective agents at the membrane level (tocopherol) or protect the photosynthetic complex by non-photochemical quenching (NPQ) (xanthophylls).

The thylakoids consist of a lipid bilayer enclosing a lumen, resulting in disc-shaped "sacs". The majority of thylakoids are stacked (granal thylakoids) and interconnected by non-stacked lamellae (stromal thylakoids) (Daum and Kühlbrandt 2011). At the curved regions of the thylakoid membrane, globular lipid droplets, named plastoglobules (PG), are present (Austin II et al. 2006). PG were discovered by electron microscopy owing to their highly osmiophilic properties that are due to the presence of unsaturated lipids (Greenwood et al. 1963). They consist of a membrane lipid monolayer surface surrounding a core of neutral lipids. This membrane lipid surface is studded with proteins (Kessler et al. 1999), many of which are implicated in lipid metabolism (Grennan 2008; Eugeni Piller et al. 2012) (Figure 1.1).

Since the characterization of PG proteomes from Arabidopsis chloroplasts and red pepper chromoplasts, the concept has emerged that PG are not only implicated in the storage of neutral lipid molecules but actively contribute to their synthesis (Vidi et al. 2006; Ytterberg et al. 2006; Lundquist et al. 2012b). Around 30 proteins are associated with the PG polar monolayer (Table 1.1, see (Lundquist et al. 2012b) for a complete list).

Their expression may be regulated in response to stress or developmental conditions (Bréhélin and Kessler 2008). For example, an effect of abiotic conditions, such as prolonged darkness or high light, was observed on the level of PG protein accumulation (Ytterberg et al. 2006; Lundquist et al. 2013). However, the mechanisms of their regulation at the protein level and their targeting to PG remain largely unsolved. Although none of the known PG proteins have predicted transmembrane domains, (Austin II et al. 2006) showed that part of the PG-localized tocopherol cyclase VTE1 (vitamin E-deficient 1) is exposed at the PG surface while another extends across the polar lipid monolayer, allowing direct contact with the neutral lipid content of the PG (Austin II et al. 2006; Kobayashi and

DellaPenna 2008; Mène-Saffrané and DellaPenna 2010). PG proteins belong to three different functional groups: (1) presumed structural proteins called fibrillins (FBN) or plastoglobulins; (2) enzymes implicated in lipid metabolism and (3) uncharacterized proteins. Proteins are recruited to the PG in response to stress or developmental stage. Changes of the PG protein composition may directly and indirectly affect PG lipid composition, because several prenyllipid biosynthetic enzymes and regulatory kinases are located in PG.

It has been suggested that the membrane curvature facilitates PG formation whereby the PG stay physically connected to the thylakoid membrane through the outer membrane lipid leaflet of the thylakoid membrane (Austin II et al. 2006). Moreover, a specific bilayer composition might influence the formation of PG as it has been proposed for lipid droplets (LD). LD are structurally related to the PG and arise at the endoplasmic reticulum membrane. LD serve as lipid reservoir and site of lipid metabolism and are essential in membrane formation and maintenance (Murphy 2012). The molecular mechanisms of LD formation are still under debate (Walther and Farese 2012). One of the models proposes that the products of specifically recruited neutral lipid biosynthetic enzymes accumulate between the lipid leaflets of the membrane bilayer leading to LD formation. This model is equally applicable to PG has they also host enzymes that contribute to neutral lipid biosynthesis and accumulation.

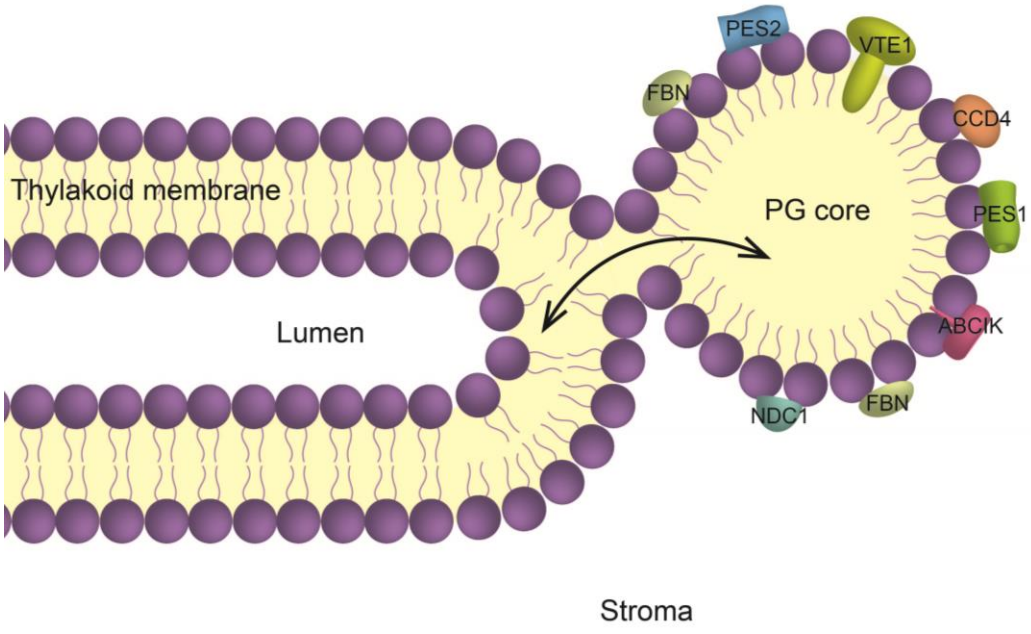

Figure 1.1 Representation of the physical connection between the thylakoid membrane and the plastoglobule (PG).
Within the chloroplast, the thylakoids are immersed in the stroma. The thylakoid membrane, composed of a polar lipid bilayer (mainly MGDG and DGDG), surrounds the lumen. At the curved regions of the thylakoid membrane, a PG buds from the outer thylakoid leaflet. Surrounded by a polar lipid monolayer, the PG core contains neutral lipids such as prenylquinones, carotenoids, fatty acid phytyl ester and triacyglycerol. The monolayer surface of PG is studded with specific proteins many of which are involved in prenyllipid metabolism. The contact site between PG and thylakoid membrane may provide a conduit for lipid trafficking (arrow). ABC1K, activity of bc1 complex-like kinases; CCD4, carotenoid cleavage dioxygenase 4; FBN, fibrillins; NDC1, NAD(P)H dehydrogenase C1; PES1, phytyl ester synthase 1; PES2, phytyl ester synthase 2; VTE1, tocopherol cyclase. Figure from (Rottet et al. 2015).

Table 1.1 Characterized plastoglobule (PG) proteins. This table provides a link between PG proteins and their roles in lipid remodeling. Despite quite numerous studies, the functions of many PG proteins remain unknown (c.f. (Lundquist et al. 2012b) for a complete list). Table from (Rottet et al. 2015).

ID	Common name	Symbol	Function(s) in lipid metabolism	Organism	References
At4g32770	Tocopherol cyclase	VTE1	Tocopherol biosynthesis and recycling	Arabidopsis	(Porfirova et al. 2002; Vidi et al. 2006)
At5g08740	NAD(P)H dehydrogenase C1	NDC1	VitK biosynthesis, PQ and tocopherol turnover	Arabidopsis	(Eugeni Piller et al. 2011; Eugeni Piller et al. 2014)
At1g54570	Phytyl ester synthase 1	PES1, DGAT3	TAG and FAPE biosynthesis	Arabidopsis	(Lippold et al. 2012)
At3g26840	Phytyl ester synthase 2	PES2, DGAT4	TAG and FAPE biosynthesis	Arabidopsis	(Lippold et al. 2012)
At4g31390	Activity of bc1-like kinase 1	ABC1K1	Regulation of prenylquinone biosynthesis	Arabidopsis	(Lundquist et al. 2013; Martinis et al. 2014)
At1g79600	Activity of bc1-like kinase 3	ABC1K3	Regulation of prenylquinone biosynthesis	Arabidopsis	(Lundquist et al. 2013; Martinis et al. 2013)
At4g19170	Carotenoid cleavage dioxygenase 4	CCD4, NCED4	Carotenoid oxidative cleavage	Arabidopsis	(Huang et al. 2009b; Gonzalez-Jorge et al. 2013)
At4g04020	Fibrillin 1a	FBN1a, PGL35	PG structural maintenance, JA biosynthesis	Arabidopsis,	(Deruère et al. 1994; Youssef et al. 2010)
At4g22240	Fibrillin 1b	FBN1b, PGL33	PG structural maintenance, JA biosynthesis	Arabidopsis	(Deruère et al. 1994; Youssef et al. 2010)
At2g35490	Fibrillin 2	FBN2, PGL40	PG structural maintenance, JA biosynthesis	Arabidopsis	(Deruère et al. 1994; Youssef et al. 2010)
At3g23400	Fibrillin 4	FBN4, PGL30.4	PG structural maintenance, Stress resistance	Arabidopsis, Apple	(Deruère et al. 1994; Singh et al. 2010; Singh et al. 2012)
gi|1583601	ζ-carotene desaturase	ZDS	Carotenoid biosynthesis	Red pepper	(Ytterberg et al. 2006)
gi|12643508	Lycopene β-cyclase	LYC-β	Carotenoid biosynthesis	Red pepper	(Ytterberg et al. 2006)
gi|2956671	β-carotene β-hydroxylase	CrtR-β	Carotenoid biosynthesis	Red pepper	(Ytterberg et al. 2006)

VTE, vitamin E-deficient; VitK, phylloquinone; PQ, plastoquinone; DGAT, diacylglycerol acyltransferase; TAG, triacylglycerol; FAPE, fatty acid phytyl ester; NCED, 9-cis-epoxycarotenoid dioxygenase; PGL, plastoglobulin; JA, jasmonate.

Thin layer chromatography, and recently mass spectrometry have allowed the identification of lipids in PG, but the complete lipidomic of PG is not available (Lichtenthaler and Tevini 1970; Ghosh et al. 1994; Zbierzak et al. 2010; Besagni et al. 2011; Martinis et al. 2011; Lippold et al. 2012; Singh et al. 2012; Martinis et al. 2013; Eugeni Piller et al. 2014; Kessler and Glauser 2014; Martinis et al. 2014). The neutral lipid core contains prenylquinones, carotenoids, triacylglycerol (TAG) and phytyl esters. The fact that PG and thylakoid membrane share the same kinds of neutral lipids must be emphasized even though the proportions may vary between the compartments. Concerning the polar lipid monolayer, the situation is ambiguous. In the past, galactolipids were either considered components of PG (Greenwood et al. 1963; Leggett Bailey and Whyborn 1963; Lichtenthaler 1968) or thylakoid contaminants because they were undetected in some studies but not in others (Steinmüller and Tevini 1985; Tevini and Steinmüller 1985). Topologically, PG are contiguous with the outer leaflet of the thylakoid membrane bilayer and therefore logically should share the same polar lipids.

It has been proposed that the thylakoid membrane adapts to changing environmental conditions and developmental cues by lipid remodeling. Lipid turnover is essential to ensure longevity and stress resistance of membranes. Such dynamics are clearly evident in extraplastidic membranes under phosphate deficiency where a large proportion of phospholipids are replaced by DGDG (Härtel et al. 2000; Andersson et al. 2003; Dörmann 2007; Gaude et al. 2007).

Interestingly, Lichtenthaler in 1968 already suggested that PG have a dynamic composition according to the stage of development (Lichtenthaler 1968). This hypothesis has been expanded during the last few years as it became clear that PG are sites of lipid metabolism. It can now be proposed that the PG serve to supply and maintain (neutral) lipids required for remodeling in response to environmental or developmental changes (Figure 1.2).

It is therefore of high interest to elucidate the functions of PG. To achieve this goal, a wide range of methods are being used. Application of stresses and description of the resulting macro- and microphenotypes of plants were among the early approaches, followed by reverse genetics in conjunction with metabolomics analyses. In the following, the implication of PG in thylakoid lipid remodeling under various developmental and stress conditions will be reviewed.

4 Role of plastoglobules in plastid differentiation

4.1 Photomorphogenesis: From the etioplast to the chloroplast

In the dark or under low light intensity, proplastids develop into etioplasts, the chloroplast precursor organelles (Solymosi and Schoefs 2010). Etioplasts are characterized by the presence of the paracrystalline prolamellar body (PLB) that contains molecular building blocks for the chloroplast thylakoid membrane. Light triggers the conversion of the etioplast to the chloroplast. During this conversion, the PLB disappears while the thylakoid membrane emerges accompanied by the production of large quantities of chlorophyll. Dark-grown etiolated tissues have a pale yellow color due to the presence of carotenoids. In addition, etioplasts accumulate the chlorophyll precursor

protochlorophyllide, the conversion of which to chlorophyllide and then chlorophyll occurs almost instantly in response to light (Philippar et al. 2007).

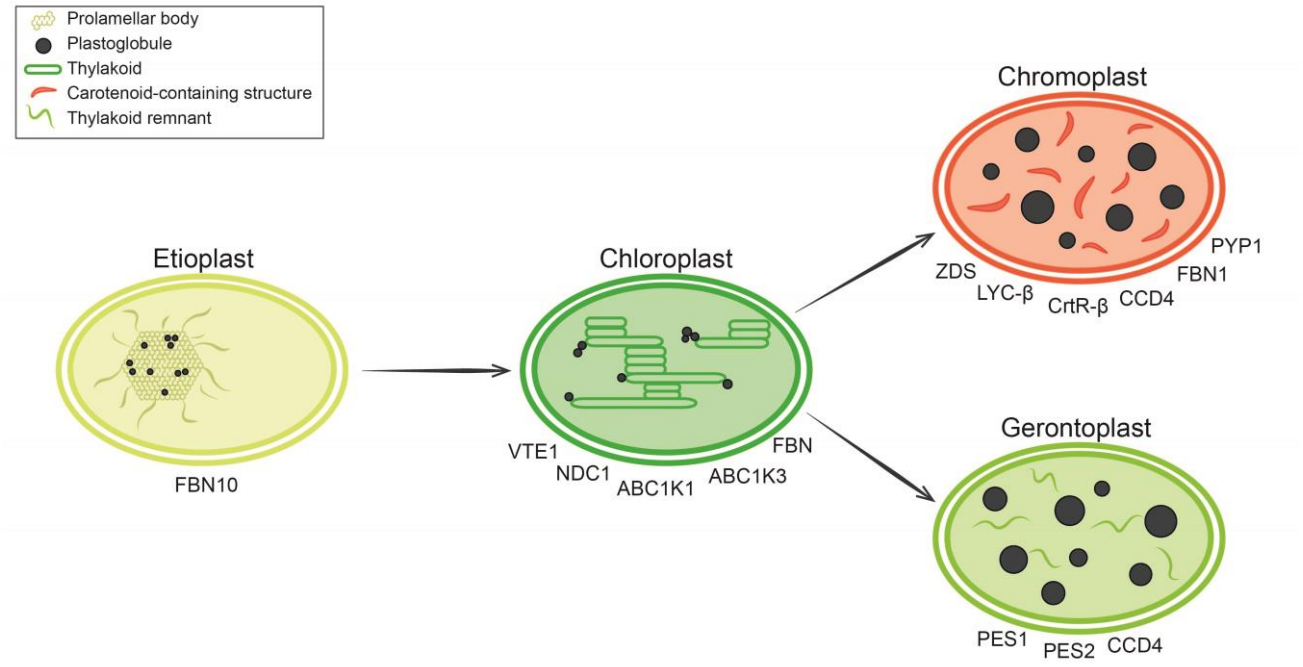

Figure 1.2 Roles of plastoglobules (PG) in plastid differentiation.
Etioplasts, chloroplast precursors, are present in the dark. They are characterized by the paracrystalline prolamellar body (PLB) that is interspersed with numerous small PG. As a known lipid reservoir, PG may assist in the rapid formation of thylakoid membranes upon illumination. Ytterberg et al. (2006) identified the homolog of the thylakoid-associated FBN10 in low-density lipid particles that correspond to the PLB of rice etioplasts (Ytterberg et al. 2006). FBN10 may serve to channel lipids to the nascent thylakoids. Chloroplasts contain the internal thylakoid membrane network. PG are coupled to the thylakoid membrane and involved in lipid remodeling. Tocopherol metabolism is upregulated under high light, involving the PG-located proteins tocopherol cyclase (VTE1), NAD(P)H dehydrogenase C1 (NDC1), activity of bc1 complex-like kinases (ABC1K) and fibrillins (FBN). Chromoplasts in reproductive tissues (fruits and flowers) differentiate from chloroplasts to attract pollinators and seed disseminators. These plastids are characterized by thylakoid disassembly and an appearance of carotenoids stored and produced in PG or carotenoid fibrils with the help of ζ-carotene desaturase (ZDS), lycopene β-cyclase (LYC-β) and two β-carotene β-hydroxylases (CrtR-β). Carotenoid cleavage dioxygenase 4 (CCD4) cleaves carotenoids to release apocarotenoids that contribute to scent and flavor. The tomato pale yellow petal 1 (PYP1) is required for xanthophyll esterification and hence normal yellow petal pigmentation. Gerontoplasts differentiate from chloroplasts during senescence. Chlorophyll and thylakoid membranes are dismantled, releasing large amounts of fatty acids and phytol. These catabolic products are sequestered in triacylglycerol (TAG) and fatty acid phytyl ester (FAPE) by phytyl ester synthase 1 (PES1) and 2 (PES2), two PG-located enzymes. TAG and FAPE contribute to the formation of giant PG. Carotenoids remaining in gerontoplasts are degraded by CCD4. Figure from (Rottet et al. 2015).

Thylakoid membrane formation requires the coordinated assembly of the lipid bilayer with membrane proteins. These are mostly nuclear-encoded, imported proteins, and many are assembled to photosynthetic complexes together with cofactors such as pigments or metal ions. Galactolipids constitute 80% of the thylakoid membrane lipids. Synthesized at the inner envelope membrane, they contain fatty acids (FA) originating from the endoplasmic reticulum. FA are then incorporated into phosphatidic acid, imported into the chloroplast by the trigalactosyldiacylglycerol complex at the inner envelope and converted into diacylglycerol (DAG) (Benning 2009; Wang et al. 2012; Mehrshahi et al. 2013; Mehrshahi et al. 2014). Monogalactosyldiacylgycerol synthase 1 and digalactosyldiacylglycerol synthase 1 are required for galactolipid synthesis. Both enzymes are embedded in the inner envelope of the chloroplast and catalyze the conversion of DAG into MGDG and DGDG respectively, the two main galactolipids present in thylakoid membranes (Aronsson et al. 2008).

Several mechanisms of lipid transfer from the site of synthesis at envelope membrane to the nascent thylakoid membrane have been proposed. These include transport vesicles as well as membrane tubes emerging from the inner envelope or the PLB (Andersson et al. 2001; Kobayashi et al. 2007; Chigri et al. 2012; Kobayashi et al. 2012; Vothknecht et al. 2012; Rütgers and Schroda 2013).

During chloroplast biogenesis, lamellar prothylakoids have been observed to emerge from the PLB (Gunning 2001; Grzyb et al. 2013). The PLB itself consists of tubular structures interspersed with numerous PG (Lichtenthaler 1968). Both PLB tubules and prothylakoids are composed mainly of MGDG and DGDG, the PLB being enriched in MGDG (Aronsson et al. 2008). Apart from membrane lipids, the PLB also contains protochlorophyllide and proteins that are required for rapid chloroplast biogenesis. Proteomics analysis of purified PLB revealed two major functional groups of proteins: (1) Proteins implicated in pigment synthesis, such as the abundant NADPH protochlorophyllide oxidoreductases A/B and chlorophyll synthase. (2) Known thylakoid proteins implicated in photosynthetic reactions (e.g. ATP synthases, cytochrome b_6f, ferredoxin-NADPH oxidoreductases, PSII subunits). The protein and metabolite compositions provide the evidence that the PLB plays a role in chloroplast biogenesis and functions as a precursor of the chloroplast thylakoid membranes (Blomqvist et al. 2008; Solymosi and Schoefs 2010).

In etioplasts, the PLB cages a high number of PG. After exposure to light, PG number decreases in de-etiolated tissue simultaneously with the rise of thylakoid membranes from the PLB (Lichtenthaler and Peveling 1966; Sprey and Lichtenthaler 1966; Lichtenthaler 1968; Nacir and Bréhélin 2013). PG as a lipid reservoir may assist in the rapid formation of thylakoid membranes in greening tissues by releasing structural thylakoid lipids (MGDG) and their precursors (TAG, DAG). Supplying lipid building blocks for membrane expansion may explain why PG become small and rare during thylakoid formation and larger and more abundant in the mature chloroplast (Lichtenthaler 1968). PG also contain tocopherol and other prenylquinones, therefore PG have also been proposed to protect the nascent membrane by supplying lipid antioxidants during chloroplast biogenesis (Eugeni Piller et al. 2014).

However, two questions remain unsolved: how small hydrophobic molecules can be transferred from PG to thylakoid membrane and the extent to which PG and associated proteins are involved in thylakoid membrane formation.

While most likely the contact sites between PG and thylakoids provide the conduit for small molecules, FBN may also be involved in lipid transfer. Indeed, FBN possess a predicted lipocalin motif that has the ability to bind and transport small hydrophobic molecules (Flower 1994; Flower 1996; Flower et al. 2000; Kim et al. 2001; Singh and McNellis 2011). The members of the FBN family constitute the most abundant proteins in PG. Together seven FBN (out of 13 identified in Arabidopsis) represent 53% of the PG proteome mass (FBN1a-At4g04020, FBN1b-At4g22240, FBN2-At2g35490, FBN4-At3g23400, FBN7a-At3g58010, FBN7b-At2g42130, FBN8-At2g46910) (Lundquist et al. 2012b). Initially considered structural proteins, recent studies indicate that FBN function may extend to chromoplast pigment accumulation, resistance to biotic and abiotic stresses as well as protection of the photosystem from photodamage (Giacomelli et al. 2006; Leitner-Dagan et al. 2006; Singh et al. 2010; Youssef et al. 2010). These roles are in agreement with FBN expression patterns, which vary with plant developmental stage, hormonal treatment and various stresses (Pozueta-Romero et al. 1997; Gillet et al. 1998; Singh and McNellis 2011; Lundquist et al. 2013; Gámez-Arjona et al. 2014). Unfortunately, a PG proteome of etioplasts is still missing. Ytterberg et al. (2006) attempted to establish the PG proteome of rice etioplasts (Ytterberg et al. 2006). However, the isolated low-density particles are dominated by protochlorophyllide reductase and showed no overlap with other PG proteomes. For this reason, it was concluded that these low-density particles most likely represented PLB. Interestingly, a member of the FBN family was identified in these low-density particles of rice etioplasts. In Arabidopsis, the probable ortholog is FBN10 (At1g51110). FBN10 is mainly present in thylakoids but not particularly enriched in PG. Nevertheless, it is tempting to speculate on the implication of FBN10 in lipid trafficking during thylakoid formation.

In conclusion, the main ultrastructural modification induced by light during the transition from etioplast to chloroplast is the formation of thylakoid membrane that emerges from the PLB and is presumably assisted by the PG lipid reservoir.

4.2 Reproduction: From the chloroplast to the chromoplast

Higher plants have evolved flowers and fruits, which are specialized tissues for reproduction. Often the color of fruits and flowers are conferred by chromoplasts. Chromoplasts differentiate from chloroplasts during floral development and fruit maturation. During the process the well-developed thylakoid membrane network that characterizes chloroplasts is dismantled and replaced by carotenoid-containing structures and enlarged PG in chromoplasts (Egea et al. 2010). During this transition, the degradation of chlorophyll is concomitant with carotenoid biosynthesis and sequestration (Li and Yuan 2013; Othman et al. 2014).

Carotenoids are widespread pigments synthesized and localized in plastids. They are subdivided in two classes, carotene hydrocarbons that may be cyclized at one or both ends and xanthophylls that contain extra oxygen atoms in the form of hydroxyl or epoxide groups. Carotenoids are highly esterified in fruits and flowers (Hornero-Méndez and Mínguez-Mosquera 2000; Breithaupt and Bamedi 2001). The esterification seems to enhance carotenoid stability (Schweiggert et al. 2006) and to increase their lipophilic properties, which may facilitate their sequestration into carotenoid-containing structures (Deruère et al. 1994).

During chloroplast to chromoplast conversion in red pepper, thylakoids and chlorophyll disappear whereas PG strongly enlarge. In chromoplasts, PG may transform into rod-like structures (fibrils) filled with carotenoids. The major protein associated with the fibrils was termed FBN and turned out to be the first identified member of the FBN family (Deruère et al. 1994; Vishnevetsky et al. 1999). Interestingly, chromoplast fibril self-assembly occured when FBN was added to a mixture of carotenoids and polar lipids (MGDG, DGDG and phospholipids). Fibril reconstitution only occurred when the lipid-protein ratio was close to the in vivo ratio. Furthermore, linear carotenoids such as lycopene inhibited fibril assembly. Cyclic carotenoids (β-carotene, zeaxanthin and capsanthin) gave intermediate results, while esterified carotenoids (zeaxanthin diester and capsanthin diester) worked best (Deruère et al. 1994). This important experiment suggested that FBN play a role in the formation and stabilization of fibrils and PG.

High expression of pepper FBN1 in tomato fruits leads to enlarged PG and protects the thylakoids from degradation during chloroplast-to-chromoplast transition (Simkin et al. 2007). Indeed, an increase in carotenoid content and a delay in thylakoid disintegration were observed under FBN overexpression. These data were interpreted in two different ways. FBN may act directly on the thylakoid membrane. Alternatively, FBN may act indirectly by enhancing PG formation and/or stabilizing their structure, including their thylakoid connections. FBN are often upregulated under abiotic and biotic stresses (for review see (Singh and McNellis 2011)), supporting the idea of their protective role for thylakoid membranes, be it direct or indirect.

In chloroplasts as well as chromoplasts, PG participate in carotenoid metabolism. Ytterberg et al. (2006) identified four enzymes in the PG proteome of red pepper chromoplasts that are implicated in carotenoid biosynthesis, including ζ-carotene desaturase (ZDS), lycopene β-cyclase (LYC-β) and two β-carotene β-hydroxylases (Ytterberg et al. 2006). ZDS introduces conjugated double bonds which are required for the biosynthesis of lycopene, the red pigment of tomato chromoplasts (Ben-Shaul and Naftali 1969), from phytoene. LYC-β catalyzes the cyclization of one or both ends of lycopene to yield α- or β-carotene. The next step in carotenoid biosynthesis is to generate xanthophyll products by the incorporation of oxygen molecules into carotene cycles. By the action of carotenoid hydroxylases, α- and β-carotene are converted into lutein and zeaxanthin, respectively (Ruiz-Sola and Rodríguez-Concepción 2012).

Carotenoids can also be metabolized further by oxidative cleavage to produce apocarotenoids (Auldridge et al. 2006b). Apocarotenoids have important metabolic functions since they act as phytohormones (abscisic acid, strigolactone), pigments (β-citraurin), aromatic volatiles (β-ionone, β-cyclocitral, geranial) or signaling molecules (β-cyclocitral). Phytohormones are essential for growth regulation, stress responses and much more (Hirayama and Shinozaki 2007; Gomez-Roldan et al. 2008; Jia et al. 2013). As an aromatic volatile, β-ionone is a pollinator attractant in flowers but also contributes to fruit flavor (Simkin et al. 2004a). β-cyclocitral functions as a stress signal produced under high light. It increases the tolerance to photooxidative stress by modulating the expression of genes involved in the singlet oxygen response (Ramel et al. 2012). The oxidative cleavage of carotenoids may occur spontaneously under oxidative stress or require enzymatic activity (Havaux 2014). The enzymes involved in carotenoid cleavage are grouped into the family of carotenoid cleavage dioxygenases (CCD). Members of this enzyme family have divergent roles in different tissues and species (Auldridge et al. 2006a; Ohmiya 2009). A subgroup termed 9-cis-

epoxycarotenoid dioxygenases is essential for abscisic acid biosynthesis (Schwartz et al. 2003; Tan et al. 2003). Notably, PG proteomes contain CCD4 which cleaved 8'-apo-β-caroten-8'-al to release β-ionone in *Arabidopsis thaliana* (Huang et al. 2009b). Interestingly, simultaneous absence of PG-localized ABC1K1 and ABC1K3 (activity of bc1 complex-like kinase) resulted in a threefold downregulation of CCD4, whereas protein abundance levels of several other PG-localized metabolic enzymes were not affected (Lundquist et al. 2013). Thus, CCD4 stability may depend upon phosphorylation by these two PG kinases. CCD4 is a good example for the divergent roles of the CCD family even though the substrates are not fully known. The following examples strongly suggest a range of CCD4 substrates in different species.

In chrysanthemum (*Chrysanthemum morifolium* Ramat.), CmCCD4a is responsible for white color formation in petals. The expression level of CmCCD4a in yellow-flowered cultivars is extremely low, while it occurs at high levels in petals of white-flowered cultivars. Since carotenoid biosynthesis is unaffected in both cultivars, and lutein is the predominant carotenoid in yellow petals (Zhu et al. 2010), it is likely that CmCCD4a cleaves lutein into colorless apocarotenoids thus disrupting the accumulation of carotenoids. Despite the fact that CmCCD4a shares 61% of homology with AtCCD4, its association with PG remains experimentally unexplored (Ohmiya et al. 2006; Yoshioka et al. 2012).

During Satsuma mandarin (*Citrus unshiu*) fruit ripening, the upregulation of CitCCD4 correlates with the accumulation of β-citraurin, a red pigment typical for the Yamashitabeni-wase variety. Actually, CitCCD4 was shown to cleave β-cryptoxanthin and zeaxanthin in vitro at the 7,8 and 7',8' position to yield β-citraurin. It was concluded that CitCCD4 is substrate specific since no activity was detected with lycopene, α-carotene, β-carotene and violaxanthin (Ma et al. 2013).

Heterologous expression of the saffron (*Crocus sativus*) protein shows that CsCCD4 preferentially cleaves β-carotene (but also lutein, neoxanthin and violaxanthin) into β-ionone and β-cyclocitral during stigma development. Furthermore, the expression of CsCCD4-GFP resulted in a spot-like pattern inside chloroplasts reminiscent of PG localization (Rubio et al. 2008; Rubio-Moraga et al. 2014).

Recent insight into carotenoid sequestration stems from a study on tomato flowers (Ariizumi et al. 2014). The *pyp1* (pale yellow petal 1) mutant shows reduced yellow pigmentation in flowers and altered chromoplast development due to a lack of xanthophyll esters (mainly neoxanthin and violaxanthin esterified with 14:0 and 16:0 FA). Esterification enhances carotenoid stability (Schweiggert et al. 2006) and may therefore be favored in the chloroplast-to-chromoplast transition. Interestingly, tomato PYP1 shared 58% identity (73% similarity) with phytyl ester synthase 1 (PES1) (Ariizumi et al. 2014) which is localized in PG of *A. thaliana*. Previously named diacylglycerol acyltransferase 3 (DGAT3), PES1 contributes to TAG and fatty acid phytyl ester (FAPE) synthesis in chloroplasts (Lippold et al. 2012). Besides, its implication in carotenoid esterification is probable as PES1 was found in PG of chromoplasts of red pepper (Ytterberg et al. 2006).

In conclusion, the chromoplast PG proteome differs strongly from that of the chloroplast (Ytterberg et al. 2006). It is customized to assist the chloroplast-to-chromoplast transition. This is particularly

apparent by the presence of the carotenoid metabolic enzymes. These are specifically recruited for the purpose of depositing carotenoids in the emerging colored PG and fibrils.

4.3 Senescence: From the chloroplast to the gerontoplast

During senescence, nutrients are relocated from senescing tissue to the developing seeds and perennial tissues which must survive the challenges of winter (Quirino et al. 2000; Hörtensteiner and Feller 2002). Leaf senescence has aspects of a recycling process and is important for reproduction and plant fitness. Thus, plant senescence is a highly regulated process composed of a cascade of events, ultimately leading to cell death (Besagni and Kessler 2013). It is induced by external factors (e.g low/high temperature, shading or lack of nutrient) or internal factors such as plant age and phytohormones. Developmental factors and stresses lead to the synthesis of jasmonate (JA), abscisic acid, salicylic acid or auxin, which initiate the transcription of genes implicated in senescence. Highly expressed during senescence, the large set of senescence associated genes plays a central role throughout senescence. A number of senescence associated genes function to catalyze catabolic events leading to the transition from chloroplast to gerontoplast. This transition is accompanied by dramatic ultrastructural reorganization that is characterized by the dismantling of the thylakoids and the appearance of giant PG (Ghosh et al. 2001).

Chlorophyll breakdown is the most striking activity taking place in chloroplast to gerontoplast transition (Matile et al. 1999). However, mutants have been identified in which chlorophyll degradation is perturbed. In the most dramatic cases this results in a stay green phenotype that may be either functional (photosynthetically active) or just cosmetic (green but photosynthetically inactive) (Thomas and Howarth 2000).

Free phytol is a catabolic product released from chlorophyll by pheophytin pheophorbide hydrolase (PPH) (Schelbert et al. 2009; Zhang et al. 2014). This hydrolytic product has to be metabolized to minimize its toxicity (Ischebeck et al. 2006). A first pathway implicates the conversion of free phytol to phytol monophosphate by phytol kinase VTE5 followed by a second phosphorylation step and its incorporation into tocopherol (Ischebeck et al. 2006; Valentin et al. 2006). In a second pathway, phytol is incorporated into FAPE by the esterification with free FA. These FA may either be synthesized de novo or result from hydrolysis of galactolipids during thylakoid dismantling. The hydrolysis of galactolipids by lipases releases a pool composed mainly of C18:3 and C16:3 free FA. FA may also be deposited in TAG.

It appears likely that the huge size of PG in gerontoplasts is at least partly due to the accumulation of these senescence-associated catabolic products. Moreover, TAG and FAPE are excellent examples to illustrate the participation of PG in chloroplast lipid remodeling during senescence both at the biochemical and ultrastructural levels. Biochemically, remodeling here refers to the synthesis of FAPE and TAG while galactolipids as well as chlorophyll are broken down. Ultrastructurally, remodeling is observed by electron microscopy: thylakoids disappear and are replaced by massively enlarged PG. Moreover, PG do not only serve to deposit FAPE and TAG but actively participate in their synthesis by the presence of three PG enzymes.

PPH (At5g13800), which dephytylates pheophytin and thereby releases free phytol, was recently identified in the PG of the *abc1k1abc1k3* double mutant lacking two PG-associated kinases (Lundquist et al. 2013). The transient association of PPH with PG may be viewed as a response to the increased chlorophyll turnover observed in *abc1k1abc1k3* light-stressed leaves (see chapter I, 5.1).

A reverse genetic study revealed that PES1 and PES2, previously named DGAT3 and DGAT4, are overexpressed during senescence and required for FAPE and TAG production in gerontoplasts (Lippold et al. 2012). Indeed, heterologous expression in yeast and in vitro assay show that both proteins, members of the esterase/lipase/thioesterase family, have diacylglycerol acyltransferase activity allowing the production of TAG and FAPE from FA esterified respectively to DAG or phytol (Lippold et al. 2012; Besagni and Kessler 2013). In addition, *pes1pes2* mutant plants under nitrogen starvation accumulate far less TAG and FAPE.

PES1 and PES2, however, are not predicted to function exclusively as acyltransferases. It is tempting to speculate that they function as galactolipid lipases at the thylakoid membrane. This idea is supported by the presence of a predicted lipase domain in both proteins, their ability to release FA from MGDG *in vitro* (Lippold et al. 2012) and because the *pes1pes2* double mutant exhibits a delay in senescence characterized by a prolonged persistence of thylakoid membranes and of pale green color whereas wild type (WT) plants are yellow.

In autumn, the progressive disappearance of chlorophyll in tree leaves reveals the carotenoids that are degraded more slowly (Keskitalo et al. 2005). CCD4 identified in the PG proteome has recently been shown to cleave β-carotene during seed maturation and senescence (Gonzalez-Jorge et al. 2013). Moreover, Tevini and Steinmüller (1985) observed in beech leaves (*Fagus sylvatica*) that carotenoids liberated from the thylakoid membrane were esterified and deposited in PG during senescence (Tevini and Steinmüller 1985). This suggested an implication of carotenoids in FA sequestration as carotenoid esters. This is reminiscent of the PES1 homolog PYP1 in tomato flowers that is required for normal carotenoid ester production in petal chromoplasts (Ariizumi et al. 2014). It therefore appears likely that PES1 and PES2 may catalyze the equivalent reaction in senescent chloroplasts.

In conclusion, the transition from chloroplast to gerontoplast occurs in close relationship with PG which serve not only to store catabolic products but also participate in their release and transformation into storage compounds.

5 Role of plastoglobules in chloroplast during stress conditions

Plants are confronted with various stress conditions, including nitrogen starvation, drought, heavy metal toxicity, temperature variations, pathogen infection and high light. In many cases, these conditions induce oxidative stress within the chloroplast.

5.1 Implication of PG in thylakoid maintenance during high light stress

Noxious reactive oxygen species (ROS) are formed during high light stress, especially singlet oxygen that is responsible for most chloroplast photooxidative damage (Triantaphylidès et al. 2008). Under high light, the major photoprotective mechanism at the thylakoid membrane is NPQ of excess light energy (Jahns and Holzwarth 2012) and the production of membrane antioxidants. NPQ refers to the xanthophyll cycle that dissipates the excessive light energy in the form of heat, thereby reducing ROS formation (Demmig-Adams and Adams 1996; Jahns and Holzwarth 2012), while carotenoids and most of the prenylquinones accumulated in PG are antioxidant molecules playing an important role in photoprotection (Avalos and Limón 2014).

Tocopherol is a well-studied membrane antioxidant and its production is strongly increased under high light (Havaux et al. 2005). Belonging to the tocochromanol family, tocopherol, commonly called vitamin E, refers to four compounds. They differ by the methylation degree of their chromanol ring (α, β, γ and δ). They are lipid-soluble antioxidant molecules (Mène-Saffrané and DellaPenna 2010). α-tocopherol (α-T) is the predominant form in photosynthetic tissues, while γ-tocopherol (γ-T) accumulates mainly in seeds. Tocopherols protect membrane lipids against peroxidation and preserve PSII from photoinactivation (Havaux et al. 2005). Vitamin E-deficient mutants led to the identification of the enzymes involved in tocopherol biosynthesis (Porfirova et al. 2002; DellaPenna 2005). VTE1 is tocopherol cyclase and catalyzes the cyclisation of 2,3-dimethyl-6-phytyl-1,4-benzoquinone to γ-T (Vidi et al. 2006). Surprisingly, VTE1 appears to be localized mainly in PG whereas the remainder of the enzymes of the pathway (VTE2, VTE3 and VTE4) were localized at the chloroplast inner envelope membrane (Soll et al. 1985; Cheng et al. 2003; Vidi et al. 2006; Kobayashi and DellaPenna 2008; Zbierzak et al. 2010). The differential localization of VTE1 in PG and the other enzymes at the inner envelope suggest that tocopherol metabolites need to traffick between the compartments (Bréhélin et al. 2007).

VTE1 is not only implicated in the de novo synthesis of tocopherol but also in the recycling of the tocopherol oxidation product α-tocopherol quinol (α-TQH_2) that is produced upon reaction with lipid peroxides. Cyclization by VTE1 completes the conversion of α-TQH_2 into α-T (Kobayashi and DellaPenna 2008; Eugeni Piller et al. 2014). It is interesting to note that reduced quinones are the preferred substrate of VTE1 (Grütter et al. 2006; Kobayashi and DellaPenna 2008).

Interestingly, this regeneration pathway implicates another PG protein, NDC1 (NAD(P)H dehydrogenase 1), which reduces α-tocopherol quinone to α-TQH_2. In the *ndc1* mutant α-tocopherol quinone accumulates to a higher degree than in the WT. NDC1 has a wide substrate specificity and also catalyzes the reduction of plastoquinone (PQ) to plastoquinol contained within PG. In the *ndc1* mutant more PQ is present than in the WT under high light conditions. In higher plants, however, this reaction is inconsequential for bulk photosynthetic electron flow unlike *Chlamydomonas* where NDC1 rather than the NAD(P)H-plastoquinone oxidoreductase complex is responsible for cyclic electron flow around PSI (Jans et al. 2008). NDC1 is also required for the efficient production of plastochromanol (PC-8) from PQ that also depends on VTE1. PC-8 is also known to accumulate in PG. PC-8 inhibits lipid peroxidation and is an efficient oxygen scavenger (Olejnik et al. 1997; Gruszka et al. 2008) primarily produced during senescence rather than under high light (Szymańska and Kruk 2010; Eugeni Piller et al. 2014). Finally and surprisingly NDC1 is also required for the

conversion of 2-phytyl-1,4-naphthoquinone, the immediate precursor of phylloquinone, to phylloquinone in *A. thaliana* (Eugeni Piller et al. 2011; Eugeni Piller et al. 2014). This step requires methylation of the naphthoquinone intermediate by AtMenG (Lohmann et al. 2006). The role of NDC1 in the methylation step is not clear (Eugeni Piller et al. 2011). It is interesting to note, however, that neither *atmenG* nor the *ndc1* mutant have an apparent phenotype and the naphthoquinone intermediate can functionally replace phylloquinone except under high light conditions where oxidative damage of PSI was observed in *atmenG*.

The *Arabidopsis* PG proteomes revealed a surprisingly high number of ABC1-like kinases (ABC1K9-At5g05200, ABC1K1-At4g31390, ABC1K3-At1g79600, ABC1K5-At1g71810, ABC1K6-At3g24190, ABC1K7-At3g07700) (Lundquist et al. 2012a; Lundquist et al. 2012b). In bacteria and mitochondria, ABC1 homologs regulate ubiquinone synthesis (Poon et al. 2000; Xie et al. 2011). Recently, it has been demonstrated by two independent studies that two PG ABC1-like kinases, ABC1K3 and ABC1K1, regulate prenylquinone metabolism probably through the phosphorylation of VTE1 (Martinis et al. 2013; Martinis et al. 2014). Martinis et al. characterized the single mutants *abc1k1* and *abc1k3*, while Lundquist et al. concluded that ABC1K1and ABC1K3 are likely to form a complex and consequently focus their work on the characterization of the double mutant *abc1k1abc1k3* (Lundquist et al. 2013). *abc1k1* and *abc1k1abc1k3* showed sensitivity to light stress, expressed by a rapid leaf bleaching and an inability to accumulate anthocyanin. In the *abc1k1* and *abc1k3* single mutants, VTE1 failed to localize in PG leading to reduced vitamin E (α-T, γ-T and δ-tocopherol) content under high light stress. Surprisingly, however the transcript level of VTE1 was increased. Comparable findings were also made for FBN1a and FBN2 in both single mutants (Martinis et al. 2013; Martinis et al. 2014). This hints at an underlying post-translational regulation of protein stability. ABC1-like kinase-dependent phosphorylation may stabilize the proteins and/or affect their recruitment to PG. But these results are partially in conflict with those for *abc1k1abc1k3*. A very robust mass spectrometry-based quantification (Lundquist et al. 2013) showed that the levels of VTE1, FBN1a and FBN2 are unaffected in isolated PG of *abc1k1abc1k3* compared to WT. In addition, CCD4, ABC1K5 and ABC1K6 levels are strongly downregulated, suggesting that they are stabilized by ABC1K1 and ABC1K3 is required. Moreover, an enrichment of lipoxygenase 3 and 4 (respectively At1g17420 and At1g72520) was observed in isolated PG of *abc1k1abc1k3* under light stress. These two newly identified PG proteins are involved in the synthesis of the plant hormone JA using FA. Recruitment of the JA biosynthetic pathway to PG suggests an increased lipid remobilization for JA production in *abc1k1abc1k3*. An extensive quantification of prenylquinones and carotenoids was also provided, with a specific focus on their distribution and redistribution between PG and thylakoid membrane. Compared to the WT, *abc1k1abc1k3* showed an increased amount of PQ, phylloquinone and β-carotene that are relocated to the PG rather than to the thylakoid membranes. In accordance with a reduced activity of VTE1, they also observed a lower level of PC-8 and α-T that are redistributed toward the thylakoid membranes. Interestingly, a novel quinone (molecular mass of 746.6) was identified in isolated PG of *abc1k1abc1k3*. This putative quinone could be an unknown intermediate of the quinone biosynthesis pathway or an oxidation product of prenyllipids.

The degreening phenotype of *abc1k1abc1k3* is not a strict light stress effect as the same phenotype was obtained under drought stress or nitrogen starvation (Lundquist et al. 2013). The inability of

abc1k1abc1k3 to adapt to elevated light intensity, water or nitrogen deficiency probably leads to excessive singlet oxygen production. The implication of singlet oxygen retrograde signaling in the degreening phenotype is supported by the elevated level of β-cyclocitral found in *abc1k1abc1k3* under light stress (Ramel et al. 2012).

In conclusion, regulation of VTE1 activity by the phosphorylation of ABC1K3 and ABC1K1 is a common finding, which is strongly supported by predictions and experimentation. The PhosPhAt database (The Arabidopsis Protein Phosphorylation Site Database, *http://phosphat.uni-hohenheim.de/*) shows that VTE1 has a phosphorylation hotspot near its N-terminus. Conceivably, phosphorylation at this site affects the activity of the protein. Moreover, VTE1 was shown to be phosphorylated in a phosphoproteome analysis upon nitrogen deficiency (Nakagami et al. 2010).

5.2 PG may be involved in the tolerance to the heavy metal cadmium

Heavy metals are either essential (Cu, Zn, Mn) or toxic (Cd, Pb) for plants. Small amounts of essential metals are sufficient to ensure their metabolic role while larger amounts of heavy metals are toxic to the plant (Jasinski et al. 2008). To overcome metal toxicity, phytochelatins, glutathione and ABC transporters are produced in order to sequestrate and/or extrude heavy metals (Clemens et al. 2002; Kim et al. 2007). Thus, heavy metal resistance requires the activation of a specific set of genes.

Cadmium (Cd) has a destructive effect on the chloroplast. Upon Cd treatment, the disorganization of the photosynthetic apparatus was observed. More specifically, PSI and associated (light-harvesting) antenna proteins are dismantled while PSII, cytochrome b_6f and ATP-synthase seem less affected (Fagioni et al. 2009; Villiers et al. 2011). Cd can replace other metal ions (Zn, Fe, Ca, Mg) in proteins and may affect the redox state by generating, directly or indirectly, ROS. Regarding lipids, spinach basal leaves showed an increase in xanthophyll content (neoxanthin, violaxanthin and lutein) concomitant with a chlorophyll decrease (chlorosis) in the presence of Cd. The lutein overproduction may represent a defensive mechanism against ROS (Fagioni et al. 2009). Surprisingly, upon Cd treatment, plants seem unable to produce zeaxanthin, a well-described ROS scavenging defense (Havaux et al. 2007; Dall'Osto et al. 2012). In the chloroplast, Cd toxicity mimics the symptoms observed during senescence. A notable change is a considerable increase in the number and size of PG (Jin et al. 2008). Indeed, Cd-treated *Pisum sativum* plants showed disorganized thylakoid membranes in conjunction with an increase in size and number of PG as well as in the size of starch grains. It was suggested that Cd toxicity induces oxidative stress as in leaf senescence (Sandalio et al. 2001).

Interestingly, the expression of the envelope-located ABC1K8 (or OSA1, oxidative-stress related ABC1-like protein) is strongly affected by Cd treatment (Jasinski et al. 2008). To investigate the implication of PG in Cd resistance, effect of Cd on root growth was evaluated for WT, abc1k1, abc1k3 and abc1k1abc1k3 (Lundquist et al. 2013). However all genotypes showed the same reduced root growth, indicating that ABC1K1 and ABC1K3 are not involved in Cd tolerance. Nevertheless, the PG proteome contains 4 other ABC1-like kinase candidates that have not yet been characterized.

6 Aim of this work

In recent years, the PG has emerged as an important player in chloroplast lipid metabolism operating as a thylakoid microdomain for metabolite synthesis, repair and disposal. This concerns both the neutral and polar membrane lipids. By its capacity for lipid remodeling at large, PG in different tissues are implicated in transitions from the chloroplast to the chromoplast and gerontoplast, respectively. While it has been proposed that PG contained in the prolamellar body contribute to thylakoid formation during chloroplast biogenesis, this exciting possibility remains to be demonstrated experimentally. A number of lipid components of PG have been identified, but the full PG lipidome awaits elucidation. In comparison, the PG proteome has been extensively described, but numerous PG proteins remain to be characterized. In particular the PG ABC1-like kinases remain of great interest as their regulatory functions may extend beyond lipid metabolism and affect a range of other chloroplast pathways (Lundquist et al. 2013; Martinis et al. 2014). The mechanism for protein recruitment to PG is not totally understood. Regarding FBN distribution between PG and thylakoids, Lundquist et al. have suggested that the intrinsic hydrophobicity and isoelectric point of FBN influence their localization to PG (Lundquist et al. 2012b). Moreover, it was demonstrated that the nearly entire sequence of FBN7a (Vidi et al. 2007) or FBN1a (Shanmugabalaji et al. 2013) is required to target recombinant proteins to PG.

The present research tackles two main topics in PG metabolism. The first subject concerns lipid transport. Lipid remodeling requires molecular communication between PG and thylakoids that with great likelihood implicate their contact sites. The idea of lipid trafficking between the two compartments is supported by the following observations. (1) PG size is highly dynamic, responding to stress and aging and inversely related to the extent of the thylakoid system. (2) Lipid composition of PG reflects that of the thylakoid. (3) PG enzymes produce lipids that function at the thylakoid. Because a large body of evidence supports this idea, we even postulate bidirectional transport. To date, the presumed ability of FBNs to bind and transport small hydrophobic molecules through their lipocalin domain was not experimentally demonstrated. Thus, the exact mechanism of lipid trafficking between PG and thylakoids remains mysterious. Among proteins found in PG proteomes no putative transporter was identified leading us to investigate another option. Previously, the subunit of a putative ABC transporter, NAP14 (Non-intrinsic ABC Protein 14) showed a localization similar to what is observed for PG proteins by confocal microscopy (Shimoni-Shor et al. 2010). Therefore, the first task of this thesis was to characterize NAP14 and its close relative NAP13 to determine whether they may be implicated in lipid transport between PG and thylakoids.

The second part of this work concerns the regulation of carotenoid homeostasis in leaves. First thought to be only lipid storage sites, many studies revealed that PGs actively participate in lipid synthesis and repair by hosting crucial enzymes. For instance, regeneration cycles of tocopherol and plastoquinone were largely resolved and turned out to occur at the PG interface. However, to date very little is known about the turnover of photosynthesis-related carotenoids. Interestingly, three proteomics studies revealed the presence of CCD4 (Carotenoid Cleavage Dioxygenase 4) in PG (Vidi et al. 2006; Ytterberg et al. 2006; Lundquist et al. 2012b). The second goal of this study was to evaluate the implication of PG in carotenoid homeostasis through the characterization of CCD4.

Chapter II

Characterization of chloroplast NON-INTRINSIC ABC PROTEINS 13 and -14 in *Arabidopsis thaliana*

1 Abstract

The ABC family is widespread and diverse. The ABCI subfamily gathers together the most divergent members, each typical domain being encoded by a separate gene. *NAP13* and *-14* encode two predicted nucleotide-binding domains that are targeted to the chloroplast. Suborganellar studies identified NAP13 as extrinsically bound to the chloroplast inner envelope while NAP14 cofractionated with the heaviest membrane fraction, namely the thylakoid membrane. Both mutants showed a highly pleiotropic albino phenotype, underlying the crucial function of NAP13 and -14 in plant metabolism. Mutant leaves showed an astonishing vitrified appearance, which may be explained by the abundant air space resulting from the absence of mesophyll cells. Each albino phenotype was successfully rescued by the introduction of respective cDNA constructs, indicating that the disruption of *NAP13* and *-14* are responsible for the albino phenotypes. Interestingly, *nap13* and *-14* showed a distinct lipid profile when compared with three unrelated albino mutants. The most relevant observation was the reduced level of phosphatidylethanolamine 16:0/18:3 in *nap13* and *-14*. The striking similarities shared by *nap13* and *-14* suggest that the two proteins contribute to the same, but still unknown, functional pathway. Finally, a co-immunoprecipitation assay revealed the interaction between NAP13, NAP14 and ABCI12, an ABC protein harboring a transmembrane domain.

2 Background

About 1.5 billion years ago, a eukaryotic cell engulfed an ancestral cyanobacterium resulting in a tight endosymbiosis. Nowadays, both players, that is to say plant cell and its plastid, are mutually dependent and unable to survive on their own. This functional collaboration requires a highly regulated metabolite exchange between cellular compartments. The substances that cross the plastid membranes in one or the other direction are extremely diverse (Lunn 2007; Mehrshahi et al. 2013; Hurlock et al. 2014). Note that plastids provide plant cell with necessary metabolites and signaling molecules. For instance, chloroplasts fix carbon through photosynthesis (Jensen and Bassham 1966; Black 1973). Plastids are also involved in fatty acid (FA) biosynthesis, nitrogen fixation and isoprenoid biosynthesis (MEP pathway), to cite only a few examples.

In many cases exchange of metabolites requires specialized transporters. The ATP-binding cassette (ABC) superfamily is the largest family of transporters in every kingdom of life. ABC transporters

are generally composed of four domains, two transmembrane domains (TM) and two highly conserved nucleotide-binding domains (NBD) responsible for the ATP binding and hydrolysis. These four domains may be expressed as a single polypeptide (full transporter), two polypeptides (half transporter) or as four polypeptides (prokaryotic-like transporter). The NBD is responsible for the ATPase activity and confers the driving force to translocation. The TM is involved in the channeling process and is also thought to carry substrate recognition sites. Classification of ABC proteins is based on multiple sequence alignment of the highly conserved NBD, transport direction and on functional similarities. In the former ABCISSE (ABC: Information on Sequence, Structure and Evolution) classification, three distinct classes were established, class 1 and 3 represented exporters and importers, respectively, while class 2 gathered soluble ABC proteins not involved in transport. Importers are most frequently constituted of independent polypeptides that form a multimeric complex, whereas for exporters the four domains are fused to a single or two polypeptides (Davidson et al. 2008). Note that, import processes generally required the participation of a protein specialized in substrate binding (BP). In other words, parts of an ABC importer, such as the NBD, the TM and the BP, are encoded by separate genes. Interestingly, in prokaryotes these genes are gathered in the same operon (Dean and Allikmets 1995).

Strikingly, class 3 is widespread in prokaryotes but almost absent from eukaryotic genomes. Two exceptions were recorded, algae and plants, that possess few representative members of class 3. Plant ABC proteins have been extensively reviewed in the past years and to be consistent with the Human ABC community nomenclature (subfamilies A-H), representative members of class 3 were gathered in a new subfamily termed ABCI (Theodoulou 2000; Sanchez-Fernandez et al. 2001; Martinoia et al. 2002; Garcia et al. 2004; Rea 2007; Verrier et al. 2008; Kang et al. 2011; Pang et al. 2013; Roston et al. 2014). Because of their uniqueness in eukaryotes, ABCI proteins are described as bacterial or prokaryotic-like ABC. Each gene encodes a single domain, later assembled into a multi-subunit ABC transporter in most cases (Verrier et al. 2008). Twenty-one ABCI genes have been identified in *A. thaliana* genome. Based on the ABCISSE system, ABCI proteins were tentatively subdivided in 6 groups based on their presumed functional interactions (Garcia et al. 2004) (Table 2.1). However, their phylogenetic relationships have turned out to be impossible to resolve as their divergence is too large (Kang et al. 2011). Classification suffers from the lack of overall homology between NBD, TM and BP. Based on their structural characteristics, NBD-encoding genes were previously grouped under the name of *NON-INTRINSIC ABC PROTEINS*, formerly *NAPs*.

An example of the reconstitution of a complete plant ABC importer through the association of NBD, TM and BP has been well described for the MLK group. The trigalactosyldiacylglycerol (TGD) complex is involved in ER-to-plastid lipid trafficking (Roston et al. 2012). The *tgd* mutants typically accumulate oligogalactoglycerolipids, hence their TGD designation. This putative ABC transporter at the chloroplast inner envelope is composed of a permease TGD1/ABCI14, a small ATPase TGD3/NAP11, as well as multiple BPs (Xu et al. 2003; Xu et al. 2005a; Lu et al. 2007). Two different BPs TGD2/ABCI15 and TGD4 have been shown to bind phosphatidic acid (Awai et al. 2006; Lu and Benning 2009; Wang et al. 2012). Interestingly, bacterial homologs of *TGD1*, *TGD2* and *TGD3* have been found adjacent in operons (Lu et al. 2007).

Another interesting example concerns the NO group. In 2005, Larsen et al. identified ALS3/STAR2, a protein that contains only one TM, as a crucial component of *A. thaliana* tolerance to aluminum

(Larsen et al. 2005). Afterwards, NAP3/STAR1, which displays a single NBD, was also implicated in aluminum tolerance in *A. thaliana* as well as in rice (Huang et al. 2009a; Huang et al. 2010). Coexpression analysis in onion epidermis showed that the very localization of STAR1-GFP depends on the presence of STAR2, suggesting synergy. On the one hand, a mutated version of *star1*-GFP, coexpressed with STAR2, gave a spotty pattern at the plasma membrane with no overlap with STAR2-DsRed signal. Note that this localization was identical to the one observed with the native version of STAR1-GFP expressed alone. On the other hand, STAR1-GFP when coexpressed with STAR2-DsRed gave a diffuse signal at the plasma membrane overlapping with the signal of STAR2. What is more, the authors successfully demonstrated the interaction between STAR1 and -2 by bimolecular fluorescence complementation in vesicles of rice protoplasts as well as by the yeast split-ubiquitin system. Altogether these data clearly testified that the NBD of NAP3/STAR1 interacts with the TM of ALS3/STAR2 to form a putative ABC transporter. Using *Xenopus laevis* oocytes, they also identified UDP-glucose as the substrate transported by the STAR1-STAR2 complex (Huang et al. 2009a). How this transport is involved in aluminum tolerance is unclear, especially since *nap3* and *als3* have also been shown to be highly sensitive to phosphate deprivation (Belal et al. 2015).

Table 2.1 ABC type I subfamily in *Arabidopsis thaliana*.

ABCISSE Group[1]	AGI Code	ABCI Name[2]	NAP Name[3]	Synonym	Domain
CCM	At1g63270	ABCI1	NAP10	ccmA	NBD
	Atmg00110	ABCI2	-	ccmB	TM
	Atmg00900	ABCI3	-	ccmC	TM
	At2g07681	ABCI4	-	ccmC	TM
	At2g07771	ABCI5	-	ccmC	TM
ABCX:ISB	At3g10670	ABCI6	NAP7	SufC	NBD
	At1g32500	ABCI7	NAP6	SufD	CYT
	At4g04770	ABCI8	NAP1	SufB, LAF6	CYT
	At5g44316	ABCI9	-	-	CYT
CBY:Y179	At4g33460	ABCI10	NAP13	-	NBD
	At5g14100	ABCI11	NAP14	-	NBD
	At3g21580	ABCI12	-	-	TM
MKL	At1g65410	ABCI13	NAP11	TGD3	NBD
	At1g19800	ABCI14	-	TGD1	TM
	At3g20320	ABCI15	-	TGD2	BP
NO	At2g37330	ABCI16	-	ALS3, STAR2	TM
	At1g67940	ABCI17	NAP3	STAR1	NBD
	At1g03900	ABCI18	-	-	NBD
ADT	At1g03905	ABCI19	NAP4	-	NBD
	At5g02270	ABCI20	NAP9	-	NBD
	At5g44110	ABCI21	NAP2	POP1	NBD

[1](Garcia et al. 2004), [2](Verrier et al. 2008), [3](Sanchez-Fernandez et al. 2001).
NBD, nucleotide binding domain, TM, transmembrane domain, BP, substrate binding protein, CYT, conserved soluble protein which interacts with ABC domain, CCM, cytochrome C maturation, ISB, iron sulfur center biogenesis family, CBY, family similar to putative cobalt uptake systems, Y179, similar to *M. janaschii* Y179 protein subfamily, MKL, similar to *M. leprae* MKL protein family, NO, proteins of unknown function, ADT, proteins of unknown function, which form a homogenous cluster.

In bacteria, cytochrome c biogenesis involves an ABC transporter composed of CcmA and CcmB (Giegé et al. 2008). In plants, their orthologues NAP10/ABCI1 and ABCI2 represent a NBD and a TM, respectively (Rayapuram et al. 2007). NAP10 was localized at the mitochondrial inner membrane and showed to interact with ABCI2 through a yeast two-hybrid assay. The substrate of this putative ABC transporter is, however, still unknown.

Regarding the other plant ABCI groups (ISB and ADT), no putative TM have been identified to date, which hints at housekeeping functions. NAP1, -6 and -7 are the orthologues of the bacterial SUF system components, that is to say SufB, SufD and SufC, respectively (Nachin et al. 2003; Ahn et al. 2005; Hjorth et al. 2005; Xu et al. 2005b; Xu and Moller 2006; Nagane et al. 2010). The SUF machinery is responsible for the biogenesis and maintenance of iron-sulfur clusters, which are essential cofactors of many enzymes (Takahashi and Tokumoto 2002; Xu and Moller 2008). A scarce amount of information is available on NAP2, -4 and -9. The three of them, when fused with GFP, were found in tobacco and Arabidopsis cytoplasm. NAP2 was proposed to be implicated in cell elongation (Marin et al. 2006).

In ABCISSE system, the class 3 represents BP-dependent importers; however several exceptions have been discovered such as the CBY family which regroups probable BP-independent ABC importers. The CBY family is subdivided in two subfamilies, namely CBU for cobalt and nickel transporters and Y179 for biotin and hydroxymethyl pyrimidine uptake systems (Davidson et al. 2008). In prokaryotes, the CBY:Y179 group represents ABC transporters that are composed of a heterodimeric ATPase and an homodimeric permease (Dassa 2003; Garcia et al. 2004; Zhao et al. 2004). For instance in *Spiroplasma kunkelii*, the putative ABC transporter CbiOOQ is encoded by three genes clustered on a chromosomal locus, *cbiOA-cbiOB-cbiQ*. Theoretically, it results in a transporter with two different NBDs (CbiOA and CbiOB), and two identical TMs (CbiQ) that form the permease. Based on motif analysis, that transporter is predicted to be responsible for cobalt uptake. In contrast to other putative importers, CbiOOQ lacks a substrate binding protein (BP) (Zhao et al. 2004). Similarly in plants, three proteins, ABCI10, -11, -12, constitute the CBY:Y179 family. ABCI10 and -11, also known as NAP13 and -14, are putative small ATPases while ABCI12 is obviously a TM as it contains 5 to 6 membrane-spanning helices (predicted with TMHMM and Aramemnon).

To date, available data on NAP13 and ABCI12 are extremely limited, while the sole study on NAP14 leaves open many questions. NAP14 was proposed to function as a chloroplast iron transporter based on comparisons of *nap14* and *nap11* iron contents (Shimoni-Shor et al. 2010). In this study, NAP11 is used as a " non-metal transporter" control, because C. Benning and coworkers have successfully demonstrated its implication in lipid transport as part of the TGD complex (Lu et al. 2007). Impressively, the *nap14* mutant displayed a severe albino phenotype. But as demonstrated by the authors (Shimoni-Shor et al. 2010) themselves, *nap11* was far from being albino as it grew on soil, produced green well-shaped leaves and showed normal photosynthetic activity. Surprisingly, the possible effect of these phenotypic disparities on iron contents was not considered.

The newly evolved needs for translocation across the plastid envelope membranes due to endosymbiosis together with the ancestral origin of ABCI proteins raise the question whether the CBY:Y179 members have maintained their ancestral roles, or whether they have co-evolved with the

endosymbiont to assume new functions. To answer this fascinating question, each protein as well as its associated mutants have to be carefully studied. In brief, the aim of this study is to characterize NAP13, and to give an insight into its putative function. We also present alternative interpretations and suggest a framework for a future research direction in the functional characterization of NAP14.

3 Results

3.1 Structure of AtNAP13 and AtNAP14 proteins

Non-intrinsic ABC proteins (NAPs) belong to the ATP-binding cassette superfamily (the ABC type I, more specifically), they encode a unique nucleotide-binding domain (NBD) which is most of the time part of a prokaryotic multi-subunit ABC transporter. The NBD is responsible for ATP hydrolysis and thus supplies energy to a variety of cellular processes. Here we describe the characterization of AtNAP13 and AtNAP14 (also known as ABCI10 and ABCI11, respectively). *NAP13* gene is composed of five exons encoding a protein of 271 residues with a predicted molecular mass of 29.6 kDa. On the other hand, *NAP14* is a ten-exon gene predicted to produce a 30.7-kDa protein of 278 residues. Both proteins are predicted to contain a transit peptide sequence of 48 and 49 residues, respectively, at their N-termini (*http://www.cbs.dtu.dk/services/ChloroP/*), thus probably targeting the proteins to the chloroplast. NAP13 and -14 share 26% identity and 42% similarity at the amino acid level according to Needleman-Wunsch global sequence alignment (*http://www.ncbi.nlm.nih.gov/*). Their closest homolog in Arabidopsis is NAP11, also known as TGD3 (Figure 2.1). For multiple alignment purposes, we identified NAP13 and -14 putative orthologs using Phytozome Blast in *Physcomitrella patens* and *Chlamydomonas reinhardtii*.

As depicted in Figure 2.2 their nucleotide-binding domains encompass about 200 residues and are characterized by five to six short motifs (Marchler-Bauer et al. 2015), Walker A/B and the ABC signature being the most important features (Sanchez-Fernandez et al. 2001; Rea 2007; Dassa 2011). The Walker A ($GX_4GK[ST]$) and Walker B ($(hydrophobic)_4[DE]$) are separated by approximately 120 amino acids harboring the Q-loop and the ABC signature motifs. Following the Walker A, the Q-loop consists of a conserved glutamine which is believed to mediate interactions between the ABC subunits (Davidson et al. 2008). Noteworthy, the glutamine residue is not conserved in the ADT group (i.e. AtNAP2, -4, -9). The ABC signature ($[LIVMFY]S[SG]GX_3[RKA][LIVMYA]X[LIVFM][AG]$) known as the LSGGQ motif is unique to ABC ATPases and was shown to closely interact with ATP during hydrolysis (Fetsch and Davidson 2002). Downstream the Walker B, a conserved aspartic acid constitutes the D-loop, while the H-loop contains a highly conserved histidine residue. These six motifs are remarkably conserved in AtNAP13 and -14 as well as in their respective homologs.

Genes from the same pathway tend to cluster on prokaryotic chromosomes forming what is called an operon (Osterman and Overbeek 2003). A gene neighborhood analysis using Stringdb (*http://string-db.org/*) revealed a close spatial relation between ABCI12 and NAP13, as well as between ABCI12 and NAP14 in prokaryotic genomes.

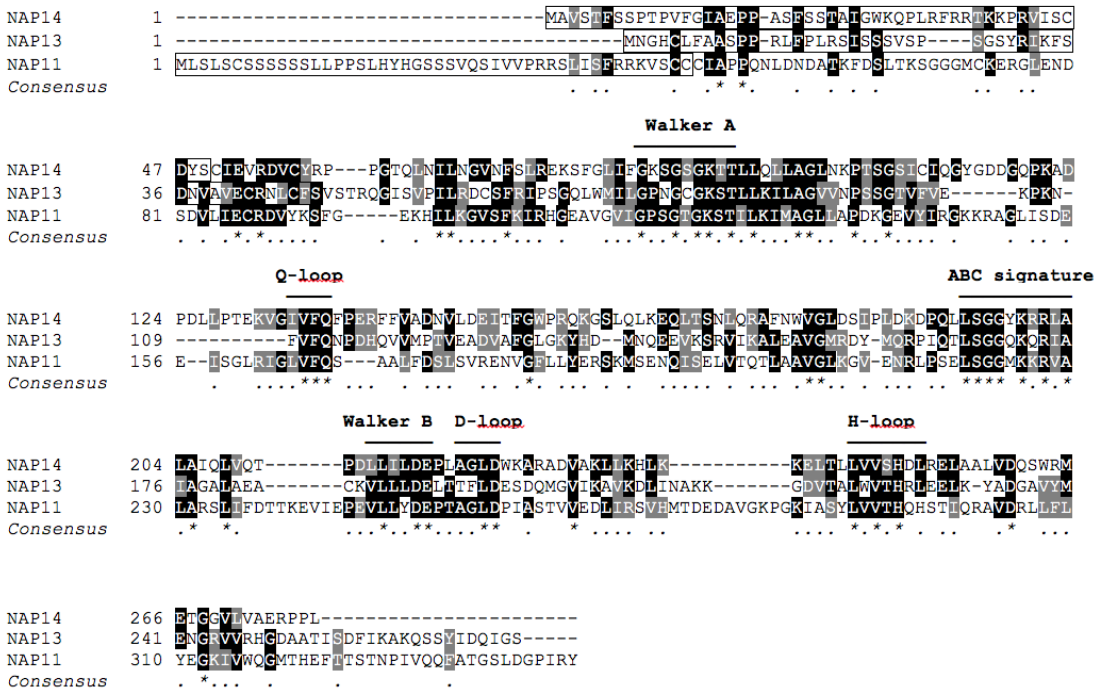

Figure 2.1 Full sequence alignment of AtNAP13, -14 and -11.
A Blast search on Phytozome 10.3 with NAP13 and -14 amino acid sequences identified NAP11 as their closest homolog in *Arabidopsis thaliana*. Multiple residue alignment was generated with ClustalW2 and formatted with BoxShade (threshold fraction of residues set up at 0.5). Conserved motifs are highlighted and predicted transit peptides are framed.

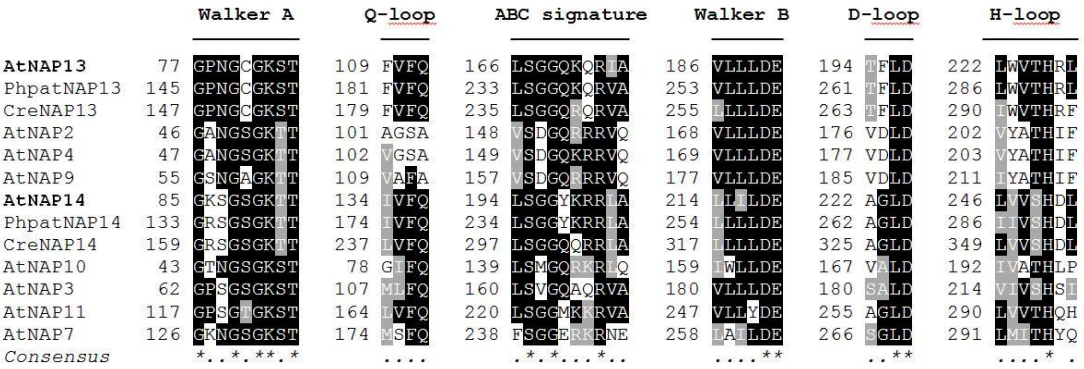

Figure 2.2 Conserved ABC motif alignment.
NAP13 and -14 putative orthologs in *Physcomitrella patens* (Phpat) and *Chlamydomonas reinhardtii* (Cre) were identified using Phytozome 10.3. Accession numbers are as follows. PhpatNAP13 (Phpat.003G116500), PhpatNAP14 (Phpat.003G101400), CreNAP13 (Cre03.g164150) and CreNAP14 (Cre16.g687550). From *Arabidopsis thaliana* (At), members of the ABCI subfamily containing one nucleotide-binding domain (NBD) were selected (see Table 2.1 for AGI code). Multiple residue alignment was generated with ClustalW2 and formatted with BoxShade.

3.2 *nap13* and *nap14* are albino mutants already affected in etioplast development

To characterize the biological function of *NAP13* and *NAP14*, we obtained two Arabidopsis T-DNA insertional mutants from the European Arabidopsis Stock Center (*http://arabidopsis.info/*). *nap13* (Salk_027270) carried a T-DNA insertion in the first exon, while *nap14* (Salk_116866) contained one in the second intron, disrupting the *NAP13* (At4g33460) and *NAP14* (At5g14100) genes respectively (Figure 2.3A). The heterozygous *nap13*/WT and *nap14*/WT mutants were isolated by genotyping-PCR using gene specific primers combined with a T-DNA left border primer. Noteworthy, they were phenotypically indistinguishable from the WT (data not shown). Seeds of heterozygous plants were grown on ½ MS supplemented with 1% sucrose. The heterozygous *nap13*/WT and *nap14*/WT resulted in about 25% albino seedlings, whereas the remaining 75% had a wild type appearance. Albinos were identified as homozygous *nap13* and *nap14* using a PCR-based screening (Figure 2.3B). Without sucrose, *nap13* and *-14* were unable to grow, pointing out the embryo lethality of these mutations. This first observation in combination with the prokaryotic origin of NAPs suggests an essential role of NAP13 and NAP14 in plant metabolism and more specifically in chloroplast development as shown later by microscopy analysis. To verify that the T-DNA insertions in *NAP13* and *NAP14* were responsible for the albino phenotype, we successfully carried out complementation which will be described later. What is more, dark-grown *nap13* and *nap14* seedlings showed early reduced pigmentation when compared with WT pinpointing a defect already in etioplast establishment. To support this idea, we applied the same treatment on *ppi2* which is known to be affected in etioplast development as it contains only a rudimentary prolamellar body (Bauer et al. 2000). Interestingly, *ppi2*, *nap13* and *-14* displayed similar etiolated seedling phenotypes (Figure 2.4). Cotyledons of the etiolated WT seedlings were deeply yellow, probably due to lutein which is the main carotenoid in etioplast (Mysliwa-Kurdziel et al. 2012), whereas those of *ppi2*, *nap13* and *-14* appeared colorless. After exposure to light, some of the albinos showed a visible stress response as they accumulated anthocyanin. It needs to be noted however that the phenomenon did not consistently appear. Note also that anthocyanin biosynthesis may be induced by the sugar present in the medium (Solfanelli et al. 2006). In comparison, WT seedlings synthesized chlorophyll and fully expanded their cotyledons as expected. At maturity *nap13* and *-14* shared a surprisingly similar phenotype. Leaves were misshaped and had a vitrified appearance. Plants never grew larger than 2cm in diameter and were totally incapable of flowering even on a medium supplemented with sucrose.

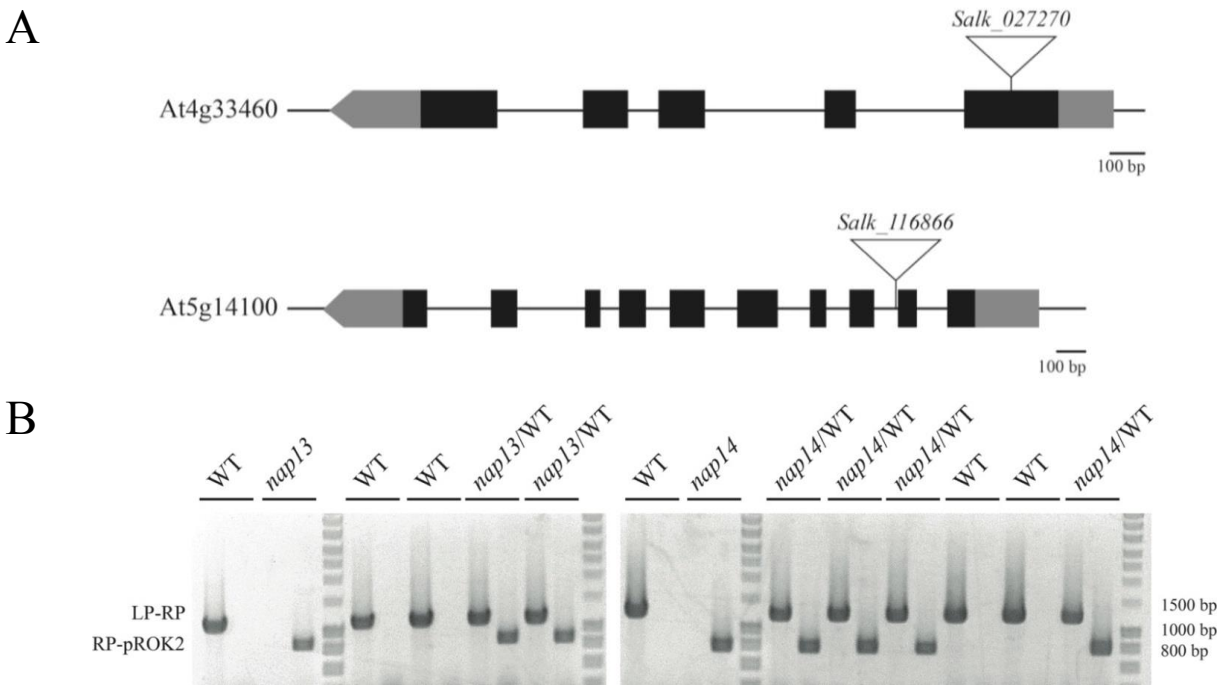

Figure 2.3 Genetic characterization of NAP13 and - 14 T-DNA insertion lines.
(**A**) Gene structures of NAP13 (At4g33460) and NAP14 (At5g14100). Exons (black boxes), UTR regions (grey boxes) and T-DNA insertions (white triangles, not to scale) are shown.
(**B**) Genotyping of Salk_027270 (*nap13*/WT) and Salk_116866 (*nap14*/WT) plant lines. Genomic DNA was extracted and subjected to PCR-based screening. Two primers flanking the T-DNA insertion (termed LP and RP) were used to detect the WT allele. Combination of the RP primer with a T-DNA-specific primer (pROK2) identified alleles harboring the T-DNA insertion. Hence, heterozygous (*nap*/WT) positively responds to both PCRs.

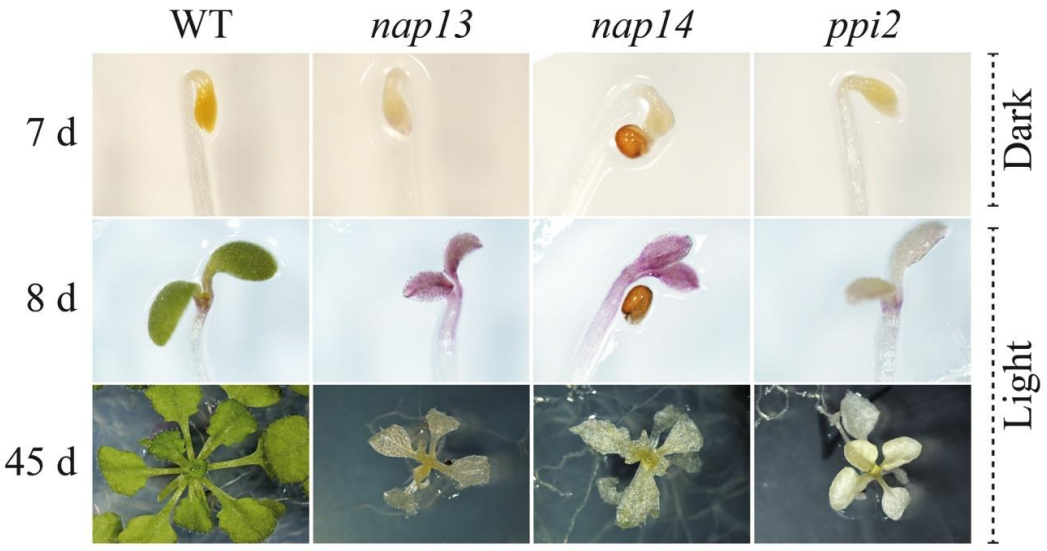

Figure 2.4 Visible phenotype of *nap13* and *-14* in comparison to WT and *ppi2*.
Sterilized seeds were sown on ½ MS supplemented with sucrose and kept in the dark at 4°C for 3 d. To induce germination, 1 h of light was applied at RT. Then, plants were grown for 7 d in darkness (first line). Etiolated seedlings were transferred to light and observed at 8 d (second line) and 45 d (third line).

3.3 *nap13* and *nap14* are complemented by NAP13- and NAP14- derived cDNA constructs, respectively

To verify that the T-DNA insertions in *NAP13* and *NAP14* were responsible for the albino phenotypes, we introduced tagged-cDNAs for *NAP13* or *NAP14* under the control of a constitutive CaMV 35S promoter into *nap13* and *nap14* mutants, respectively. To ensure that the function of NAP13 or NAP14 was not affected by the fusion, two different C-terminal tags were tested. On the one hand, we used a 21-kDa-tag adapted for the tandem affinity purification (TAP), which is composed of a calmodulin-binding peptide (CBP), a TEV-cleavage site followed by two IgG-binding domains (abbreviated 35S:NAP-TAP for complemented plants and NAP-TAP for proteins). On the other hand, we worked with the yellow fluorescent protein (YFP) fused to the human influenza hemagglutinin epitope (HA) which makes up a tag of about 30 kDa (abbreviated 35S:NAP-YFP for complemented plants and NAP-YFP for proteins). The constructs thus obtained and harboring a glufosinate resistance were introduced into the respective heterozygous knockout plants by *Agrobacterium*-mediated stable transformation. Progeny was selected on glufosinate and carefully screened by PCR to isolate individual plants homozygous for the T-DNA insertion knockout (Figure 2.5A). Nine independent transgenic plants were shown to be in the homozygous *nap13* background, one of them carried the NAP13-TAP construct and 8 harbored the NAP13-YFP construct. Moreover, we identified a total of 12 independent transgenic plants in the *nap14* background, among them 3 carried the NAP14-TAP construct while the remaining 9 were transformed with NAP14-YFP. Impressively, these twenty-one plants all displayed a normal phenotype indistinguishable from the WT despite their knockout backgrounds (Figure 2.5B). Seeds from the following generation were harvested and subjected to segregation analysis on glufosinate which allowed the selection of 10 lines carrying a single insertion of the transgene (3:1, glufosinate resistant to glufosinate sensitive). Immunoblotting was carried out to evaluate the expression level of the recombinant proteins in the different lines (Figure 2.5B). Expressing lines were selected for each construct. Plants homozygous for the transgene were further identified by segregation (100:0, glufosinate resistant to glufosinate sensitive) of their own progeny. We isolated 2, 3, 3 and 4 homozygous plants for NAP13-TAP, NAP13-YFP, NAP14-TAP and NAP14-YFP, respectively. To locate the insertion of the transgene, CTAB extraction of gDNA followed by TAIL-PCR was carried out. Fortunately, 3 lines harbored an insertion in a non-coding region of *A. thaliana* genome. NAP13-TAP was inserted on the chromosome 1 between At1g28180 and At1g28190. NAP14-TAP occurred on chromosome 2 between At2g23670 and At2g23660 and NAP14-YFP was found between At2g46300 and At2g46308. We were not able to locate the NAP13-YFP construct.

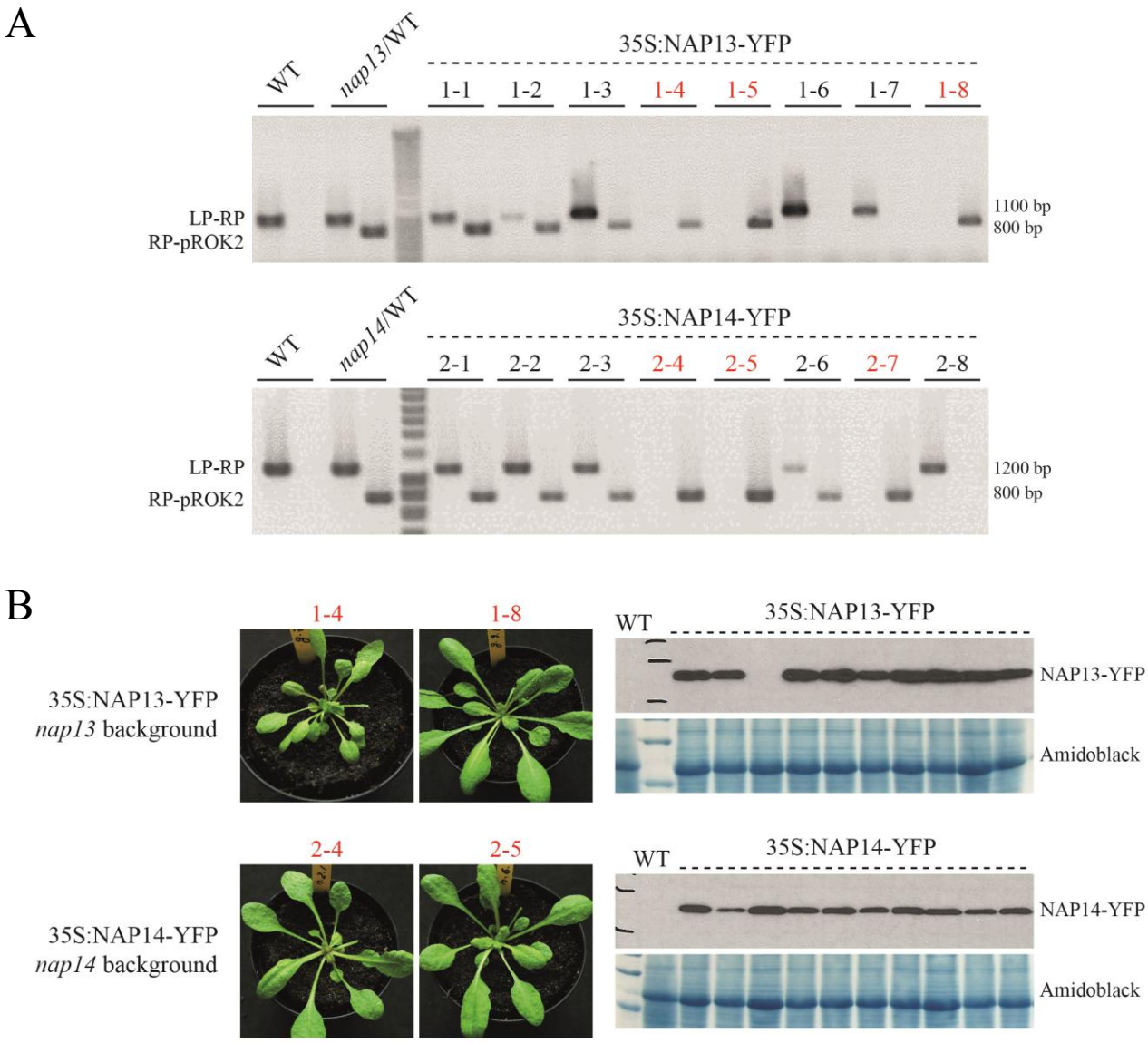

Figure 2.5 Mutant complementation using 35S:NAP13- and NAP14-YFP-HA.
Heterozygous *nap13*/WT and *nap14*/WT plants were respectively transformed with 35S:NAP13-YFP and 35S:NAP14-YFP constructs carrying a phosphinothricin marker. Resulting transgenic plants were always selected on phosphinothricin to eliminate untransformed plants.
(**A**) Representative PCRs for background determination are shown. Several independent T1 plants were subjected to gDNA extraction. Two primer sets, namely LP-RP and RP-pROK2, were used to detect either the WT allele or the disrupted allele for both genes. Homozygous knockouts carrying the YFP-HA constructs are highlighted in red.
(**B**) *nap13* and *-14* are visibly complemented by the corresponding YFP-HA fusion (left panel). Proteins were extracted from their T2 progeny and the expression of the recombinant protein was detected by immunoblotting with anti-HA-HRP (right panel).

3.4 Leaf organization and plastid ultrastructure are affected in *nap13* and *nap14*

As albinism is always associated with defective plastids and because the leaf transparency of *nap13* and -*14* was surprising, microscopic analyses were carried out. Leaf tissues of 1-month-old WT, *nap13* and -*14* plants were embedded in Spurr resin. On the one hand, samples were stained with toluidine blue and observed by light microscopy to define leaf macro-organization (Figure 2.6A). Epidermal cells of *nap13* and -*14* appeared 2- to 3-fold enlarged when compared to the WT. In addition, their inconsistent shape drew an irregular epidermal line, which resulted in highly variable leaf thickness (ranging from 60 to 230 µm). Surprisingly, mesophyll cells were mostly absent resulting in increased air space which may explain the vitrified appearance of *nap13* and -*14* leaves. Unlike the WT, palisade and spongy parenchyma were indistinguishable but vascular tissue was still present. On the other hand, transmission electron microscopy was carried out on contrasted samples to analyze plastid ultrastructure (Figure 2.6B). In *nap13* and -*14* cells, only putative plastid vestiges were observed. A disorganized network of thylakoid membranes and some high density globules were recorded in *nap13*. In *nap14*, only high density globules as exemplified in Figure 2.6B were observed. However in another study, incoherent membrane assemblies were also seen in *nap14* (Shimoni-Shor et al. 2010).

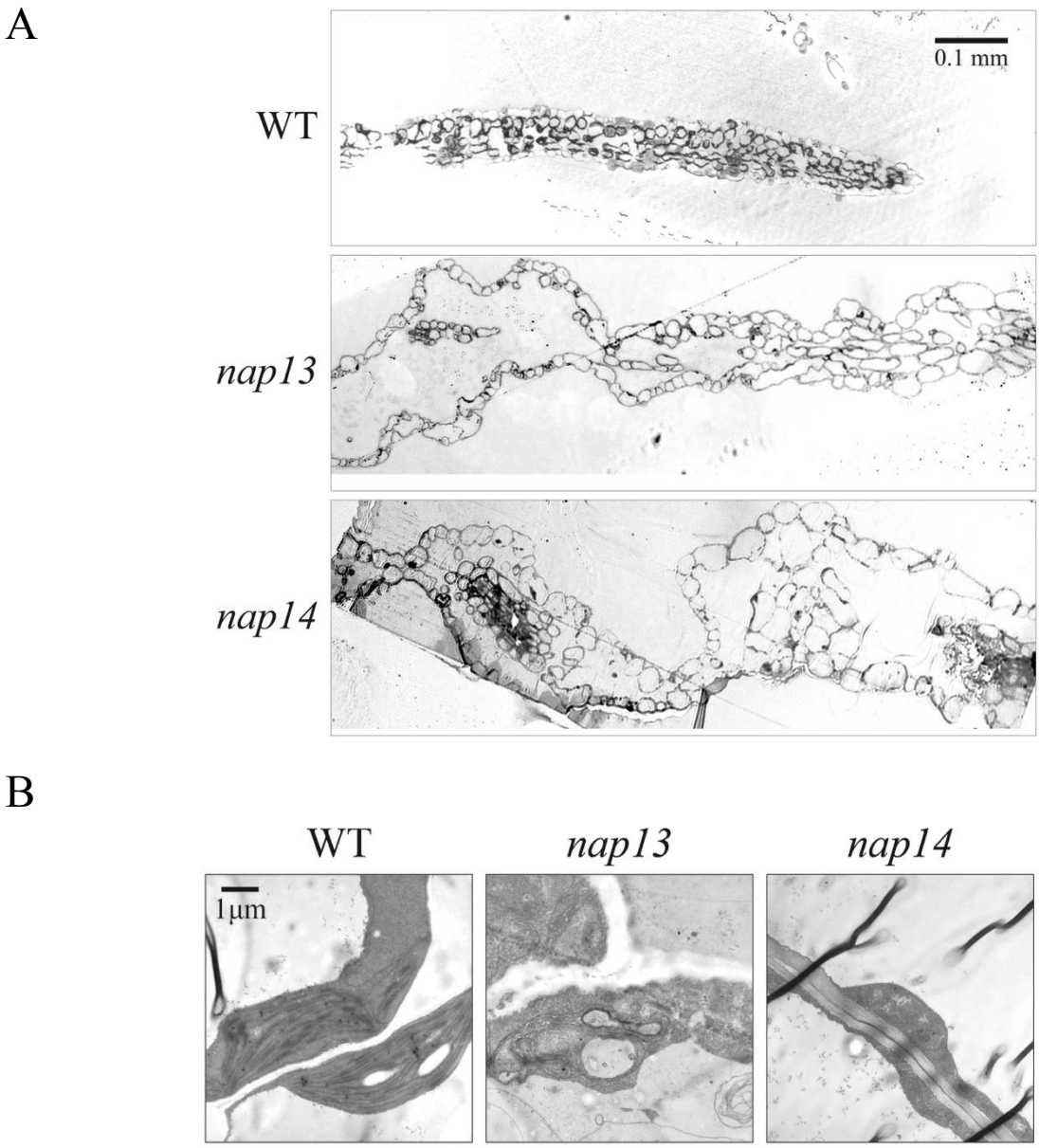

Figure 2.6 Leaf ultrastructure of *nap13* and -*14* compared to WT.
Small pieces of leaf were cut from one-month-old plants, fixed in formaldehyde and glutaraldehyde, post-fixed in osmium tetroxide and embedded in Spurr epoxy resin. Semithin (750 nm) and ultrathin (80 nm) sections were cut with a microtome.
(**A**) Light micrographs of leaf semithin sections stained with toluidine blue. In WT, mesophyll was differentiated into palisade and spongy parenchyma and surrounded by a well-defined epidermis which drew a regular and straight line. In *nap13* and -*14*, epidermal cells were 2 to 3 times larger, irregular oval shaped and drawing an irregular line which resulted in highly variable leaf thickness. The mesophyll displayed very low cell density lacking differentiation between palisade and spongy parenchyma. Vascular tissues appeared conserved.
(**B**) Transmission electron micrographs of leaf ultrathin sections contrasted with uranyl acetate and Reynolds lead solution. Two WT chloroplasts containing starch grains, thylakoid membranes and plastoglobules are shown in the first panel. Only putative plastid vestiges were observed in *nap13* and -*14* cells. A disorganized network of thylakoid membranes and some high density globules were recorded in *nap13*.

3.5 Lipid profiling of *nap13* and *nap14* reveals perturbation in phosphatidylethanolamine species

The albino phenotypes of the mutants indicate that NAP13 and -14 are essential. Unfortunately this highly pleiotropic phenotype turned out to be a major obstacle to unravel the respective functions of NAP13 and -14. To overcome this problem, we decided to compare *nap13* and *-14* to three unrelated albino mutants: the *pac* mutant presumably lacking PAC (At2g48120) a protein involved in mRNA maturation (Reiter et al. 1994; Grevelding et al. 1996; Meurer et al. 1998; Holding et al. 2000), the *cla1* mutant lacking the 1-deoxyxylulose 5-phosphate (DXP) synthase (At4g15560) responsible for the first step in isoprenoid biosynthesis through the MEP pathway (Mandel et al. 1996; Estévez et al. 2000; Crowell et al. 2003) and the *ppi2* mutant lacking Toc159 (At4g02510) a major component of the chloroplast protein import machinery (Bauer et al. 2000; Asano et al. 2004).

Based on their similarity with NAP11 (well known as TGD3), we hypothesize that NAP13 and -14 are involved in a lipid transport. This hypothesis was addressed by an untargeted comparative lipid analysis. Therefore, leaf lipid extracts from the three aforementioned albino mutants as well as WT, *nap13* and *-14* were analyzed by UHPLC-QTOFMS and compared by a PCA (Figure 2.7A). The overall lipid compositions of *nap13* and *-14* were surprisingly similar as they formed a distinct cluster from the other albino mutants. Despite their divergent phenotypes (Figure 2.7B), *cla1*, *ppi2* and *pac* were gathered in the upper right quadrant at the opposite of *nap13* and *-14* which were coming up in the lower one, the principal component 2 explaining 23.3% of this vertical variance. As expected, the main difference was recorded between WT and albinos nevertheless, and is explained at 59.9% by the principal component 1.

To further understand the distinct lipid composition of *nap13* and *-14*, the outlying PCA loadings were identified as far as possible (Figure 2.7C). Polar lipids and prenylquinones mostly contributed to the separation of the three groups (*nap13+nap14*, *pac+ppi2+cla1*, WT). The separation of WT from the albinos was mainly based on the presence of galactolipids (MGDG and DGDG), crucial components of the thylakoid membrane. Among albinos, the main variability was attributed to a phospholipid, namely phosphatidylethanolamine (PE) 18:3/16:0 nearly absent in *nap13* and *-14*. Note that the detection of other phospholipids was not possible with the method used here. Interestingly, PE species were vertically separated. Regarding their fatty acid composition, PE with palmitic acid (16:0) came up in the upper right quadrant with *ppi2*, *cla1* and *pac*. PE with two C18 chains gathered in the lower right part of the PCA loading plot. Another interesting point was a shift in MGDG molecular species, 18:3/16:3 being higher and 18:3/18:3 being lower in *nap13* and *-14* than in other albinos. Despite the lack of replicas in our lipidomic study, it is important to note that we were able to reproduce the drop in PE and the shift in MGDG by an independent analysis using only *ppi2* as control thus strengthening our observations (data not shown).

As our complemented lines were under the control of a 35S promoter, an overexpression phenotype was to be expected. Therefore, an untargeted lipid profiling was also carried out on the four complemented lines carrying either NAP13 or NAP14 fused with YFP or TAP tag. Their overall lipid content was compared with the lipid composition of WT by a multivariate analysis in triplicate (PCA). No statistical differences were recorded between the complemented lines and WT plants,

thus no overexpression phenotype was observed (data not shown). One possible interpretation is that NAP13 or -14 alone are not sufficient and that the synergistic expression of multiple proteins may be required to enhance their metabolic function. As described in literature and based on comparison with prokaryotic ABC transporters, it likely that the NBDs encoded by *NAP13* and *-14* are part of one (or two) ABC transporter(s) together with proteins representing TM and BP. Such TM and BP may be limiting NAP13 and NAP14 function.

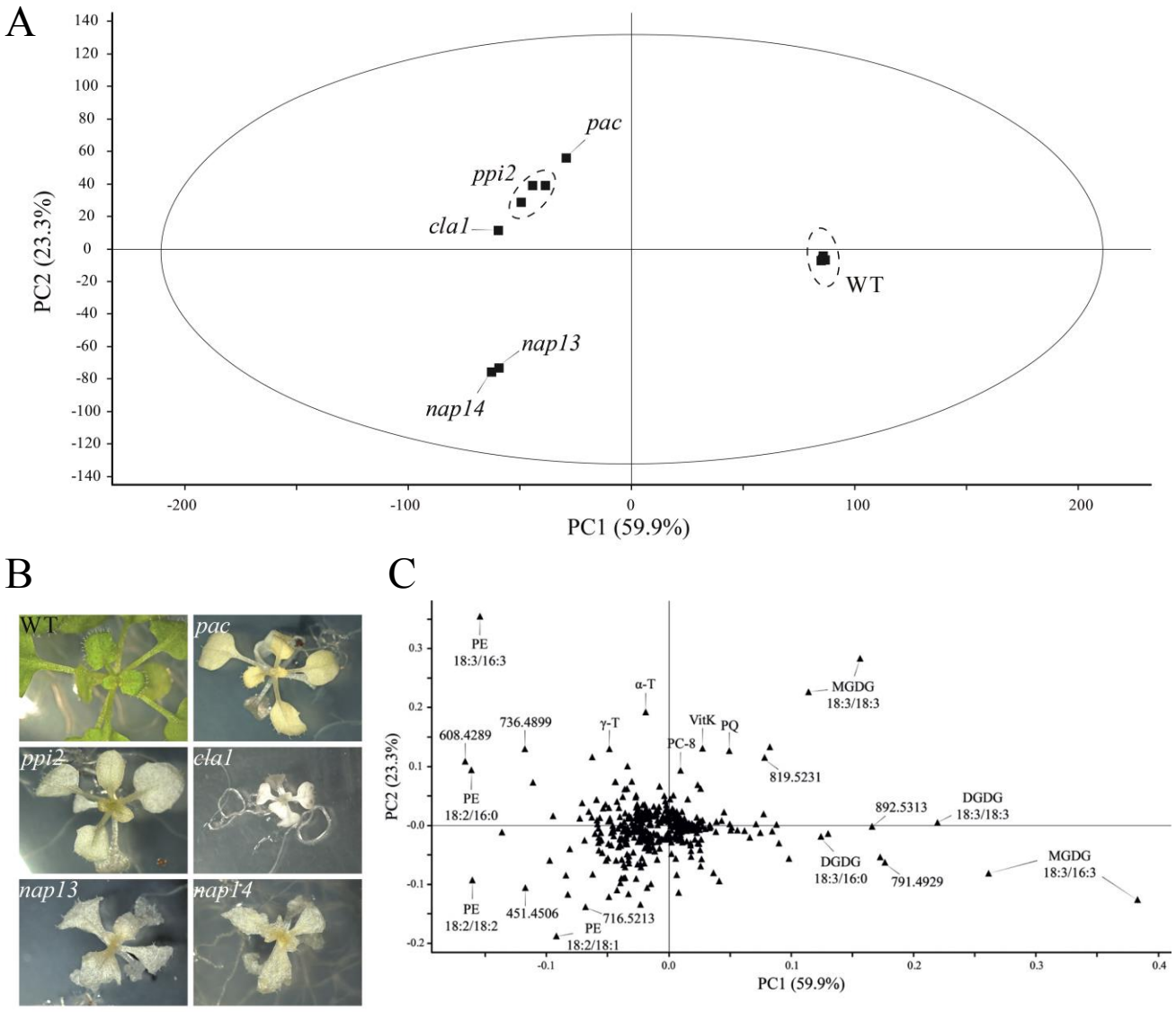

Figure 2.7 See caption on next page

.

Figure 2.7 Untargeted lipid profiling of *nap13* and *-14* compared with WT and unrelated albino mutant lines.
A mixture of plantlets, grown for 6 weeks on ½ MS supplemented with sucrose, were harvested to reach between 20 and 50 mg of FW and immediately frozen in liquid nitrogen. Aerial tissues were mechanically homogenized and lipids were extracted using five volumes of THF. Extracts were analyzed by HPLC-MS and raw data were processed for automatic peak detection with Markerlynx XS™. Normalized and pareto-scaled variables were then subjected to principal component analysis.
(**A**) Score plot showing the clustering of *nap13* and *-14* at the opposite of other albinos (*cla1*, *ppi2* and *pac*). As expected, the extremely large variance between WT and albinos is explained at 59.9 % by the first component. Unexpectedly, albino lines were subdivided in two groups opposing *nap13* and *-14* to *cla1*, *ppi2* and *pac*. The second component explains 23.3 % of this difference.
(**B**) Representative specimens were photographed at a comparable magnification before harvesting. *CLA1* encodes the DXP synthase of the MEP pathway and is essential for chloroplast development. *PAC*, encoding a chloroplast-targeted protein, is thought to be involved in mRNA maturation. *ppi2* lacks a major component of the chloroplast protein import machinery, Toc159.
(**C**) Loading plot showing the main compounds responsible for the separation between genotypes. Galactolipids (MGDG and DGDG) are accumulated in WT explaining the major difference between WT and albinos. Among albinos, the phospholipid phosphatidylethanolamine (PE) appears to explain the discrimination between *nap13/ -14* and others albinos (*cla1*, *ppi2* and *pac*).

3.6 NAP13 is an extrinsic membrane protein localized at the chloroplast envelope

NAP13 has a predicted chloroplast transit peptide of 48 residues. To verify the chloroplast localization of NAP13, its cDNA was introduced in the vector p0GWA containing a T7 promoter and an in frame hexahistidinyl tag. Then, NAP13-6xHIS was *in vitro* translated in presence of [^{35}S] methionine. The radiolabeled-protein was incubated with isolated pea chloroplasts for 15 min. The thermolysin protease, which digests cytosol-exposed proteins, was used to eliminate non-imported preprotein after the incubation. In an attempt to sublocalize NAP13-6xHIS, chloroplasts were fractionated into stroma and membranes. The protein originally detected at 32 kDa (pNAP13) appeared at about 20 kDa after 15 min of incubation (Figure 2.8A). The loss of approximately 12 kDa includes the removal of the transit peptide by the stromal processing protease (SPP). Surprisingly, the cleaved sequence estimated around 100 residues is approximately 2-time longer than the transit peptide predicted by ChloroP (48 residues). Thermolysin treatment after the import assay resulted in the degradation of the pNAP13 preprotein, while the mature form was resistant. After fractionation, the latter was found in the stromal fraction. These results demonstrate that NAP13 is imported and processed inside the chloroplast.

Chloroplast large-scale proteomic studies identified NAP13 at the chloroplast envelope membrane (Froehlich et al. 2003; Ferro et al. 2010; Huang et al. 2013). To visualize the suborganellar location of NAP13, protoplasts from the complemented 35S:NAP13-YFP line were isolated and observed by confocal microscopy (Figure 2.8B). The yellow fluorescent protein fused with NAP13 resulted in a widespread signal inside the chloroplast, although slightly more concentrated at the chloroplast periphery, close to the envelope membrane. The overlap with the thylakoid marker, namely chlorophyll that emits red autofluorescence, was not perfect and starch grains appeared free of fluorescent signals suggesting a dominant stromal location for NAP13-YFP. As a predicted non-intrinsic membrane protein, it is not surprising to detect a free form of NAP13 in the stroma,

especially in NAP13 overexpressing plants where membrane-binding sites are potentially saturable. All together, these results confirm the chloroplast localization of NAP13 and suggest dual suborganellar localization of NAP13-YFP in transgenic plants.

To further narrow down the location of NAP13, chloroplasts from 35S:NAP13-YFP plants were isolated. Broken chloroplasts were separated into membranes and stroma by centrifugation at 100'000×g. Isolated and homogenized membranes were then separated according to their density on a discontinuous sucrose-gradient. Depending on their lipid to protein ratios, chloroplast membrane fractions have either a high density (thylakoids), an intermediate (envelopes) or a low density (plastoglobules). Fractions of 200 µL were separately collected from the top to the bottom of the gradient. Proteins contained in each fraction were analyzed by SDS-PAGE and blotted onto a nitrocellulose membrane (Figure 2.9A). The distribution of NAP13-YFP, as well as typical membrane markers, in chloroplast membrane fractions was established by immunoblotting (Figure 2.9B). Antibodies against the LHCBII protein gave signals that strongly increased from fractions 7 to 24, indicating the presence of thylakoid membranes in fractions of higher density. The FBN1a protein was detected across the entire gradient, however with weaker signals in fractions 7-10, showing the typical plastoglobule pattern (Vidi et al. 2006; Eugeni Piller et al. 2011). The presence of TOC75, a marker protein of the outer envelope membrane, in fraction 7-20 was consistent with the intermediate density of chloroplast envelopes. Similarly, the inner envelope membrane protein TIC40 was detected in fractions 8-17. Interestingly, NAP13-YFP was detected in fractions 9-20. Note that NAP13-YFP also gave strong signal in the stromal fraction (data not shown), which is in accordance with our previous observations by confocal microscopy. To sum up, NAP13-YFP is mainly accumulated in the stroma but a small fraction was demonstrated to specifically cofractionate with envelope membrane markers TOC75 and TIC40.

It remains to experimentally demonstrate that NAP13 interacts with the envelope membranes as a non-intrinsic protein thus explaining its dual localization. Leaves of the 35S:NAP13-TAP transgenic line were mechanically homogenized. Soluble and membrane fractions were then separated by centrifugation at 100'000×g. Membrane-containing fractions were treated with five different extraction buffers to determine the nature of the NAP13-TAP membrane interaction. Sodium chloride is known to break weak ionic interactions, alkaline carbonate is stronger than NaCl and solubilizes extrinsically bound proteins, while increasing concentrations of the nonionic detergent Triton X-100 disrupts lipid organization and allows the solubilization of integral membrane proteins. After the treatment, solubilized and unsolubilized proteins were separated by centrifugation at 100'000×g and analyzed by SDS-PAGE and immunoblotting (Figure 2.10A). The integral membrane protein LHCBII was insensitive to NaCl and carbonate treatments. But as expected, LHCBII was increasingly solubilized by 0.1, 0.5 and 1% Triton X-100, confirming its integral membrane topology. For NAP13-TAP complete solubilization by carbonate treatment was recorded, strongly supporting the predicted extrinsic membrane character of NAP13. Nonetheless, sodium chloride was unable to solubilize NAP13-TAP, probably because the treatment is too gentle. NAP13-TAP was completely soluble upon 0.1 and 0.5% Triton X-100 treatments.

3.7 NAP14 might be an extrinsic membrane protein at the thylakoid membrane

To resolve the localization of NAP14, the same experimental strategy as used for NAP13 was applied. Pea chloroplast import of NAP14-6xHIS identified a preprotein at about 40 kDa and a processed thermolysin-resistant form at 31 kDa after 15 min of incubation (Figure 2.8A). The size reduction of 9 kDa corresponds to the cleavage of the chloroplast transit peptide. After fractionation, the mature form was detected in the stromal fraction. These results show that NAP14 is imported and processed inside the chloroplast.

Protoplasts expressing NAP14-YFP were observed by confocal microscopy to obtain an overview of NAP14 subcellular localization. In that case, the yellow fluorescent protein gave multiple intense punctuate signals inside the chloroplast (Figure 2.8B). It is noteworthy that this result is in accordance with a previous study (Shimoni-Shor et al. 2010), in that study, however, only one spot was observed per chloroplast. Remarkably this pattern of suborganellar distribution is also characteristic of plastoglobule localization (Vidi et al. 2006; Eugeni Piller et al. 2011).

To determine whether NAP14 is associated with plastoglobules, we carried out chloroplast membrane fractionation using 35S:NAP14-YFP plants. As for NAP13-YFP, membrane markers were used to identify the position of each membrane-type in the sucrose gradient (Figure 2.9C). Antibodies against TIC40 detected inner envelope membranes in fractions 8-19. The FBN1a protein showed the typical profile for plastoglobule proteins with strong signals in the first fractions (1-6), low signals in the intermediate fractions (7-12) and again strong signals in last fractions (13-24). However, NAP14-YFP was detected in fractions 10-24 with increasing intensity. Similarly, the thylakoid marker LHCBII gave strong signals in fractions 7-24. These results suggest that NAP14 is rather associated with thylakoid membrane than plastoglobules. However, it hardly explains why NAP14-YFP fluorescence was concentrated in foci. A sparse and specialized region of the thylakoid membrane is to be suspected. Interestingly, NAP14-YFP also gave a strong signal in the stroma (data not shown) suggesting that membrane-bound and free soluble forms coexist as was observed in the case of NAP13-YFP.

The nature of the interaction occurring between NAP14 and the thylakoid membrane was established by solubilization assays on isolated chloroplasts from 35S:NAP14-TAP plants (Figure 2.10B). First, stroma and membranes were separated and designated as soluble and insoluble fractions respectively. Note that NAP14-TAP was mostly found in the soluble part, while the plastoglobule protein FBN1a was more concentrated in the membrane fraction. Insoluble proteins were then tentatively solubilized using one of the following buffers: 1 M NaCl, 0.2 M Na_2CO_3, 0.1%, 0.5% or 1% Triton X-100. The treatment with sodium chloride did not release NAP14-TAP, while FBN1a was just barely detectable. The release of NAP14-TAP and FBN1a by carbonate extraction was incomplete. All FBN1a was solubilized with only 0.1% Triton X-100, whereas NAP14-TAP showed a partial resistance even to 1% Triton X-100. These results suggest that three forms of NAP14-TAP may coexist. A large part of NAP14-TAP is soluble and is probably present in the stroma. This other part is insoluble and cofractionates with membranes. In this insoluble fraction, two forms of NAP14-TAP appear to occur. On the one hand, a limited proportion is extrinsically bound to membranes as it was released by carbonate treatment. On the other hand, a larger proportion of NAP14-TAP was not solubilized by Triton X-100, which suggests its inclusion in aggregates.

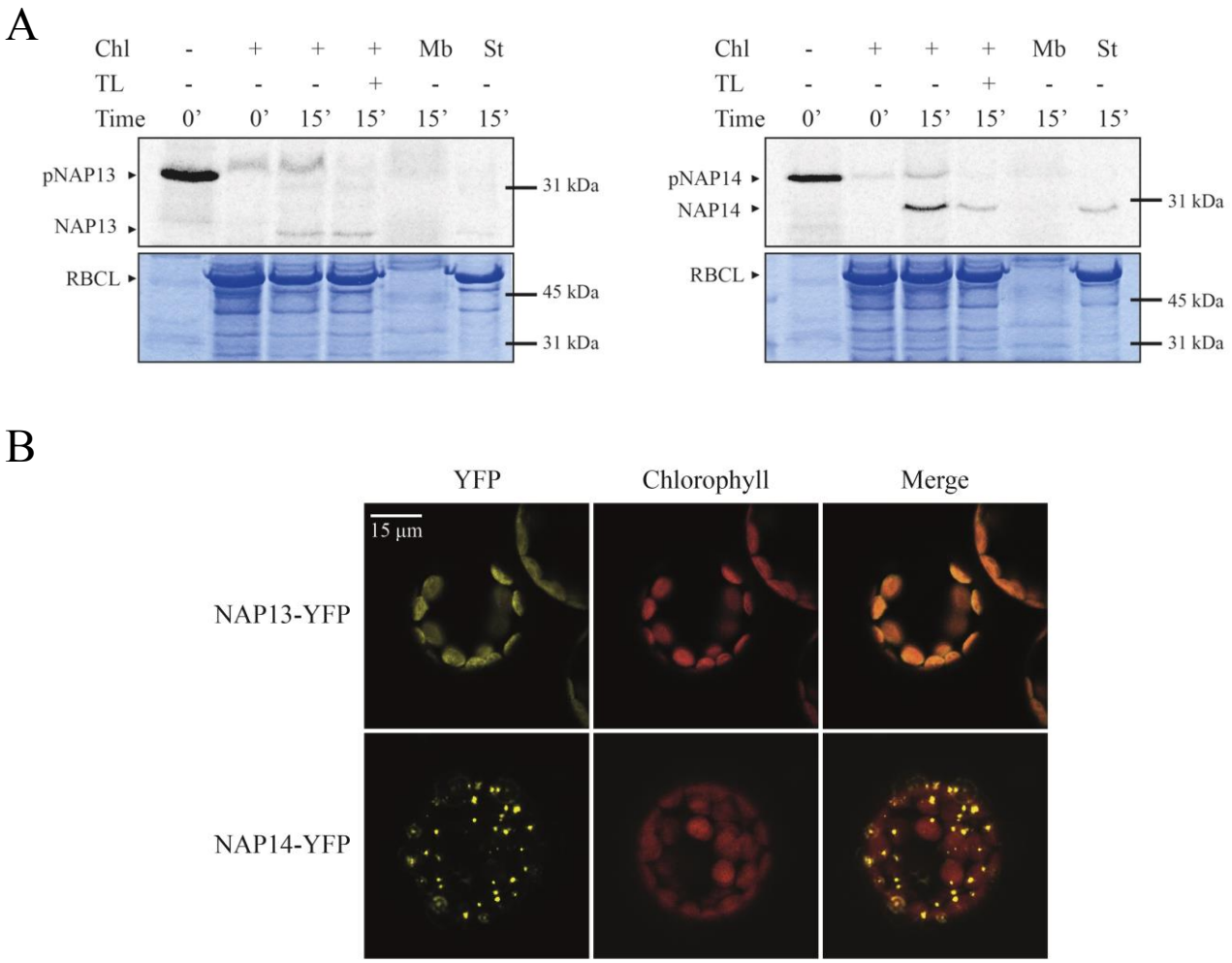

Figure 2.8 Chloroplast localization of NAP13 and -14 recombinant proteins.
(**A**) Chloroplast import assay. NAP13-6xHIS and NAP14-6xHIS were *in vitro* transcribed and translated in the presence of ^{35}S methionine (first lanes) and incubated with 20 µg (chlorophyll equivalent) of isolated and intact pea chloroplasts (Chl) in each import experiment. Incubation was at 25°C for 0 and 15 min. Chloroplasts at 15 min were either treated with thermolysin (TL) to digest non-imported proteins or broken by osmotic shock and fractionated into stroma (St) and membranes (Mb) by centrifugation at 16'000×g. For analysis, overall proteins were chloroform-methanol precipitated, separated by SDS-PAGE and stained with Coomassie blue (bottom panel). Autoradiograms of protein gels exposed to Phosphorimager plates are shown (upper panel). p, preprotein; RBCL, RuBisCO large subunit.
(**B**) Protoplasts isolated from *A. thaliana* complemented with 35S:NAP13-YFP or 35S:NAP14-YFP were analyzed by confocal laser microscopy (left hand panel). Chloroplasts are visualized by the chlorophyll autofluorescence (center panel). The merged image shows the superposition of YFP and chlorophyll (right hand panel).

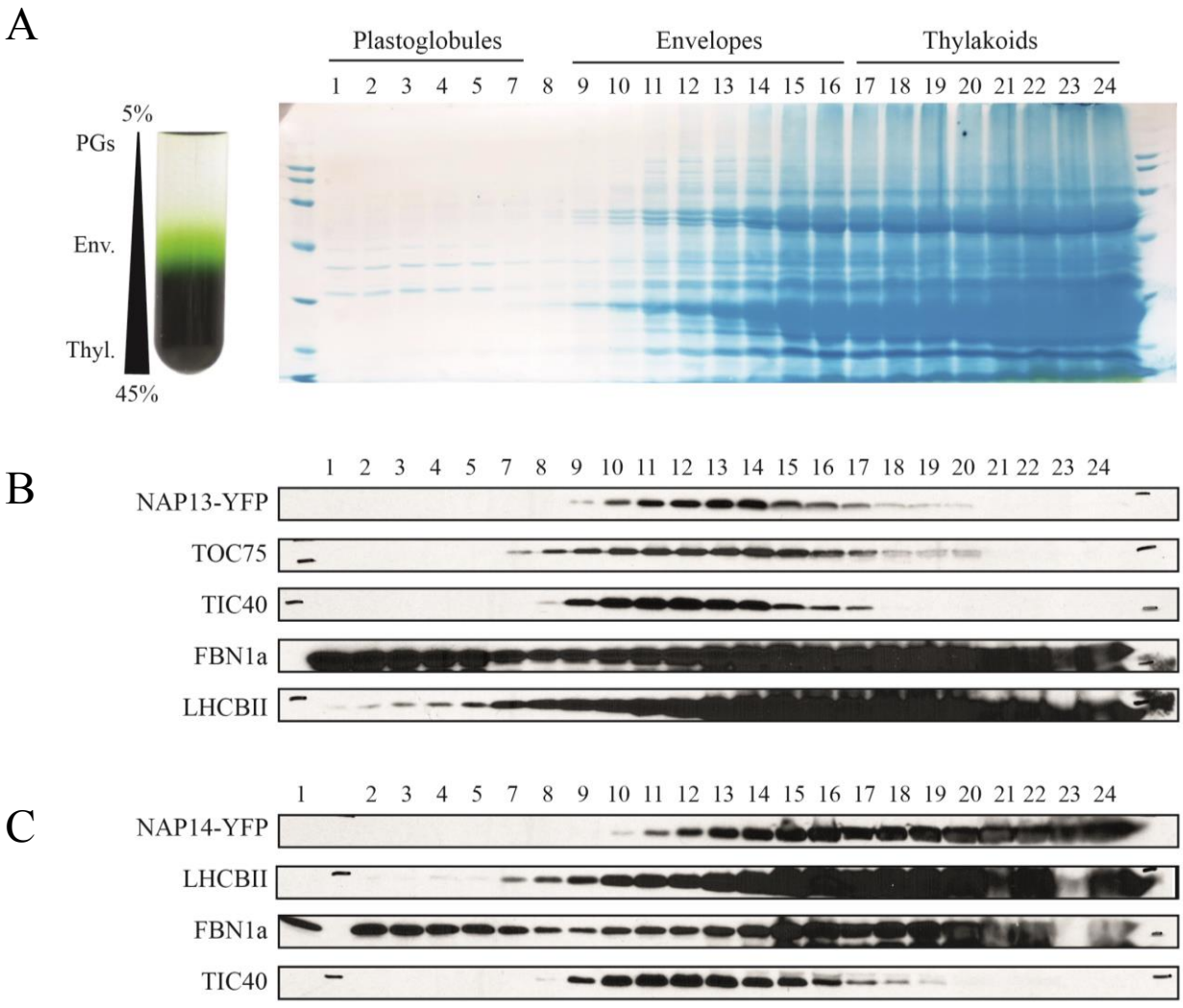

Figure 2.9 Localization of NAP13- and NAP14-YFP-HA by chloroplast membrane fractionation
(**A**) Separation of chloroplast membranes by sucrose-gradient flotation (left hand panel). Fractions of 200 µL were sequentially retrieved from the gradient to analyze their protein contents. After extraction and separation by SDS-PAGE, proteins were stained with Amidoblack (right hand panel). Fractions 1-7 correspond to low-density plastoglobules, intermediate fractions 9-16 contain envelope membranes while high-density thylakoid membranes accumulate at the bottom of the gradient (fractions 17-14). The representative separation of chloroplast membranes from 35S:NAP13-YFP plants is shown.
(**B**) Cofractionation of NAP13-YFP with envelope markers. The blot presented in (**A**) was probed with anti-TOC75 (outer envelopes), anti-TIC40 (inner envelopes), anti-FBN1a (plastoglobules) and anti-LHCBII (thylakoids) to determine membranes distribution. The anti-HA-HRP antibody was used to detect NAP13-YFP by its C-terminal HA tag.
(**C**) Cofractionation of NAP14-YFP with the thylakoid membrane marker. Chloroplast membrane separation was carried out as described in (**A**) but with 35S:NAP14-YFP plants. The resulting blot was probed with anti-LHCBII (thylakoids), anti-FBN1a (plastoglobules), anti-TIC40 (inner envelopes) and anti-HA-HRP (NAP14-YFP-HA).

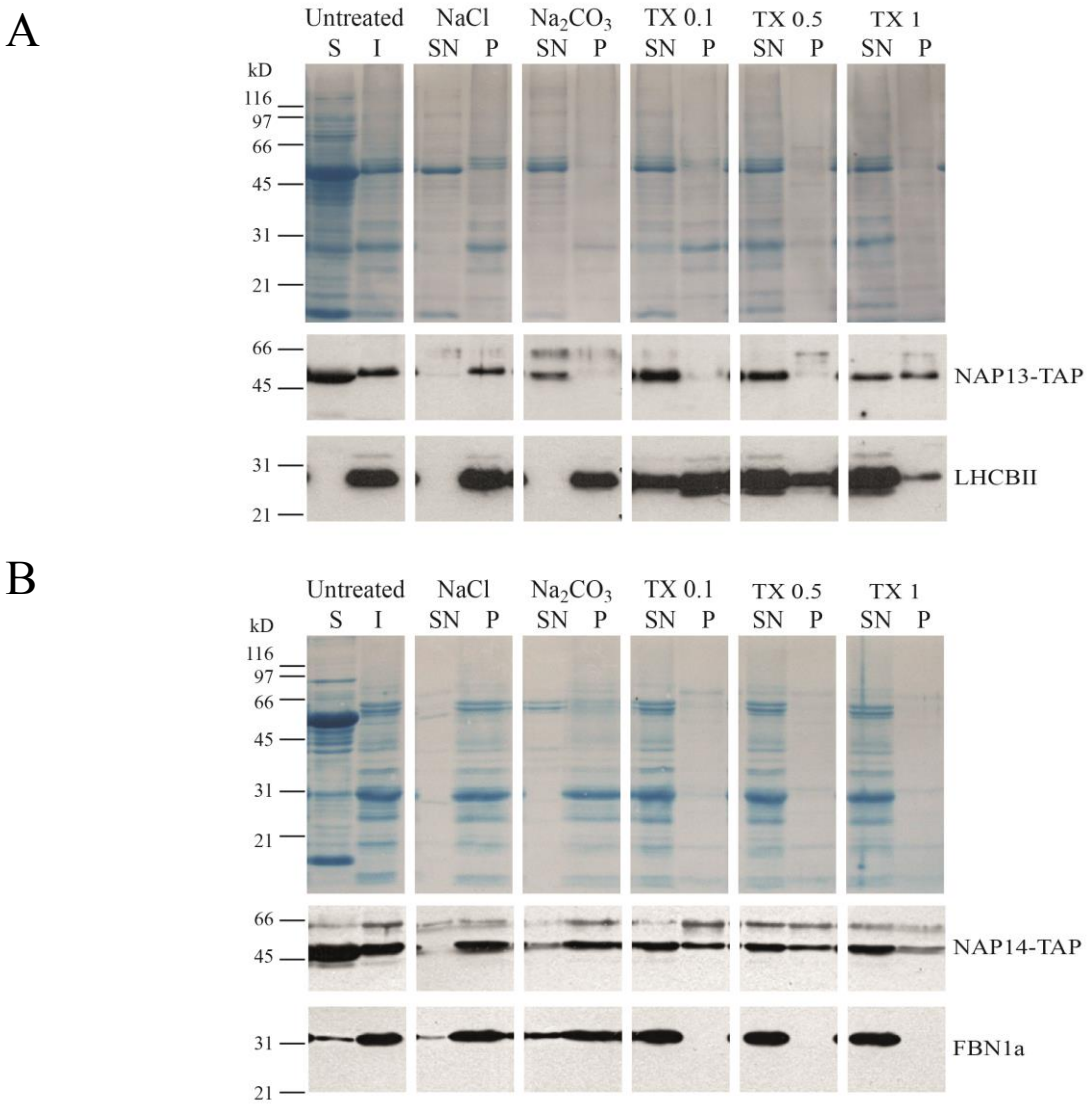

Figure 2.10 Both NAP13-TAP and NAP14-TAP are peripheral (extrinsic) membrane proteins.
(**A**) A protein extract was obtained from rosettes (8 weeks) of NAP13-TAP complemented line. Plant tissues were manually ground with pestle and mortar. Proteins were separated into soluble (S) and insoluble (I) fractions at 100'000 ×g. Then equal amounts of the insoluble fraction were treated with 1 M NaCl (NaCl), 0.2 M Na_2CO_3 (Na_2CO_3), 0.1% Triton X-100 (TX 0.1), 0.5% Triton X-100 (TX 0.5) or 1% Triton X-100 (TX 1). Samples were equally resuspended using a Dounce homogenizer and separated into supernatant (SN) and pellet (P) fractions. Proteins were analyzed by SDS-PAGE followed by immunoblotting with anti-CBP to detect NAP13-TAP. An integral membrane protein, LHCBII, was used as control.
(**B**) Intact chloroplasts were isolated from NAP14-TAP complemented plants (6 weeks). Chloroplasts were osmotically and mechanically lysed using a Dounce homogenizer in a hypotonic buffer. Proteins were then separated into soluble (S) and insoluble (I) fractions. Equal amounts of the insoluble fraction were treated with 1 M NaCl, 0.2 M Na_2CO_3, 0.1% Triton X-100, 0.5% Triton X-100 or 1% Triton X-100. Solubilized samples were finally separated into supernatant (SN) and pellet (P) fractions. SDS-PAGE and immunoblotting analyses were carried out to detect NAP14-TAP (anti-CBP) and the peripheral plastoglobule protein FBN1a in the different fractions.

3.8 NAP13 and NAP14 may physically interact with ABCI12

As described in the introduction, NON-INTRINSIC ABC PROTEINS harbor a single domain which is predicted to bind and hydrolyze ATP. Among ABC superfamily, peptides carrying a single domain resemble prokaryotic multi-subunit transporters and are therefore gathered in the ABCI family. Based on phylogenetic relationships, it is tempting to hypothesize that NAP13 and -14 interact with ABCI12, a transmembrane-harboring protein (TM) that would serve as a channel. Sometimes TM carries substrate recognition sites, although the participation of a third protein involved in substrate binding (BP) cannot be excluded.

To unravel protein-protein interactions, co-immunoprecipitation of NAP13-YFP-HA and NAP14-YFP-HA were carried out. In parallel, the experiment was also done with control proteins. One control line overexpressed the YFP-HA tag alone. The YFP-HA tag was targeted to chloroplasts by fusion to the transit peptide of RuBisCO small subunit (cYFP-HA= Ctrl1). The other control line expressed an unrelated protein responsible for carotenoid breakdown in plastoglobules (CCD4-YFP-HA= Ctrl2, see Chapter III). Chloroplasts (chlorophyll at 1mg/mL) from all lines were isolated and solubilized using 1% TX-100. After removal of debris by centrifugation, clear supernatants were incubated with anti-HA microbeads (Miltenyi Biotec). Several gentle washes were applied before the elution of protein complexes. After protein in-gel tryptic digestion, peptides were identified by quantitative Synapt Q-TOF mass spectrometry. Note that three technical replicates were obtained and that an additional biological replicate will be carried out in the near future.

As a result of three technical replicates, an impressive 454 Arabidopsis proteins were detected in NAP14-YFP sample, while only 66 and 53 proteins were identified in Ctrl1 and 2, respectively. In the NAP13-YFP co-immunoprecipitation experiment, 117 Arabidopsis proteins were found. To directly compare our samples, the YFP, a component of the tag used as bait, was quantified (Table 2.2). We detected an average of 73.24 fmoles of YFP in NAP14-YFP experiment, while only 9.07, 12.76 and 11.79 fmoles were detected for NAP13-YFP, Ctrl1 and Ctrl2 experiments, respectively. Note that these data were in accordance with the quantification of the targeted protein itself. For instance in NAP14-YFP experiment, 68.98 fmoles of NAP14 were recorded, whereas in NAP13-YFP experiment only 12.40 fmoles of NAP13 were detected on the column (Table 2.2). Taken together, these results suggest either that NAP14-YFP was more concentrated in the starting transgenic material than other recombinant proteins, or that the purification was more efficient for NAP14-YFP. Interestingly, NAP13 was not found in control experiments, emphasizing a specific purification. Unfortunately, NAP14 was detected in all samples, including controls. Due to its high abundance in NAP14-YFP experiment (68.98 fmoles), it is likely that a contamination of the column preceding the mass spectrometer occurred.

To narrow the number of candidates curated locations of each protein were retrieved from the public database PPDB (*http://ppdb.tc.cornell.edu/)*. Proteins that could not be assigned with certainty to a subplastidial location were excluded. Localization of NAP13 at the envelope membranes gave an important constraint for the identification of interaction candidates. For NAP14 as it will be explained later on, we also focused our research on envelope-located proteins. In addition as we were mainly searching for a channel, transmembrane domains were predicted using Aramemnon (*http://aramemnon.uni-koeln.de/*) and TMHMM (*www.cbs.dtu.dk/services/TMHMM/*) portals.

Finally, two criteria, namely specificity (i.e. not detected in any control) and abundance, were used to order envelope-located proteins (Table 2.3). Note that unless they are highly concentrated, proteins found also in control experiments are likely to be contaminants and should not be accounted for.

Proteomics data obtained for NAP13-YFP co-immunoprecipitation were filtered for envelope localization. As a result, six proteins with a curated location at the envelope were shortlisted ABCI12 (At3g21580) being one of them (Table 2.3). The fact that bacterial orthologues of NAP13, -14 and ABCI12 belong to the same operon, hints at the possibility of ABCI12 interacting with NAP13. ABCI12 was the only candidate that met both criteria of envelope localization and containing a transmembrane spanning domain. ABCI12 is a protein of approximately 42 kDa, which harbors 5 predicted TMs and is described as a cobalt ion transmembrane transporter by similarity. As the twelfth member of the ABCI subfamily ABCI12 is classified in the CBY:Y179 group together with NAP13 and NAP14. Moreover, the relatively low abundance of ABCI12 in our sample correlates well with the scarcity of NAP13 in large-scale proteomic study (Ferro et al. 2010). In summary, these results support a scenario in which NAP13 and ABCI12 are assembled at the chloroplast envelope to form a novel multi-subunit ABC transporter.

As will be discussed later, previous proteomics studies strongly suggested that NAP14 is localized at the chloroplast envelope membranes rather than at the thylakoid membranes (Zybailov et al. 2008; Ferro et al. 2010; Simm et al. 2013). In addition, the fact that NAP14 together with NAP13 and ABCI12 is part of the CBY:Y179 group indicates that NAP14 is likely to localize at the chloroplast envelope membranes too. Actually, the CBY:Y179 group represents ABC transporters composed of an heterodimeric NBD (NAP13 and NAP14?) and an homodimeric TM (ABCI12?). What is more, NAP14 is coexpressed with NAP13 and ABCI12 according to the ATTED-II resource (*http://atted.jp/*). Owing to these lines of evidence, we used the envelope-localization as a filter to analyze NAP14-YFP Synapt data. Twenty-one proteins were shortlisted (Table 2.3) of which six were also found in NAP13-YFP experiment amongst them NAP14 itself. An interesting finding was the presence of NAP13 and ABCI12, absent in both control experiments, in NAP14-YFP co-immunoprecipitation. In addition, a third protein, At2g38040, was exclusively found in NAP14- and NAP13-YFP. At2g38040 encodes the alpha subunit of the acetyl-CoA carboxylase carboxyltransferase (CAC3) involved in the conversion of acetyl-CoA into malonyl-CoA, an important step in fatty acid biosynthesis. Based on PPDB curated location, CAC3 is associated with the inner envelope membrane. However, according to Aramemnon and TMHMM, CAC3 is not an integral membrane protein. TM predictions revealed six potential channels at the chloroplast envelopes. These were ABCI12, TIC214, DUF1012, TIC110, SQD2 and FLU. TIC214 and TIC110, as they are involved in protein import machinery, can be reasonably excluded (Kikuchi et al. 2013). Similarly, SQD2 is known to be a sulfoquinovosyltransferase responsible for the transfer of sulfoquinovose moiety to diacylglycerol (Yu et al. 2002). Among the three remaining protein, DUF1012 a putative ion channel POLLUX-like 1 was an interesting candidate but ABCI12 was the most abundant and thus potentially the more probable interacting partner of NAP14. These data are in support our hypothesis that ABCI12 functions as the TM portion of the NAP13, -14 transporter. To sum up, three envelope proteins were exclusively found in NAP13- and NAP14-YFP experiments, and these were NAP13, ABCI12 and CAC3. Owing to their phylogenetic relations and

our proteomics results, NAP13-NAP14-ABCI12 are likely to form a multi-subunit transporter at the chloroplast envelope.

Table 2.2 Baits detected in the four co-immunoprecipitation experiments and quantified by Synapt spectrometry are shown. Data are expressed in fmoles detected on the column. Experiment-specific baits are darkened.

AGI code	Description	NAP13	NAP14	Ctrl1	Ctrl2
AT4G33460	Non-intrinsic ABC protein 13, NAP13, ABCI10	12.40	3.38	0	0
AT5G14100	Non-intrinsic ABC protein 14, NAP14, ABCI11	3.85	68.98	4.26	1.02
AT4G19170	Carotenoid cleavage dioxygenase 4, CCD4, NCED4	0	6.57	0	27.55
	Yellow fluorescent protein, YFP	9.07	73.24	12.76	11.79

Experiments, from left to right, are as follows: NAP13, NAP13-YFP-HA; NAP14, NAP14-YFP-HA; Ctrl1, cYFP-HA; Ctrl2, CCD4-YFP-HA.

Table 2.3 Analysis of co-immunoprecipitations by quantitative Synapt mass spectrometry.
Proteins co-immunoprecipitated with NAP13- and/or NAP14-YFP-HA were filtered for a curated location at the chloroplast envelope membranes. Baits are darkened and the most probable candidate for a channel at the envelope is highlighted in bold. Data are expressed in fmoles detected on the column.

1	2	AGI code	Description	NAP13	NAP14	Ctrl1	Ctrl2
E		AT4G33460	Non-intrinsic ABC protein 13, NAP13, ABCI10	12.40	3.38	0	0
IE		AT2G38040	Acetyl-CoA carboxylase carboxyltransferase subunit alpha, CAC3	1.08	3.01	0	0
E	**x**	**AT3G21580**	**Cobalt ion transmembrane transporters, ABCI12**	**0.25**	**3.51**	**0**	**0**
E		AT5G14100	Non-intrinsic ABC protein 14, NAP14, ABCI11	3.85	68.98	4.26	1.02
IE		AT5G50920	Chaperone protein ClpC1, HSP93	1.99	10.23	1.36	0.60
OE		AT3G46740	Translocon at the outer envelope membrane of chloroplasts 75-III, TOC75	0.80	3.22	0	0.16
IE	x	ATCG01130	Translocon at the inner envelope membrane of chloroplasts 214, TIC214	0	8.00	0	0
OE		AT4G02510	Translocon at the outer envelope membrane of chloroplasts 159, TOC159	0	0.91	0	0
IE		AT3G56940	Copper response defect 1 protein, CRD1	0	0.77	0	0
OE		AT1G02280	Translocon at the outer envelope membrane of chloroplasts 33, TOC33	0	0.54	0	0
E	x	AT5G02940	Putative ion channel POLLUX-like 1, DUF1012	0	0.49	0	0
E		AT2G44640	Putative uncharacterized protein	0	0.48	0	0
IE	x	AT1G06950	Translocon at the inner envelope membrane of chloroplasts 110, TIC110	0	0.37	0	0
OE		AT2G43950	Chloroplast outer envelope protein 37, OEP37	0	0.30	0	0
OE		AT5G05000	Translocon at the outer envelope membrane of chloroplasts 34, TOC34	0	0.29	0	0
E	x	AT5G01220	Sulfoquinovosyldiacylglycerol 2, SQD2	0	0.24	0	0
IE		AT5G24020	Septum site-determining protein, MIND1	0	0.21	0	0
IE		AT1G44446	Chlorophyllide A oxygenase, CAO	0	0.14	0	0
IE		AT1G01090	Pyruvate dehydrogenase E1 alpha, PDH-E1 alpha	0	0.14	0	0
IE	x	AT3G14110	Protein fluorescent in blue light, FLU	0	0.11	0	0
IE		AT5G35360	Acetyl-CoA carboxylase biotin carboxylase subunit, CAC2	0	0.08	0	0

Ctrl1 (cYFP-HA), Ctrl2 (CCD4-YFP-HA)
[1] Curated location; E, envelope; IE, inner envelope; OE, outer envelope
[2] Proteins with predicted TM (Aramemnon, TMHMM)

3.9 Implication in fatty acid biosynthesis : A shared metabolite with ACC and PDHC?

The disruption in phosphatidyletanolamine and the shift in MGDG molecular species observed in *nap13* and *nap14* suggested a defect in lipid metabolism. Additionally, co-immunoprecipitation experiments of NAP13- and NAP14-YFP both revealed the presence of CAC3, an enzyme involved in fatty acid (FA) biosynthesis. To further investigate the potential implication of the putative NAP13-NAP14-ABCI12 transporter in FA metabolism, AGI codes of 35 proteins involved in FA biosynthesis were retrieved from ARALIP (Arabidopsis Acyl-Lipid Metabolism, http://aralip.plantbiology.msu.edu/) (Li-Beisson et al. 2013). Proteomics data from Synapt mass spectrometry were searched for those enzymes involved in plastidic FA synthesis. A total of eleven proteins were found in NAP13- and/or NAP14-YFP co-immunoprecipitations (Table 2.4). Three enzymatic complexes successively involved in FA biosynthesis were represented, that is to say the pyruvate dehydrogenase complex (PDHC), the acetyl-coenzyme A carboxylase (ACC) and the fatty acid synthase (FAS). PDHC converts pyruvate into acetyl-CoA, which is then carboxylated by ACC in malonyl-CoA. Finally, FAS is responsible for the multiple and sequential condensation of two carbons on malonyl-CoA building block.

Four components of PDHC were detected in NAP14-YFP experiment, while the dihydrolipoyl dehydrogenase 2 (LPD2) was also found in NAP13-YFP. Interestingly, the carboxyltransferase of the ACC is highly represented in NAP14-YFP experiment with 3.01 fmoles of the subunit alpha CAC3 and 7.17 fmoles the subunit beta accD. As previously mentioned, CAC3 was also co-immunoprecipitated with NAP13-YFP (1.08 fmoles). Regarding FAS, low levels of two hydroxyacyl-ACP dehydratases (HAD) were detected only in NAP14-YFP and ketoacyl-ACP synthase I (KASI) appeared in NAP13- and NAP14-YFP as well as in control experiments. As PDHC and ACC are highly represented, it is likely that they shared a common substrate/product with NAP13-NAP14-ABCI12 transporter. To conclude, note that acetyl-CoA is the common metabolite between PDHC and ACC.

Table 2.4 Proteins involved in fatty acid biosynthesis and identified by Synapt spectrometry in NAP13- and/or NAP14-YFP experiments. Proteins co-immunoprecipitated with NAP13- and/or NAP14-YFP-HA were filtered according to known roles in FA biosynthesis. Data are expressed in fmoles detected on the column.

	AGI code	Description	NAP13	NAP14	Ctrl1	Ctrl2
PDHC	AT4G16155	Dihydrolipoyl dehydrogenase 2, LPD2, E3	1.28	0.52	0	0
	AT3G25860	Dihydrolipoamide acyltransferase, LTA2, E2	0	1.40	0	0
	AT3G16950	Dihydrolipoyl dehydrogenase 1, LPD1, E3	0	0.46	0	0
	AT1G01090	Pyruvate dehydrogenase E1 alpha, PDH-E1 alpha	0	0.14	0	0
ACC	AT2G38040	Acetyl-CoA carboxylase carboxyltransferase subunit alpha, CAC3	1.08	3.01	0	0
	ATCG00500	Acetyl-CoA carboxylase carboxyltransferase subunit beta, accD	0	7.17	0	0
	AT5G35360	Acetyl-CoA carboxylase biotin carboxylase subunit, CAC2	0	0.08	0	0
FAS	AT5G10160	Hydroxyacyl-ACP dehydratase, HAD	0	0.32	0	0
	AT2G22230	Hydroxyacyl-ACP dehydratase, HAD	0	n.d.	0	0
	AT5G46290	Ketoacyl-ACP synthase I, KASI	1.71	3.07	0.46	0.19
	AT5G08415	Lipoyl synthase 1, LIP1	0	0.47	0	0

Ctrl1 (cYFP-HA), Ctrl2 (CCD4-YFP-HA)
ACC, Acetyl-CoA carboxylase; ACP, acyl carrier protein; CoA, coenzyme A; FAS, fatty acid synthase; PDHC, plastidial pyruvate dehydrogenase complex; n.d., detected in only one technical replicate.

4 Discussion

4.1 Severe phenotypes that emphasize the essential roles played by NAP13 and NAP14

The mutations in *NAP13* and *-14* result in embryo lethality on MS media without sugar. When supplemented with sugar, they cause a highly pleiotropic albino phenotype affecting not only leaf pigmentation, but also leaf shape and cell macro-organization. The restoration of the WT phenotype in *nap13* and *-14* by the corresponding cDNA confirmed that these drastic phenotypes were due to the disruption of *NAP13* and *NAP14*, respectively. Embryo lethality of *nap13* and *-14* shows that these genes are essential for the viability of *A. thaliana*. Due to the severity of the phenotype, the biological processes affected are not easy to diagnose. To identify the developmental stage implicated, etioplast formation was induced by dark treatment. As a result, etiolated *nap13* and *-14* seedlings displayed whitish cotyledons, which suggests a defect in differentiation of proplastids into etioplasts. Plastid primary transitions will have to be analyzed in-depth to further appreciate the respective roles of NAP13 and -14. Still, our results point out an essential action of these proteins at the proplastid stage which is corroborated by large-scale proteomics studies. Hardly detectable in leaf extracts or isolated chloroplasts, maize orthologs of NAP13 (GRMZM2G111511) and NAP14 (GRMZM2g116634) have primarily been identified in *Zea mays* proplastids (Friso et al. 2010; Majeran et al. 2012; Huang et al. 2013), suggesting their implication in early plastid development. Interestingly, disruption of *NAP14* has been shown to cause the *angulata 9* phenotype, a mutant isolated after EMS mutagenesis and showing a defect in leaf morphogenesis. The *anu9-1* has pale-green leaves with irregular margins and prominent teeth (Mateo-Bonmati et al. 2014). Compared with *nap14*, *anu9-1* presents an interesting, because less severe, phenotype with leaf pigmentation partially retained. This intermediate phenotype is due to a point mutation inducing a premature stop, 16 residues before the end of *NAP14*. The truncated protein seems to maintain its function to a certain extent. These data suggest that NAP14 is playing an important role in leaf morphogenesis rather than exclusively in chloroplast differentiation. As previously mentioned pleiotropic effects related to albinism are major constraint, thus the availability of leaky mutants such as *anu9-1* is of great interest to further explore the function of NAP14. Similarly, isolating such a leaky mutant for NAP13 should be seriously considered.

4.2 The distinct lipid phenotypes of *nap13* and *-14* points to a defect in lipid metabolism

Not only defective in plastid ultrastructure, *nap13* and *-14* have an astonishingly low number of mesophyll cells as well as irregular leaf margins and thickness resulting in a unique vitrified appearance. Albinism alone cannot explain this disruption in leaf morphology as suggested by the leaky *anu9-1* mutant. Despite the fact that pigmentation is partially maintained in *anu9-1*, leaf morphogenesis remains abnormal. A better understanding of *nap13* and *-14* phenotypes resulted from untargeted lipid analysis. Abnormalities in their lipid profile were highlighted against three unrelated albino mutants (*pac*, *ppi2*, *cla1*) that were used to compare. Results of the principal component analysis were surprising. Albinos and WT clustered at the opposite according to the

principal component 1 (59.9%) which is mainly due to the higher level of overall galactolipids in WT. Supporting the notion that NAP13 and -14 act on the same biochemical pathway, the two mutants formed a cluster at the opposite of the other three albinos. This segregation between albinos, explained at 23.3% by the principal component 2, was mainly due to phospholipid content. The sole detectable phospholipid namely phosphatidylethanolamine (PE) dropped in *nap13* and *-14*, especially the 18:3/16:0 molecular species. Phospholipids are major constituents of the plasma membrane and endomembrane system that define a cell, thus a reduced number of cells would result in a decrease in phospholipids. However, the drop in PE is hard to attribute to the only fact that mesophyll tissues are scattered as identical quantities of fresh weight tissues were used. Actually the same reduction in number of mesophyll cells, thus increasing the proportion of air space, has been observed in the *cla1* mutant, one of our albino controls (Estévez et al. 2000). Plastids being arrested early in development, it has been proposed that the chloroplast-nucleus coordination is altered in most albinos which compromises the last stages of mesophyll differentiation (Chatterjee et al. 1996; Keddie et al. 1996; Leon et al. 1998; Rodermel 2001). Despite this pleiotropic effect related to albinism, *cla1* was not clustering with *nap13* and *-14*. On the contrary, its level of PE was close to that of WT plants. What is more, in *cla1* cell size, leaf shape and thickness are not drastically modified in comparison with WT plants (Estévez et al. 2000). Regarding galactolipids, an interesting fact was the shift in molecular species of MGDG. The 18:3/16:3 species was more accumulated in *nap13* and *-14* while the 18:3/18:3 species was increased in other albinos. Noteworthy, these two MGDG species originate from two distinct pathways. MGDG 18:3/18:3 derives from the eukaryotic pathway, whilst MGDG 18:3/16:3 is assembled through the prokaryotic route directly inside plastids (Jarvis et al. 2000; Awai et al. 2001).

Note that phospholipid and galactolipid syntheses fundamentally rely on fatty acid (FA) availability. In plants, fatty acid biosynthesis mainly occurs in plastids (Li-Beisson et al. 2010; Li-Beisson et al. 2013). Acetyl-coenzyme A (CoA) found in plastids is believed to be the building block used to synthesize fatty acids. Quite interestingly, enzymes involved in the two first committed steps of FA biosynthesis were specifically co-immunoprecipitated with NAP13- and NAP14-YFP. These include the dihydrolipoyl dehydrogenase 2 (At4g16155), a component of the pyruvate dehydrogenase complex responsible for the synthesis of acetyl-CoA from pyruvate, and the acetyl-CoA carboxylase carboxyltransferase subunit alpha (At2g38040) that assists with the conversion of acetyl-CoA in malonyl-CoA (Reverdatto et al. 1999; Chen et al. 2010). In summary these data give rise to the hypothesis that NAP13 and -14 may contribute trafficking functions toward the vital process of lipid metabolism, probably at the level of FA biosynthesis.

4.3 Is NAP14 really associated with the thylakoid membrane?

NAP14-YFP produced punctuated fluorescent signals in chloroplasts, which we first interpreted as potential plastoglobule localization. To verify this hypothesis, membranes from 35S:NAP14-YFP were fractionated and plastoglobules were isolated. Immunoblotting revealed the absence of NAP14-YFP in plastoglobule fractions. This finding is in accordance with the absence of NAP14-YFP from established plastoglobule proteomes (Vidi et al. 2006; Ytterberg et al. 2006; Lundquist et al. 2012b). Instead, NAP14-YFP cofractionated with the thylakoid marker LHCBII suggesting its association with specialized domains of the thylakoid membranes. It is important to note that nucleoid-located

proteins also gave a punctuated fluorescence in the chloroplast (Terasawa and Sato 2005; Newell and Gray 2010) and that disruption of the plastid transcription machinery often leads to chlorotic or albino phenotypes (Pfalz and Pfannschmidt 2012). Knowing that multiple nucleoids are associated with the thylakoid membrane in mature chloroplasts (Liu and Rose 1992; Jeong et al. 2003), it would be of great interest to determine nucleoid distribution in membrane fractions using antibodies against a well-described nucleoid markers. Alternatively, colocalisation by fluorescence microscopy of NAP14-YFP with the DNA marker DAPI would be interesting. However, the maize ortholog of NAP14 (GRMZM2g116634) was not identified in nucleoid-enriched proteomes from *Zea mays* chloroplasts (Majeran et al. 2012). It is interesting to note that NAP14 was detected in maize proplastids (Huang et al. 2013). An important point to mention is the extremely low abundance of NAP14 in WT plants, since only one peptide (VGIVFQFPER) with 2 spectral counts was recorded in a chloroplast proteome study (Zybailov et al. 2008). In contradiction to our results, NAP14 was found in the low-density membrane fraction (likely to correspond to envelopes) rather than in thylakoid membrane. What is more, ten spectral counts of NAP14 were identified in the chloroplast envelope membranes by a large-scale proteomics study (Ferro et al. 2010). More recently, a detailed proteome of chloroplast envelope membranes reveals NAP14 in the inner envelope membrane of *Pisum sativum* (Simm et al. 2013). NAP14 was therefore classified as a putative chloroplast envelope transporter (Mehrshahi et al. 2013). Taken together these data suggest that the localization of NAP14-YFP to thylakoid membranes may be erroneous. One should consider the possibility that an artifact of overexpression may have resulted in protein aggregates, explaining fluorescence concentrated in foci and hence cofractionating with the densest membranes, the thylakoids. In the near future, it will be necessary to further investigate the subcellular location of NAP14 as it is directly related to its function. Since NAP14-TAP was demonstrated to partially behave as an extrinsic membrane protein in alkaline carbonate extraction experiments, a dual localization, one at a membrane and the other in the stroma might be predicted.

4.4 NAP13 is conditionally associated with the chloroplast inner envelope membrane

Despite difficulties to functionally characterize NAP13, we are now reasonably certain about the localization of NAP13 at the stromal face of the chloroplast inner envelope membrane. In previous proteomics studies, NAP13 was detected in envelope membranes from the C_3 plant Arabidopsis (Froehlich et al. 2003) and from the C_4 plant maize (*Zea mays*), but not from the C_3 plant pea (*Pisum sativum*) (Bräutigam et al. 2008). A large-scale proteomics study of Arabidopsis chloroplasts recorded NAP13 at 100% in the envelope subfraction (Ferro et al. 2010). Only 8 spectral counts were measured suggesting that the native NAP13 is relatively rare. In accordance with these studies, we demonstrated by two independent experimental approaches that NAP13 is located in chloroplasts. In addition, a convincing membrane fractionation experiment in this thesis clearly indicated that NAP13 is localized at the chloroplast envelope membranes. A dual localization between envelopes and stroma was noticed for NAP13-YFP as well as NAP13-TAP. Because NAP13 was shown to be an extrinsic membrane protein, we attributed this observation to an artifact of overexpression possibly due to the saturation of NAP13 binding sites at the membrane. To know whether a protein is associated with the outer or inner envelope membrane, trypsin resistance after import into isolated pea chloroplast assay is the most common indicator. In our protein import experiment, NAP13-

6xHIS was only detected in the stromal fraction already suggesting an aberrant localization. The subplastidial location of NAP13 in pea chloroplasts is likely to be different than in Arabidopsis since the native NAP13 was not detected in envelope membranes of *Pisum sativum* (Bräutigam et al. 2008). In conclusion, a protein import experiment in isolated Arabidopsis chloroplasts followed by trypsin treatment will be necessary to clarify the exact topology of NAP13. Nevertheless, the stromal localization of NAP13 observed by confocal microscopy and by chloroplast fractionation together with the resistance of NAP13-6xHIS to thermolysin treatment after protein import assay suggested that NAP13 is located on the stromal side of the chloroplast inner envelope membrane.

4.5 Discovery of a novel prokaryotic-type ABC transporter in *A. thaliana*

NAP13 and *-14* encode two small putative ATPases (NBD) that likely interact with a membrane-spanning protein (TM). Several lines of evidence collected by STRING database predicted ABCI12 as a functional partner of NAP13 and vice versa. Both proteins together with NAP14 are assigned to the CBY:Y179 group, which suggests that they are acting in the same pathway as has been observed for other ABCI groups (Table 2.1). For example, the three components of the TGD complex, namely NAP11, TGD1 and TGD2, are classified in the MLK group (Roston et al. 2012). NAP10/AtCcmA and AtCcmB whose bacterial orthologs are involved in maturation of c-type cytochromes in the periplasm are gathered in the CCM group (Rayapuram et al. 2007). A third instance is the ABC transporter required for aluminum tolerance and phosphate deficiency responses. That transporter consists of NAP3/STAR1 and ALS3/STAR2, both belonging to the NO group (Larsen et al. 2005; Huang et al. 2009a; Huang et al. 2010; Belal et al. 2015). Furthermore, NAP14 is coexpressed with NAP13 and ABCI12 according to the ATTED-II resource supporting our hypothesis regarding their role in the same functional pathway. In this study, we demonstrated a promising direct interaction of NAP13, NAP14 and ABCI12. A confirmation of this interaction as well as the identification of other interaction candidates (e.g. substrate binding protein) will require repeating the isolation of the native complex with a reasonable number of replicates. Nevertheless, our current data together with phylogenetic relationships clearly suggest that a core ABC transporter possibly consisting of the NAP13-NAP14 ATPases and the ABCI12 permease is assembled at the chloroplast inner envelope. Intriguingly, the SALK_101753 T-DNA insertion in *ABCI12* does not result in a lethal or albino phenotype as suggested by the fact that the homozygous line is available to order (Ajjawi et al. 2010; Roston et al. 2014). This information should be regarded with particular caution, since whether *ABCI12* is properly disrupted by this T-DNA insertion, to our knowledge, has not been experimentally confirmed to date. This presumed absence of a strong growth phenotype for *abci12* together with the observed lethal phenotypes of *nap13* and *-14* raises the question whether ABCI12 function is redundant, or whether NAP13 and -14 assume multiple roles.

Regarding the direction of the translocation, it was mentioned in the introduction that ABCI family belongs to the class 3 that contains all predicted importers. In prokaryotes, importers are constituted of independent polypeptides and need a substrate binding protein (BP) subunit to successfully capture their substrate in the periplasmic space. Although, NAP13, -14 and ABCI12 belong to the CBY:Y179 bacterial-like transporter subsystem which is known to harbor only ATPases and permease (Zhao et al. 2004). Devoid of the typical BP to capture the substrate, CBY:Y179 transporters cannot conclusively be classified as importers (Davidson et al. 2008). A functional

divergence during evolution leading to an inversion of the transport polarity may explain the lack of BP. Thus, transport polarity as well as oligomeric state and transported substrate remain challenging questions to be elucidated in a near future.

5 Conclusion

To summarise, the localisation of NAP13 at the chloroplast inner envelope was well demonstrated. This led to the discovery of ABCI12, the most probable TM partner of NAP13 at the envelope. Owing to the specific presence of ACC and PDHC components in NAP13-YFP co-immunoprecipitation, it is imaginable that NAP13-ABCI12 are involved in translocation of metabolites needed for FA synthesis (Figure 2.11, upper part). This is supported by the distinct lipid phenotype of *nap13*, which had a reduced phosphatidylethanolamine level and showed an imbalance in the main galactolipid molecular species. The substrate and directionality of the transport are still unknown.

Regarding NAP14, localization results were less convincing. A specialized domain of thylakoid membrane was pointed out by confocal microscopy and chloroplast membrane fractionation. Lipid trafficking at the plastoglobule-thylakoid junction was the first assumption regarding NAP14 (Figure 2.11, lower part), which was called in question by chloroplast membrane fractionation experiments and established plastoglobule proteomes. As a second hypothesis, nucleoid localization was proposed but available proteome data in maize do not support this assumption. Finally, we thoroughly searched the literature for proteome data. Based on three independent studies, we reached the conclusion that NAP14 is most likely located at the chloroplast inner envelope membrane. Co-immunoprecipitation of NAP14-YFP revealed three potential interacting TM at the envelope, including ABCI12. Due to their prokaryotic origin and according to our results, it is likely that NAP13, -14 and ABCI12 are assembled at the chloroplast envelope membrane to form an ABC transporter (Figure 2.11).

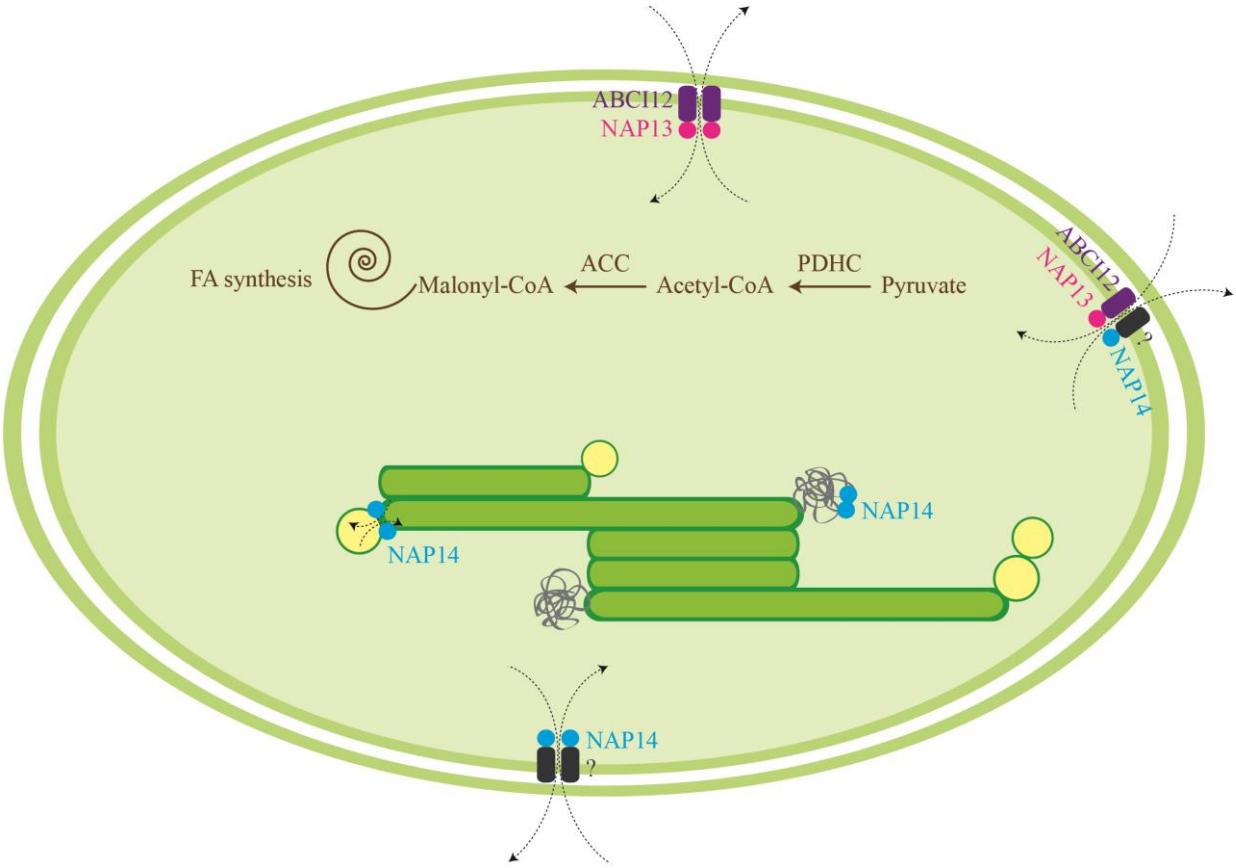

Figure 2.11 Putative models for localizations and interactions of NAP13 and NAP14.
The outer and the inner envelope membranes delimit the chloroplast. Inside the chloroplast, thylakoid membranes are shown (deep green) with burgeoning plastoglobules (yellow) and nucleoids (grey). First committed steps in fatty acid (FA) biosynthesis are depicted. Pyruvate is converted into acetyl-CoA through the action of the pyruvate dehydrogenase complex (PDHC). A component of this complex, LPD2, was specifically co-immunoprecipitated with NAP14 and NAP13, while LTA2, LPD1 and PDH-E1 alpha were found exclusively with NAP14. Then the carboxylation of acetyl-CoA into malonyl-CoA is carried out by the multisubunit acetyl-CoA carboxylase (ACC). Interestingly, the CAC3 subunit was specifically found in NAP13 and NAP14 co-immunoprecipitations, In addition, accD and CAC2 were detected in NAP14 experiment.

Chapter III

Constitutive expression of CAROTENOID CLEAVAGE DIOXYGENASE 4 leads to a reduced level of photosynthesis-related carotenoids during senescence

1 Abstract

Plastoglobules (PG) are lipid droplets inside chloroplasts. PG are stably attached to the curved portion of the thylakoid membrane via the outer polar lipid leaflet. Therefore PG can be seen as a thylakoid membrane microdomain. Around 30 proteins and enzymes reside at the PG surface. These include: fibrillins, tocopherol cyclase (VTE1), NAD(P)H dehydrogenase C1 (NDC1) and carotenoid cleavage dioxygenase 4 (CCD4). The PG core contains neutral lipids, such as prenylquinones, carotenoids, phytyl esters and triacylglycerol. These are shared with the thylakoids. Functioning as more than just a storage site, PG actively participate in lipid remodeling in thylakoids under varying environmental and developmental conditions. To advance our knowledge of PG each constituent protein needs to be characterized. Here, we describe the characterization of CCD4, a carotenoid cleavage dioxygenase, and its close physical association with PG. A chloroplast import assay demonstrates the presence of a cleavable transit peptide in CCD4 and its chloroplast localization *in vitro*. Fluorescence-tagged CCD4 resulted in a punctate pattern typical of PG localization *in vivo*. To discover the function of CCD4, a lipidomics study of Arabidopsis *ccd4* mutants compared to the wild type was carried out under varying conditions (light stress, senescence, *Pseudomonas syringae* infection). We observed a strong effect not only on β-carotene content during leaf senescence in *ccd4* as previously described (Gonzalez-Jorge et al. 2013) but also on lutein. To further investigate the function of the enzyme, we engineered 35S:CCD4-YFP overexpressing lines. In these lines a strong degradation of β-carotene, lutein and violaxanthin was observed during dark-induced senescence. In conclusion, our findings indicate that CCD4 degrades β-carotene, lutein and violaxanthin *in vivo* during chloroplast to gerontoplast differentiation.

2 Background

In chloroplasts, plastoglobules (PGs) are lipoprotein microdomains emerging from thylakoid membranes and undoubtedly implicated in prenyllipid homeostasis (reviewed in (Rottet et al. 2015; Spicher and Kessler 2015)). PGs have been reported to be composed of about 30 proteins,

prenylquinones, carotenoids, triacylglycerol (TAG), fatty acid phytyl esters (FAPEs), as well as polar lipids such as galactolipids (Vidi et al. 2006; Ytterberg et al. 2006; Lundquist et al. 2012b). As suggested by previous studies, a physical continuum between PGs and thylakoid membranes may allow the transport of lipids from the one compartment to the other (Austin II et al. 2006). To date, a metabolic activity related to lipid synthesis, repair or disposal has been demonstrated for about 10 PG-associated proteins. The most remarkable being VTE1 (tocopherol cyclase) and NDC1 (NAD(P)H dehydrogenase C1) which have been implicated in the synthesis of tocopherol and phylloquinone, respectively, as well as in the regeneration of tocopherol after oxidation (Vidi et al. 2006; Eugeni Piller et al. 2011; Eugeni Piller et al. 2014; Fatihi et al. 2015). Furthermore, ABC1K1 and ABC1K3 (activity of bc1 complex-like kinase) have been reported to regulate thylakoid lipid metabolism, presumably by phosphorylating specific target proteins such as VTE1 (Lundquist et al. 2013; Martinis et al. 2013; Martinis et al. 2014). Synthesis of TAG and FAPEs has been attributed to the activity of PES1 and PES2 (phytyl ester synthase) sequestering noxious products (phytol, free FA) released during thylakoid dismantling (Lippold et al. 2012). The fibrillin FBN4 has been implicated in lipid trafficking owing to a lipocalin domain (Singh et al. 2010), while thylakoid maintenance during chloroplast to chromoplast transition has been observed in FBN1 overexpressing tomato plants (Simkin et al. 2007). Interestingly, jasmonate biosynthesis appears to depend on FBN1a, FBN1b and FBN2 accumulation (Youssef et al. 2010).

Plastoglobule proteomes have revealed the presence of a carotenoid cleavage dioxygenase, termed CCD4, in chromoplast as well as in chloroplast plastoglobules (Vidi et al. 2006; Ytterberg et al. 2006; Lundquist et al. 2012b). CCD4 belongs to the carotenoid cleavage dioxygenase (CCD) family which is composed of nine members in *A. thaliana*. The 9-cis-epoxycarotenoid dioxygenase (NCED) subfamily is involved in stress signaling through the biosynthesis of ABA (Tan et al. 1997). CCD7 and CCD8 have been reported to be responsible for the formation of the growth hormone strigolactone (Auldridge et al. 2006a; Seto et al. 2014), while CCD1 and CCD4 were mainly related to apocarotenoid release conferring scent, flavor, or color to specific plant organs (Simkin et al. 2004a; Simkin et al. 2004b; Ohmiya et al. 2006). Apocarotenoids make up a family composed of highly diverse molecules, ranging from volatile C_{13} to colored C_{30} compounds (Auldridge et al. 2006b; Floss and Walter 2009; Walter et al. 2010). Their synthesis is initiated by the oxidative cleavage of carotenoids by CCDs or by a spontaneous oxidation (Havaux 2014). The volatile β-cyclocitral is believed to be a stress signaling molecule generated under high light through spontaneous oxidation. Nonetheless, evidence excluding a role of CCDs from β-cyclocitral synthesis are sparse (Ramel et al. 2012). Interestingly, the emission of volatile apocarotenoids such as β-ionone has been proposed as herbivore repellent in *A. thaliana* (Wei et al. 2011). In some cases, apocarotenoids were reported to be further metabolized by other enzymes such as glycosyltransferases (Moraga et al. 2004; Moraga et al. 2013; Lätari et al. 2015).

CCD4 has been studied in many plant species and tissues resulting in several observations which are sometimes confusing or even contradictory. Multiple copies of *CCD4* have been recorded in *Chrysanthemum morifolium* (Ohmiya et al. 2012; Yoshioka et al. 2012; Imai et al. 2013), *Citrus clementina*, *Citrus sinensis* (Rodrigo et al. 2013), *Crocus sativa* (Rubio et al. 2008; Ahrazem et al. 2010) and *Vitis vinifera* (Lashbrooke et al. 2013). Gene duplication leading to functional diversification may explain the difficulty in characterizing the physiological role of CCD4 when

comparing between species. The gene expression pattern is a crucial factor determining the biological function of CCD4. For instance, in *Citrus sinensis*, CCD4a is expressed in leaves, while CCD4b1 occurs in fruit peels thus excluding the function of CCD4a in fruit color formation (Rodrigo et al. 2013). Therefore, there has been a growing interest in deciphering the CCD4 promoter region in recent years (Ahrazem et al. 2010; Imai et al. 2013). Substrates and products which have been recorded to date are disparate. For example, CmCCD4a has been linked to white color formation in *Chrysanthemum* petals (Ohmiya et al. 2006). In that case, it is believed that β-carotene is cleaved symmetrically at the position 9,10 and 9',10' to produce two volatile β-ionone molecules. In *Crocus sativa* the same conclusion was reached, this time for the stigma (Rubio et al. 2008; Ahrazem et al. 2010; Rubio-Moraga et al. 2014). On the other hand, the cleavage of zeaxanthin and β-cryptoxanthin at the position 7,8 and 7',8' was observed in *Citrus* species (Ma et al. 2013; Rodrigo et al. 2013). In contrast to colorless apocarotenoids produced in *Chrysanthemum* and *Crocus*, the biological function of CCD4 in *Citrus* appeared to be the production of a bright red apocarotenoid termed β-citraurin in tangerine fruit. Interestingly, a natural variation usually due to the interruption of *CCD4* by a transposon has been observed in some species. In peach (*Prunus persica*), the functional allele is responsible for the ancestral white flesh color of the cultivar White Redhaven, while the mutated allele results in the yellow flesh color observed in Redhaven cultivar (Brandi et al. 2011; Adami et al. 2013; Fukamatsu et al. 2013). What is more, in *Brassica napus* (rapeseed) *CCD4* is interrupted by a CACTA-like transposon resulting in yellow flowers instead of white (Zhang et al. 2015).

To date, only few data are available for CCD4 from *Arabidopsis thaliana*. In the earliest study, AtCCD4 has been reported to interact with VAR3 from yeast two-hybrid assay and to be targeted to the chloroplast by a cleavable transit peptide (Naested et al. 2004). Interestingly, *var3* exhibits yellow variegated leaf sectors, in contrary to what is observed with *immutans* where variegations are white. In *var3*, an absence of carotenoid degradation in defective plastids is probably responsible for the yellow pigmentation. The fact that carotenoids are maintained in *var3* variegated sectors suggests that VAR3 positively regulates CCD4 activity. Concerning the *AtCCD4* expression pattern, a cis-acting element implicated in circadian control has been identified in the promoter (Ahrazem et al. 2010). In addition, data collected by Dalchau and coworkers (Dalchau et al. 2010) clearly demonstrate that *CCD4* is a circadian-regulated gene as expression oscillations are repressed by nicotinamide under continuous light (Figure 3.1A). Moreover, *AtCCD4* expression is repressed under high light conditions according to Genevestigator (www.genevestigator.com, Figure 3.1B) and a previous study (Ramel et al. 2012). Finally unlike *AtNCED3*, *AtCCD4* expression was not induced by drought stress (Iuchi et al. 2001). Regarding the chemical function, Huang and coworkers have performed *in vitro* enzyme assays and concluded that AtCCD4 is able to cleave β-apo-8'-carotenal thereby releasing β-ionone. In contrast to other studies, β-carotene did not appear to be a substrate of AtCCD4 (Huang et al. 2009b). First insight into the biological function of AtCCD4 arose from a plastoglobule proteome study, where dark treatment resulted in a 2-fold accumulation of CCD4 in PG compared with high light treatment (Ytterberg et al. 2006). Therefore, CCD4 has been predicted to play a role in dark-induced breakdown of carotenoids. Later it was observed that CCD4 is downregulated in *abc1k1abc1k3* which may explain the increased level of carotenoids measured in PGs of *abc1k1abc1k3* when compared to WT (Lundquist et al. 2013). However, direct evidence is lacking. Using linkage mapping and genome-wide association studies, *AtCCD4* has been identified as a negative regulator of carotenoid content during seed desiccation. What is more, *AtCCD4* was

also implicated in carotenoid breakdown during dark-induced senescence in leaves. Direct evidence was obtained by quantifying carotenoids in *ccd4*. In both seed and leaf, β-carotene was recorded as the most affected carotenoid (Gonzalez-Jorge et al. 2013). More recently, *AtCCD4* has been implicated in the formation of an unknown apocarotenoid that serves as a signaling molecule in *zds/clb5*, an albino mutant arrested in early chloroplast development and defective in carotenoid synthesis (unable to convert ζ-carotene into lycopene) (Avendano-Vazquez et al. 2014). *AtCCD4* was correlated with the formation of C_{13}-apocarotenoid glycosides that occur in PSY overexpressing plants (Phytoene SYnthase being the rate-limiting step in carotenoid biosynthesis) (Lätari et al. 2015). Taken together, these results suggest that CCD4 acts on carotenoid turnover in leaves of *A. thaliana* producing apocarotenoids that may be metabolized further. Besides, a role of CCD4 directly or indirectly in the production of retrograde signaling molecules relaying information on the chloroplast state and regulating nuclear gene expression appears very probable.

In the last decade, due to the requirement of β-carotene (pro-vitamin A) as precursor of vitamin A in human diet, important efforts have been made to increase carotenoid content in crops (e.g. Golden rice) (Ye et al. 2000). Carotenoid biosynthesis enzymes have been the first target for genetic modification, followed by a growing interest in reducing carotenoid degradation (Campbell et al. 2010; Gonzalez-Jorge et al. 2013). CCD4, which is predicted to cleave carotenoids, was identified as a PG enzyme by three independent proteomics studies (Vidi et al. 2006; Ytterberg et al. 2006; Lundquist et al. 2012b), thus placing PGs at an important position in carotenoid turnover. Before exploring the possible implication of PGs in carotenoid breakdown, the localization of AtCCD4 at the PG has to be demonstrated by biochemical and cellular methods. Note that the overexpression of *AtCCD4* has not yet been investigated and that a deeper analysis of PG lipid content will be of great interest.

This thesis presents our finding regarding AtCCD4 localization and function, especially under senescence conditions. To go into CCD4 function in depth, we characterized *ccd4* mutants under standard growth conditions. Unexpectedly, petal color did not change and no visible phenotype was observed. Therefore, we applied various stress (light stress, *Pseudomonas syringae* infection) or developmental stage (senescence) conditions to identify the biological process affected by the loss of CCD4. Furthermore, we created overexpressing lines enabling us to study the localization as well as the function of CCD4.

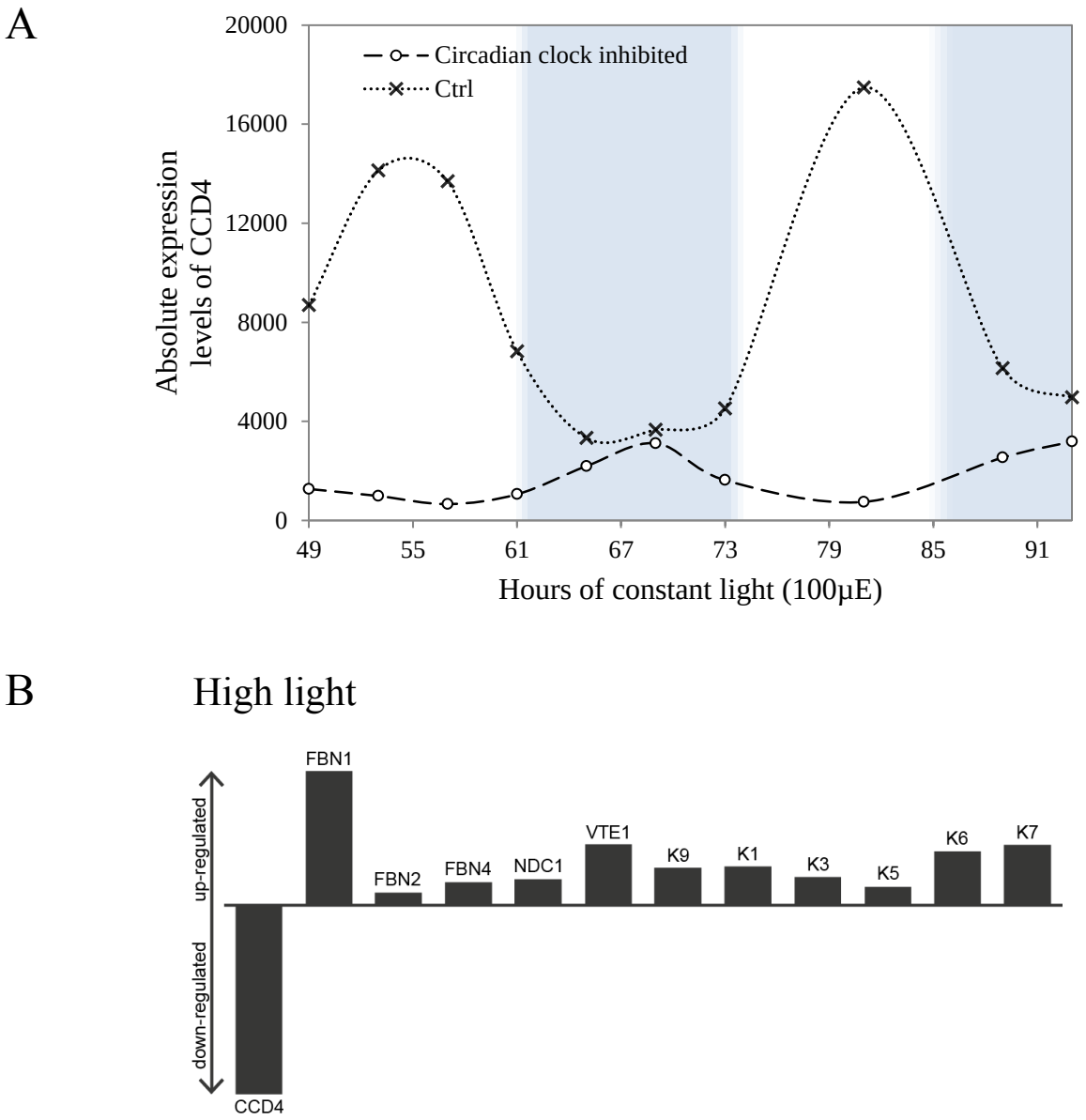

Figure 3.1 *CCD4* expression patterns (redrawn from Genevestigator data).
(**A**) *CCD4* is a circadian-regulated gene. Aerial tissue samples of C24 plants (containing CAB2:LUC and 35S:AEQ transgenes) grown under 12h light/12h dark cycles, 70 µmol·m^{-2}·s^{-1}, 19°C for 11 days, were transferred to constant light (100 µmol·m^{-2}·s^{-1}) on day 12 and treated with 50 mM nicotinamide every 2 hours over a period of 93h to inhibit the circadian clock. The control (Ctrl) did not receive nicotinamide treatment. Uncolored background represents the subjective day periods, while subjective night periods are shaded (Dalchau et al., 2010).
(B) *CCD4* is down-regulated under high light, while other PG proteins are up-regulated. FBN, fibrillin; NDC1, NAD(P)H dehydrogenase C1; VTE1, tocopherol cyclase; K1, -3, -5, -6, -7 and -9, activity of bc1 complex-like kinases.

3 Results

3.1 Mutant characterization through loss-of-function and complementation

To study the function of AtCCD4, knockout mutants are valuable tools especially since *ccd4* seeds were shown to contain significantly more carotenoids than the WT (Gonzalez-Jorge et al. 2013). Thus, T-DNA insertion lines were obtained via the TAIR website. Homozygous *ccd4-2* and *ccd4-4* lines were confirmed by PCR based on Salk Institute Genomic Analysis Laboratory (SIGnAL) instructions (Figure 3.2A and B). Loss-of-function was tested upon dark-induced senescence (Gonzalez-Jorge et al. 2013) and a phenotype possibly related to carotenoid retention was observed in *ccd4-2* and *ccd4-4* (Figure 3.2C). Moreover *CCD4* and *CCD1* transcript abundance in *ccd4-2* and WT was measured by qRT-PCR showing the lack of *CCD4* mRNA in *ccd4-2* whereas *CCD1* transcript level is not affected when compared with WT (Figure 3.2D). Under standard growth conditions, general phenotypic observations (flower color and root length) revealed no difference between mutants and WT (data not shown) but a molecular phenotype was detected by untargeted lipidomics. PCA allowed the clustering of WT and *ccd4-2* separately and a PLS-DA subjected to a permutation test barely validates the model (data not shown). However, no particular compound seems to be statistically responsible for the discrimination between WT and *ccd4-2*. We identified the following as being slightly but significantly (WT *n=6*, *ccd4-2 n=9*, $P<0.05$) higher in *ccd4-2*: PE 18:2/16:0, PE 18:3/16:0, DGDG 18:3/16:0, DGDG 18:3/16:3, MGDG 18:3/16:3 and MGDG 18:3/18:3. Therefore, a slight tendency to an increased prokaryotic FA (18:n/16:n) metabolism is observed in *ccd4-2*. We concluded that the difference observed is a combination of complex factors and not the results of one particular change in the metabolism of *ccd4-2* under standard growth conditions.

To investigate CCD4 subcellular localization and *in vivo* function, *ccd4-2* and *ccd4-4* were transformed with a construct carrying a phosphinothricin resistance marker and a fusion between CCD4 and the yellow fluorescent protein (YFP) tagged with human influenza hemagglutinin (HA) under control of the constitutive cauliflower mosaic virus (CaMV) 35S promoter (35S:CCD4-YFP-HA). Resulting plants were *ccd4-2*::35S:CCD4-YFP (35S:CCD4.2) and *ccd4-4*::35S:CCD4-YFP (35S:CCD4.4). 10-independent-glufosinate resistant T1 plants were selected because they gave a visible band by immunoblotting with anti-HA at the expected mass of 94.7 kDa (Figure 3.3A). T2 progeny of 9 lines segregated 3:1 (glufosinate resistant to glufosinate sensitive) indicating a single insertion of the transgene. Among their T3 progeny, 6 independent homozygous plants were identified. Interestingly, healthy 35S:CCD4 plants showed a normal phenotype regardless of the genetic background (Figure 3.3B). Complementation was assessed by phenotypic observations under dark-induced senescence in leaves (Figure 3.3C). Surprisingly, most of the transgenic lines displayed a whitish phenotype of their leaves, meaning that their carotenoid contents seem even lower than the WT. However, some 35S:CCD4.4 lines also showed yellowish leaves similarly to *ccd4-4*. Thus CCD4-YFP seems able to complement *ccd4-2* and *ccd4-4* with some exceptions probably related to truncated transgene or misfolded proteins. Noteworthy, some complemented lines failed to complement locally as demonstrated by yellow spots. The spots may be attributed to local gene silencing (Figure 3.3C, first line, 11^{th} leaf). To quantify our observations, total carotenoids were

quickly extracted and analyzed by spectrophotometry (Figure 3.3D). As expected, the complemented 35S:CCD4 lines contained significantly (P<0.001) less carotenoids than the WT suggesting a kind of "over-complementation". In conclusion, the overexpression of CCD4-YFP-HA did not cause a particular phenotype under standard growth conditions, although transgenic plants exhibited elevated carotenoid degradation under dark-induced senescence as supported by the notable whitish color of leaves and the total carotenoid contents.

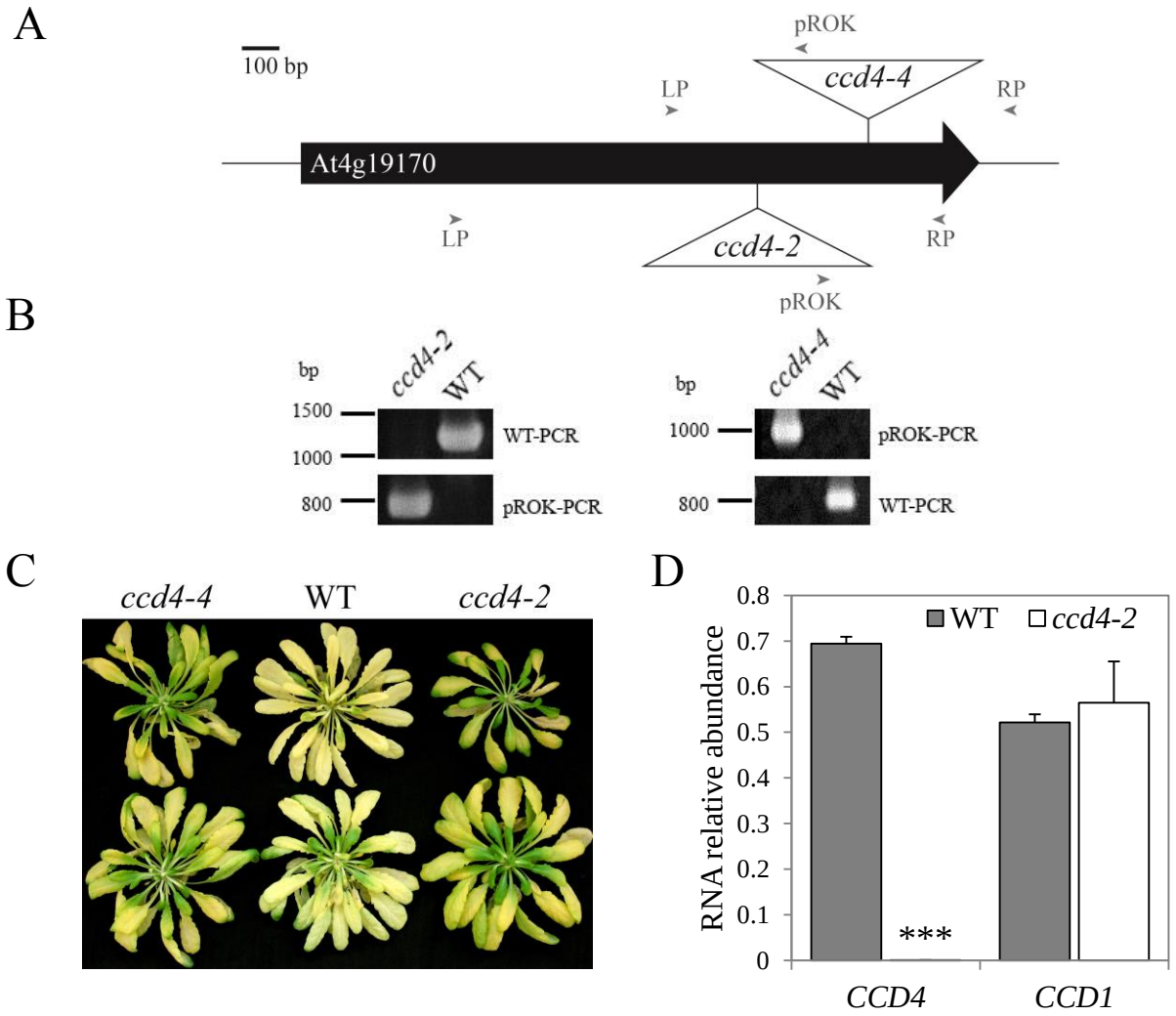

Figure 3.2 Identification of two CCD4-deficient mutants.
(**A**) Structure of *CCD4* (At4g19170). The coding DNA sequence (1788 bp) is composed of a unique exon (black arrow). Positions of T-DNA insertions *ccd4-2* (Salk_097984) and *ccd4-4* (Salk_010751) are showed (white triangles). Position of primers used for genotyping PCRs in (**B**) are indicated by arrowheads.
(**B**) Genotyping by PCR on genomic DNA of *ccd4-2* (left hand panel) and *ccd4-4* (right hand panel) compared with WT. Combination of LP and RP primers (WT-PCR) allows the identification of the WT gene. The T-DNA insertion is detected with the pROK primer combined either with a RP primer (*ccd4-2*), or with a LP primer (*ccd4-4*) (pROK-PCR).
(**C**) Loss-of-function evaluated by dark-induced senescence. Mature rosettes were placed in darkness for 8 d.
(**D**) Transcripts of *CCD4* and *CCD1* (At3g63520) were quantified by qRT-PCR in WT and *ccd4-2*. Primers CCD4-For and CCD4-Rev were used (Gonzalez-Jorges et al., 2013). The relative abundance of *CCD4* and *CCD1* transcripts were normalized to *ACTIN2* (At3g18780) transcript abundance. Means ± SD (*n=3*). Statistical significance was determined by a Student's t-test (unpaired heteroscedastic, two-tailed, ***P<0.001).

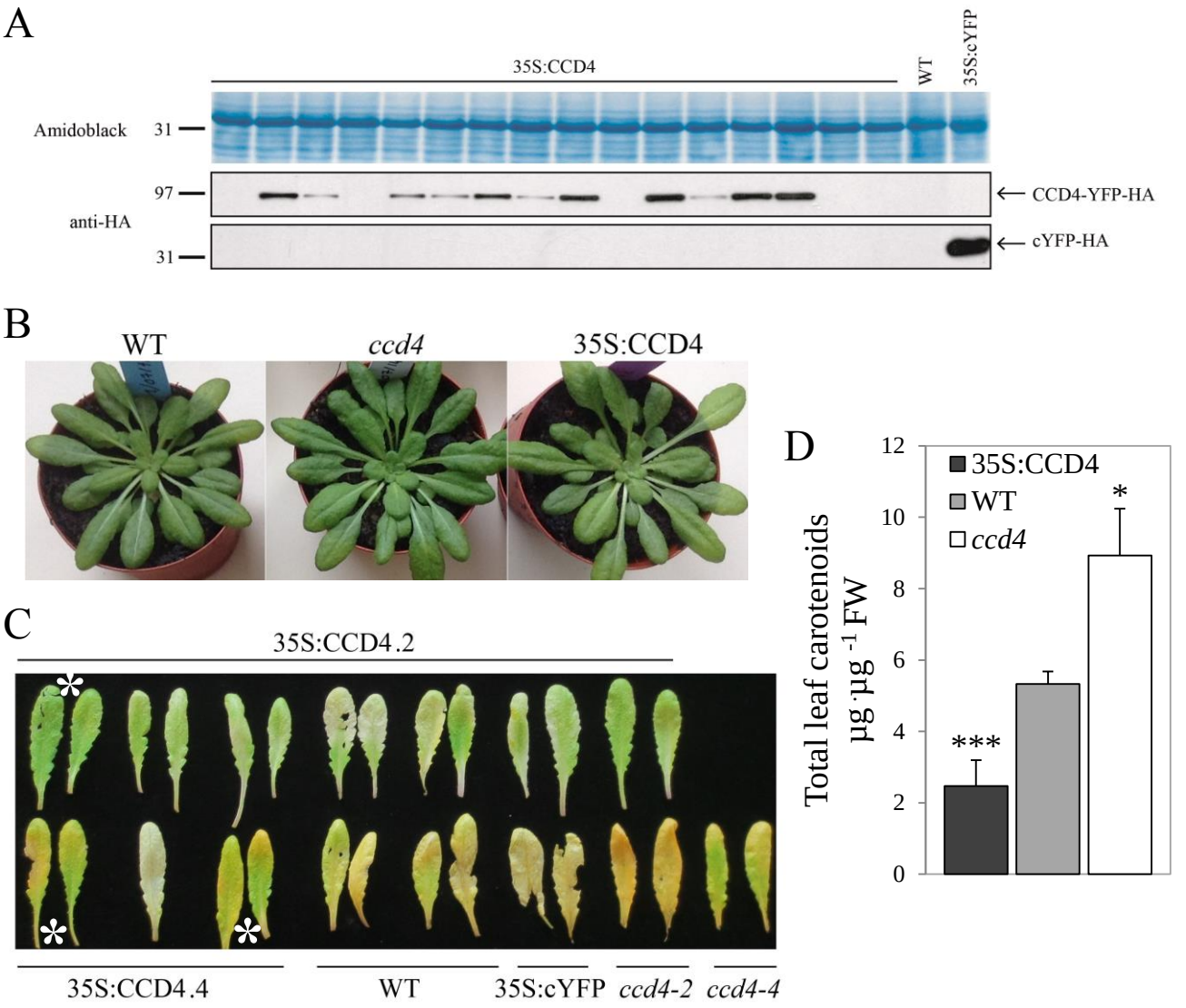

Figure 3.3 Overexpression of CCD4-YFP-HA and complementation analysis.

(**A**) Selection of plant lines that contained a detectable level of the recombinant protein. Relative amounts of CCD4-YFP-HA and cYFP-HA proteins were assessed by immunoblot analysis with an anti-HA-HRP. A representative blot is shown.

(**B**) The absence of a particular phenotype in 35S:CCD4 and *ccd4* plants. Representative individuals were shown.

(**C**) Complementation analysis of 35S:CCD4 by a leaf dark-induced senescence. Detached leaves were subjected to a dark-induced senescence for 10 d and complementation efficiency was evaluated based on the phenotype. An "over-complementation", apparent in whitish leaves, was generally observed. Two 35S:CCD4.4 plants were not complemented as they showed a yellowish color similar to *ccd4-4*.

(**D**) Total carotenoids were extracted from the leaves shown in (C) (NB: the white asterisk marks the leaves that were excluded for the calculations, 35S:cYFP was considered as WT) using five volumes of DMF. Amount ($\mu g \cdot \mu g^{-1}$ FW) of carotenoids was established with a spectrophotometer according to the equations of Wellburn (1994). Means ± SD were calculated for 35S:CCD4 (*n*=7), WT (*n*=3) and *ccd4* (*n*=2). Deviation from the WT level is significant for both mutants (35S:CCD4 and *ccd4*). Statistical significance was determined by a Student's t-test (unpaired homoscedastic, two-tailed, *P<0.05, *** P<0.001).

3.2 Subcellular localization of AtCCD4 in plastoglobules

Three earlier proteomics studies identified CCD4 as a plastoglobule protein (Vidi et al. 2006; Ytterberg et al. 2006; Lundquist et al. 2012b). *AtCCD4* encodes a protein of 595 amino acids with a predicted molecular weight of 65.6 kDa. A chloroplast transit peptide of 34 residues was predicted by ChloroP algorithm at the N-terminal of the sequence. In this study, the targeting of CCD4 to the chloroplast and the presence of a cleavable transit peptide was assessed using an *in vitro* import assay in pea chloroplast. CCD4-6xHIS was imported and processed in chloroplast leading to a mature thermolysin-resistant protein (data not shown). Transient expression of CCD4-YFP in tobacco (*Nicotiana benthamiana*) protoplasts strongly supported chloroplast localization (data not shown). Interestingly, YFP fluorescence was concentrated in fluorescent spots within chloroplasts that were reminiscent of plastoglobules (Vidi et al. 2006).

To determine the suborganellar localization of CCD4 using an independent method, we performed chloroplast membrane fractionation by floatation on a sucrose gradient (Figure 3.4A). As the antibody against the native form of CCD4 was not sufficiently sensitive, Arabidopsis plants carrying the 35S:CCD4-YFP-HA construct were used. From these plants intact chloroplasts were isolated, separated into soluble stroma and a total membrane fraction from which thylakoids, envelope membranes and plastoglobules were isolated. Equal volume fractions were collected. From these, proteins were isolated by chloroform/methanol precipitation. After a separation by SDS-PAGE and transfer to nitrocellulose, immunoblotting with a series of antibodies was done to establish the membrane distribution across the gradient. The following proteins were used as membrane markers: LHCBII which is highly abundant in the thylakoid membranes, Tic40 (translocon at the inner envelope membrane of chloroplasts) present in the chloroplast inner envelope membranes and FBN1a, an established PG protein (Lundquist et al. 2012b). Due to their low density, PG float to the top of the gradient as shown by the presence of FBN1a in fractions 1 to 6 (Figure 3.4A). Their high content in proteins makes the thylakoid membranes the densest (found mainly in fractions 17 to 24), while the envelopes are found in the middle of the gradient (mainly in fractions 9 to 16). Interestingly, CCD4-YFP cofractionates with the PG marker FBN1a on the gradient. Both proteins showed a high concentration in the first six fractions followed by an increasing amount across the last fractions (11-24) which is mainly explained by the fact that some PGs stay attached to the thylakoid membrane during the process of separation.

In addition, the colocalization of CCD4 with FBN1a was observed in protoplasts of transgenic *A. thaliana* plants constitutively overexpressing CCD4-YFP and transiently transformed with FBN1a-CFP (Figure 3.4B). Protoplasts were carefully observed by confocal microscopy. Chloroplasts were identified by their red autofluorescence due to the presence of chlorophyll. As observed in transiently transformed protoplasts of tobacco (data not shown), CCD4-YFP resulted in punctate fluorescence inside the chloroplasts. The YFP fluorescence, in most cases, colocalized with that of FBN1a-CFP, indicating that CCD4 is mainly found in plastoglobules.

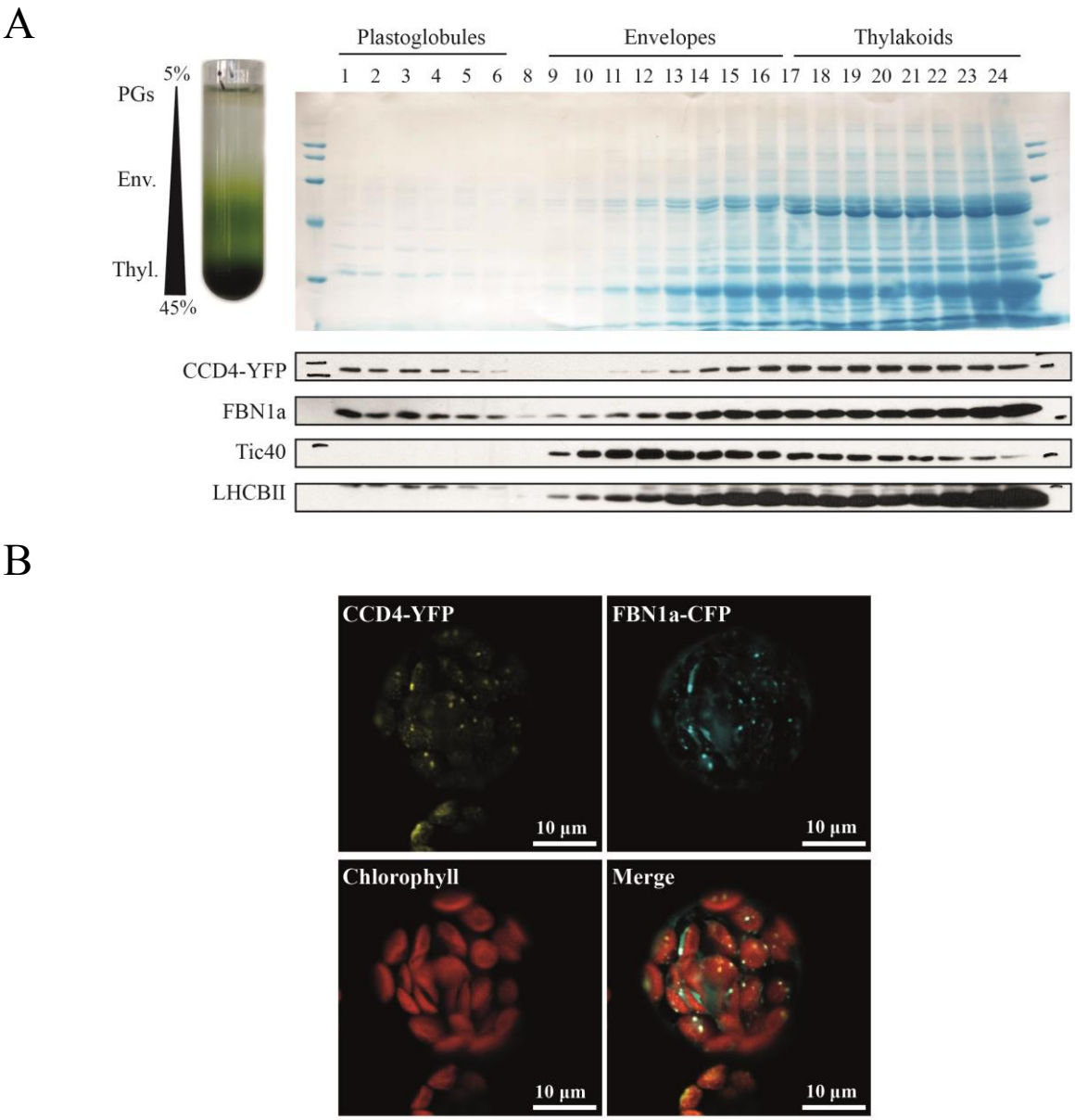

Figure 3.4 Localization of CCD4-YFP-HA at the plastoglobule, a chloroplast lipid droplet.
(A) Chloroplast membranes fractionation on a discontinuous sucrose gradient (5%-45%). On the top left of the panel, the gradient is shown, where percentage of sucrose and type of membranes are indicated (PGs, plastoglobules; Env, envelopes; Thyl, thylakoids). On the top right of the panel, proteins of each fraction (no.1-24, 5% →45%) were separated by SDS-PAGE, transferred to nitrocellulose and colored with Amidoblack. Immunoblots are presented at the bottom of the panel. To detect and localize CCD4 across the gradient, blot was probed with anti-HA-HRP. Tic40, FBN1a and LHCBII are envelope, plastoglobule and thylakoid markers, respectively.
(B) Colocalization analysis of CCD4 and the plastoglobule marker FBN1a. Protoplasts were isolated from 35S:CCD4-YFP-HA plants and transformed with FBN1a-CFP construct. Protoplasts were observed by confocal microscopy 30 h after transformation. CFP, YFP and chlorophyll fluorescence were monitored using distinct excitation wavelengths and detection windows.

3.3 Carotenoid accumulation in *ccd4* occurs mainly in senescence

To identify biological pathways affected by the loss of CCD4, three unrelated conditions were applied on WT and *ccd4-2* rosettes. Biotic stress was induced by the bacterial pathogen *Pseudomonas syringae* and an abiotic stress was applied by increasing light intensity. In addition, senescence, as a developmental state was artificially induced by a combination of dark and nutrient starvation. Lipids were extracted from grinded-rosettes with tetrahydrofuran and separated by HPLC-MS. Untargeted lipidomics analyses underlined differential responses of WT and *ccd4-2* to those conditions. Principal component analysis (PCA) was carried out from pareto-scaled variables showing a clear separation between treatments and more interestingly between genotypes (Figure 3.5A). Partial least squares-discriminant analyses (PLS-DA) were used to evaluate the strength of the model for each treatment separately. WT and *ccd4-2* formed two separate clusters under each condition. Over-fitting was detected by a permutation test (*n=200*) in light stress and *P. syringae* treatments, in other words the model is not valid and genotypes are not statistically different. The PLS-DA showing the separation of WT and *ccd4-2* in senescence (Figure 3.6B) was approved by the model-validation test meaning that the two senescent genotypes are statistically different in their lipid composition. These results are in accordance with the PCA model (Figure 3.5A) where the discrimination between WT and *ccd4-2* is greater in senescence than in light stress or during *P. syringae* attack. In addition, a visible phenotype was exclusively observed in senescence (Figure 3.6A). In the light of these results, we decided to tackle senescence PCA in more depth.

Using the loadings plot of the senescence-PLS-DA, we identified the main compounds responsible for the separation along the first axis (component 1 explaining 34.8% of the variability) between WT and *ccd4-2* in senescence (Figure 3.6C). Interestingly, two photosynthesis-related carotenoids, namely lutein and β-carotene, appeared in the upper right quadrant indicating that they contribute greatly to the separation between WT and *ccd4-2*. In addition, an unidentifiable xanthophyll (m/z 600.4172, at 0.83 min) plotted close to β-carotene. The ion at m/z 600.4172 was associated to the molecular formula $C_{40}H_{56}O_4$ (error = -1.2 ppm, confidence 92.4%) corresponding to violaxanthin and neoxanthin structures. Due to their high molecular similarity, neoxanthin and violaxanthin were not separated by the untargeted HPLC method. Consequently, their discrimination is not possible in this particular analysis. Four galactolipids (DGDG 18:3/16:3, 18:3/18:3, MGDG 18:3/16:3 and 18:3/18:3), probably largely due to their massive abundance, were also revealed as outlying compounds. Moreover, two unknown compounds (m/z 608.4282 at 1.90 min and 806.5175 at 2.10 min) showed an outlying distribution. The ion at m/z 608.4282 (Figure 3.6C) plotted near *ccd4-2* and at the opposite of m/z 806.5175 (Figure 3.6C). On the one hand, the ion at m/z 608.4282 corresponds to the elemental composition $C_{35}H_{60}O_8$ (error = -1 ppm, confidence 100%). It is worth to note that a steroidal glycoside (namely 24(*R*)-stigmastan-3*β*,5*α*,6*β*-triol- 25-ene 3-*O*-*β*-glucopyranoside) with the same elemental formula was identified in fruits of *Momordica charantia* (Cucurbitaceae) (Liu et al. 2009). What is more, in an ethyl acetate extract of *Delonix regia* (Fabaceae) leaves, a molecular ion peak was observed at m/z 608 corresponding to the molecular formula $C_{35}H_{60}O_8$ and tentatively designated as stigmastien-diol-3-*O*-glucoside (Mariajancyrani et al. 2013). On the other hand, the ion at m/z 806.5175 corresponds to the elemental formula $C_{45}H_{74}O_{12}$ (error = -0.5 ppm, confidence 99.9%). Lipoxygenases (= non-heme iron containing dioxygenases) were reported to oxygenate galactolipid acyl moieties resulting in the formation of oxylipins (Nakashima et al. 2011). An *in vitro*

assay allowed the identification of lipoxygenase products using MGDG from *Trifolium repense* (18:3 plants) as substrate. Interestingly, two peaks at m/z 805.04 corresponding to the elemental composition $C_{45}H_{74}O_{12}$ were assumed to be monohydroperoxylated MGDG (18:3/18:3) (Nakashima et al. 2011). In addition, an oxylipin (mass 806, $C_{45}H_{74}O_{12}$) termed 18:3-2O/18:3 MGDG was detected in *Arabidopsis thaliana* leaves (Buseman et al. 2006; Vu et al. 2012). Interestingly, our compound at m/z 806.5175 seems closely related to MGDG 18:3/18:3 (m/z 773.5192 at 2.11 min) as they have almost identical retention time. As we can see, the literature offers a multitude of hypotheses to explore. Nevertheless, a deeper characterization of those two molecules will be necessary to properly identify them.

Relative quantification and univariate statistics (Student's T-test) were carried out to determine whether these outlying compounds are significantly dissimilar between *ccd4-2* and WT in senescence. Compounds which appeared to be significantly different were mostly carotenoids. As shown in Figure 3.5B, *ccd4-2* contained significantly ($P<0.01$) more lutein and β-carotene than WT and this exclusively during senescence. The xanthophyll (m/z 600.4172) is also more concentrated in *ccd4-2* ($P<0.05$). While α-tocopherol, a dominant PG prenyllipid, had a comparable level in WT and *ccd4-2* regardless of the conditions (Figure 3.5B). In senescence, the outlying galactolipids were concluded as not significantly disparate except for DGDG 18:3/16:3 which was more abundant in *ccd4-2* ($P<0.05$). Finally, in senescent *ccd4-2* the ions at m/z 608.4282 and m/z 806.5175 were not significantly ($P>0.05$) divergent from the WT (Figure 3.6C).

To sum up, plants treated with light stress and *P. syringae* showed no statistical difference in their lipid composition using our methods. The main difference between WT and *ccd4-2* occurred during senescence where *ccd4-2* accumulated significantly more carotenoids than the WT.

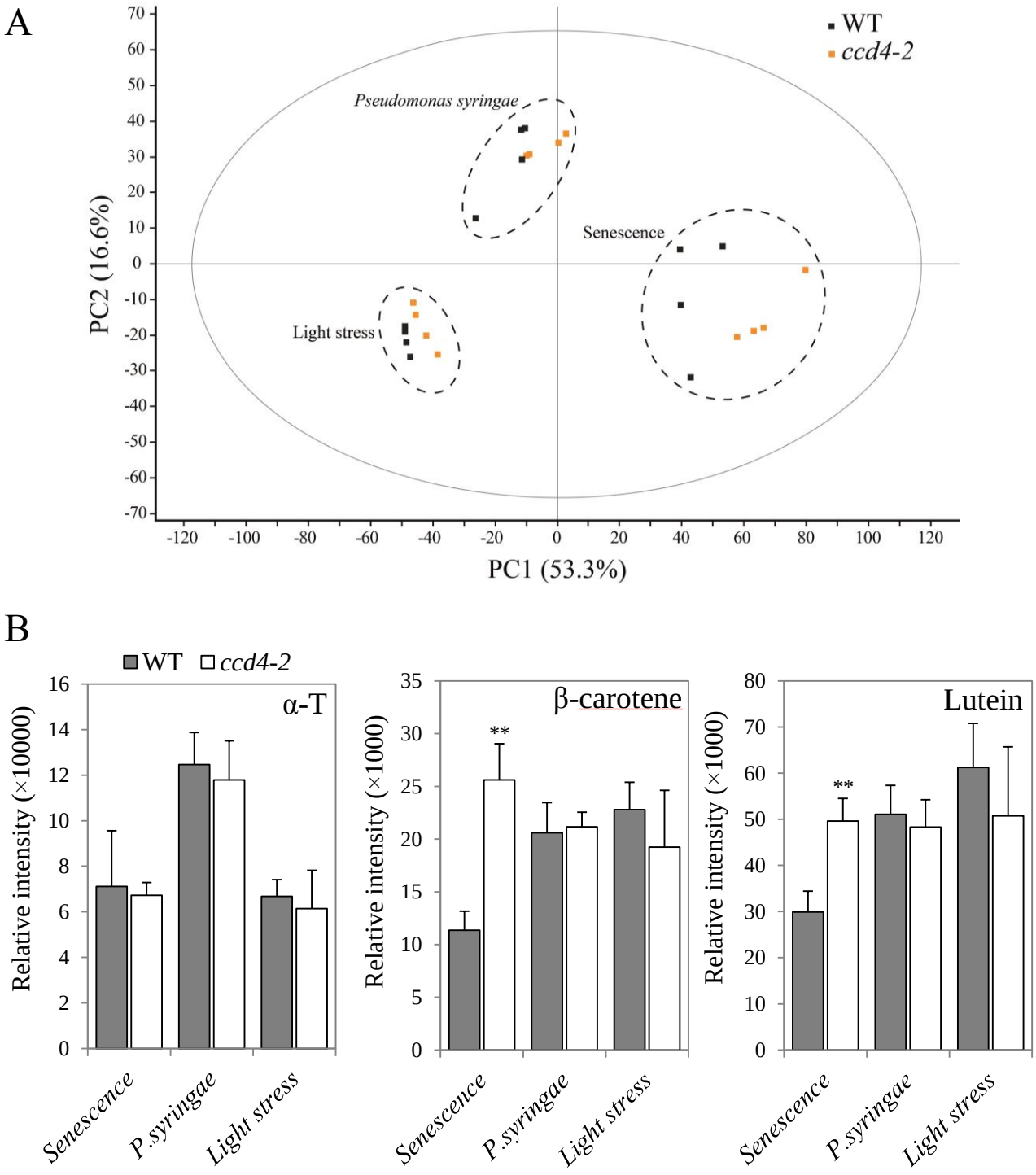

Figure 3.5 Untargeted prenyllipid profiling of *ccd4-2* and WT under various conditions.
(**A**) Responses to environmental stress (light stress, *Pseudomonas syringae*) and developmental stage (senescence) between WT and *ccd4-2* assessed by a PCA analysis. Prenyllipids were extracted with tetrahydrofuran from treated rosettes and analyzed by HPLC-MS.
(**B**) Relative quantification of a representative plastoglobule prenyllipid, α-tocopherol (α -T) and two identifiable carotenoids, lutein and β-carotene in treated WT and *ccd4-2*. Means ± SD (*n=4*). Significance of the deviation from WT value was determined by a Student's t-test (unpaired heteroscedastic, two-tailed, **P<0.01).

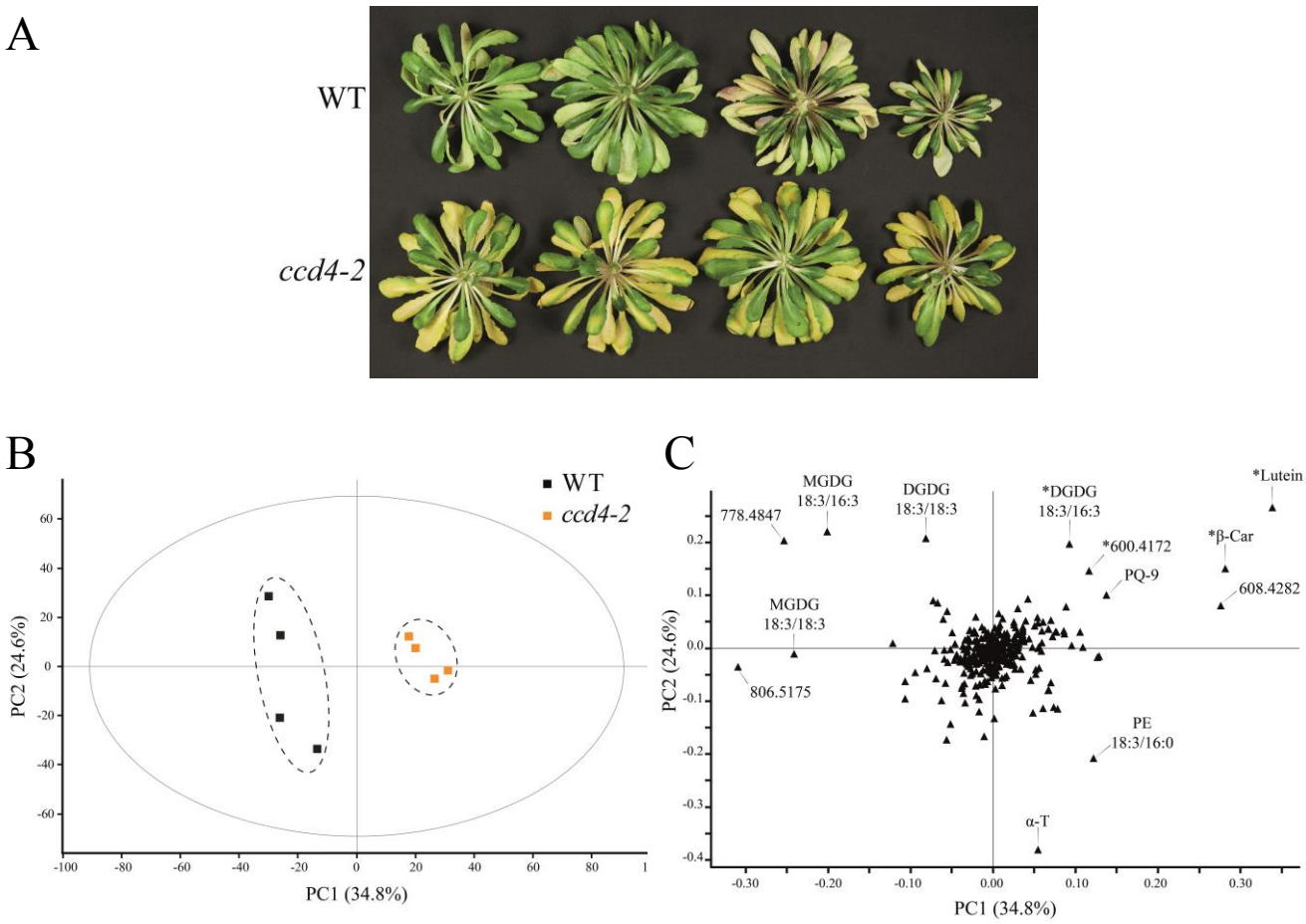

Figure 3.6 Untargeted prenyllipid profiling of *ccd4-2* and WT in senescence.
(**A**) Four mature WT and *ccd4-2* rosettes after 7 d of dark-induced senescence.
(**B**) Prenyllipids were extracted with tetrahydrofuran from WT and *ccd4-2* rosettes which had been subjected to dark-induced senescence for 7 d (*n=4*). PLS-DA analysis score plot (PC1×PC2) with the percentage of explained variance is shown. The principal component 1 explains 34.8% of the difference.
(**C**) The corresponding loading plot shows the variables responsible for the separation of WT and *ccd4-2* .The difference is mainly related to the accumulation of lutein and β-carotene in *ccd4-2*. See Figure 3.5B for relative quantification. *Statistically significant according Student's T-test (unpaired heteroscedastic, two-tailed).

3.4 Plastoglobules of senescent *ccd4* contained more β-carotene and lutein

Owing to the localization of CCD4 at PG and knowing that PGs are a site of high lipid metabolic activity during senescence (Besagni and Kessler 2013; Springer et al. 2015), we investigated the lipid composition of PGs during natural senescence in *ccd4-2*. Chloroplasts were isolated from 3-month-old plants. Isolated membranes (corresponding to 30 mg of chlorophyll) were homogenized with a Dounce homogenizer and separated by flotation on a standard-sized sucrose-gradient (25 × 89 mm) (Figure 3.7A). The experiment was simultaneously and fortuitously carried out on a senescing unrelated plant (*nap13*::35S:NAP13-YFP). The upper part of the gradient, corresponding to PGs, appeared orange for *ccd4-2* while it is normally pale-yellow as shown with the 35S:NAP13-YFP gradient. The visible difference between the two gradients was unexpected and impressive leading us

to use 35S:NAP13-YFP experiment as a control (Ctrl) (Figure 3.7A). Knowing that an overexpressor is not the ideal control, we compared the overall lipid content of the 35S:NAP13-YFP line with WT plants. Fortunately, the lipid profile of 35S:NAP13-YFP showed no statistical discrimination with the WT (data not shown). To study PG lipid composition, fractions of 1 mL were collected from the 30-mg-chlorophyll gradient described above. The 4 first fractions on the top of the gradient were pooled and designated as isolated PGs hereafter.

The visible difference observed in isolated PGs led us to carry out a quick spectroscopic analysis (Figure 3.7B). Thirty microliters of PGs were subjected to a lipid extraction with ethyl acetate. To attain a 3-fold concentration, solvent was evaporated and the lipid pellet was dissolved in 10 µL of ethyl acetate. The absorption spectra of the PG lipid extracts revealed a carotenoid-typical peak composed of maxima at 420, 450 and 470 nm for *ccd4-2* which was absent in the control (Figure 3.7B). A calibration curve established with dilution of a commercial β-carotene standard in ethyl acetate allowed a relative quantification of total carotenoids (Figure 3.7C). Carotenoid content was 5-fold higher in *ccd4-2* PGs than in the control explaining the visible phenotype of the gradient.

To further investigate the particularity of *ccd4-2* PGs, profiling was executed by HPLC on lipids extracted from 400 µL of isolated PGs. Major compounds are shown by comparable-scaled chromatograms in Figure 3.8. The typical PG prenylquinones were observed in both samples, namely α-tocopherol, vitamin K, plastochromanol and plastoquinone. MGDG 18:3/16:3 appeared as the dominant galactolipid in both PG extracts. Two compounds at m/z 255.2320 (RT: 1.25 min) and m/z 283.2632 (RT: 1.66 min) were tentatively identified as fatty acids 16:0 ($C_{16}H_{31}O_2$, error = -1.6 ppm) and 18:0 ($C_{18}H_{35}O_2$, error = -1.8 ppm), respectively. Chemical formula of FA 16:0 is $C_{16}H_{32}O_2$ and FA 18:0 is $C_{18}H_{36}O_2$ obviously a hydrogen molecule is missing in our predictions as expected in negative mode acquisition $[M-H]^-$.

For the kinds of analyses performed hereafter, the normalization of PG concentration remains critical step. Here we chose to consider the total amount of prenylquinone as an internal standard for PG concentration (Lundquist et al. 2013). Thus relative intensity of α-tocopherol-quinone, α-, δ-, γ-tocopherol, vitamin K, plastochromanol-8 and plastoquinone were added up and used to normalize our data. Noteworthy, these prenylquinone contents were not significantly affected by the loss of CCD4 in a whole plant extract (Figure 3.5B + data not shown). A better overview of PG variation was obtained by calculating the fold change of lipid normalized intensity between *ccd4-2* and Ctrl. Results are summarized in Table 3.2 and showed a 5-fold and a 3-fold concentration of β-carotene and lutein, respectively, in *ccd4-2*. At the opposite, fatty acid 16:0 and 18:0 concentration was about 2 times higher in Ctrl. In addition, galactolipids MGDG 18:3/16:3 and 18:3/18:3 were about 2 to 3 times more abundant in *ccd4-2*.

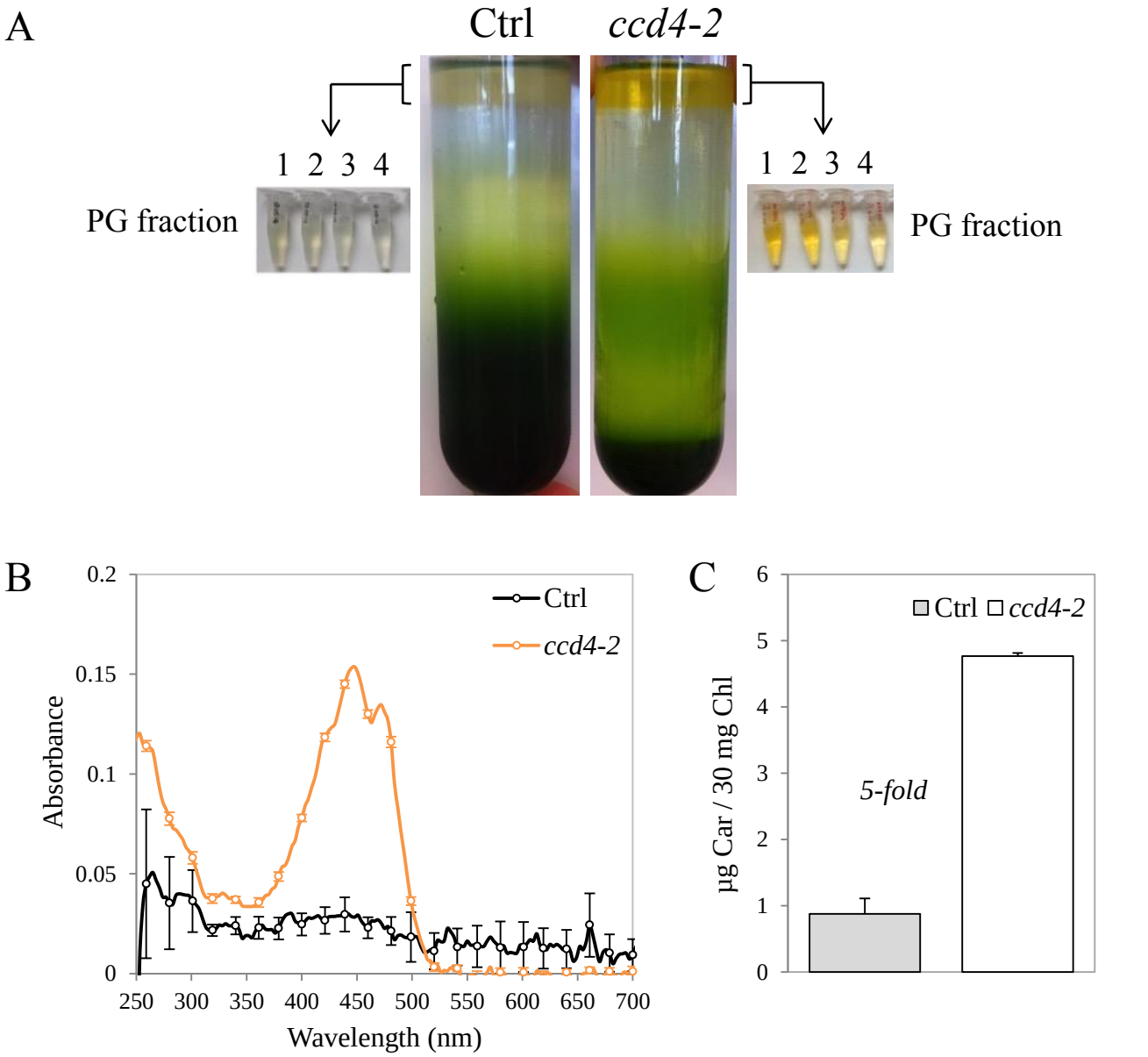

Figure 3.7 Carotenoids accumulated in senescent plastoglobules of *ccd4-2*.
(**A**) Chloroplast membrane fractionation. Naturally senescent *ccd4-2* rosettes (3 months) were used for chloroplast isolation and a chlorophyll-equivalent of 30 mg of membranes were loaded under a discontinuous sucrose gradient (5%-45%). After floatation centrifugation, fractions of 1 mL were collected from the top to the bottom of the gradient (no.1-36). Fractions 1 to 4 were pooled and considered as the plastoglobule fraction. Besides, the experiment was carried out on control (Ctrl, 35S:NAP13-YFP) plants in which *CCD4* gene is intact and thus CCD4 native protein is functional.
(**B**) Plastoglobule fraction from the gradient showed in (A) were examined by spectrophotometry. Lipids were extracted with ethyl acetate. Absorption spectrum of plastoglobule lipid extracts are shown. Three maxima around 450 nm, typical of carotenoid absorption spectra, were detected in *ccd4-2* PGs.
(**C**) Quantification of total carotenoid contents based on a calibration curve established with dilutions of β-carotene in ethyl acetate. Absorbance at 448 nm was recorded. Carotenoid content is expressed in µg of β-carotene equivalent per total membranes loaded (mg of chlorophyll).

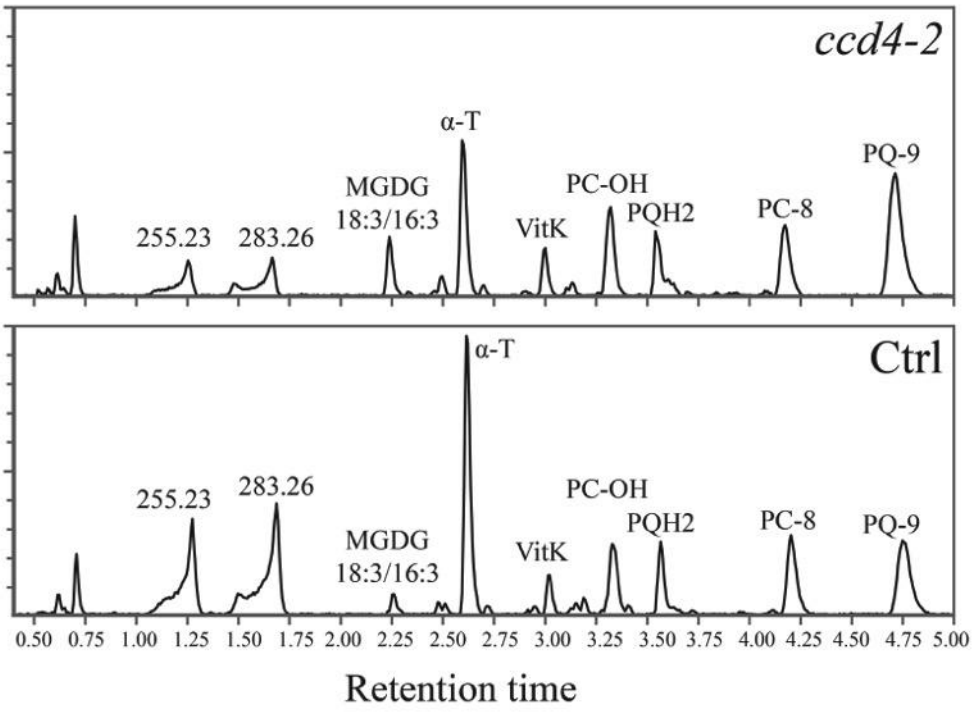

Figure 3.8 Prenyllipid and carotenoid profiling in plastoglobules of *ccd4-2* under natural senescence. Chromatograms obtained from carotenoid-targeted HPLC analysis of plastoglobule fraction (no.1-4 mixed) showing predominant lipids in PGs. Two compounds at m/z 255.23 and 283.26 were tentatively identified as 16:0 and 18:0 fatty acids, respectively. From relative peak intensity, fold change between *ccd4-2* and Ctrl were calculated and presented in Table 3.2.

Table 3.2 Lipid content from PGs of *ccd4-2* compared with PGs of 35S:NAP13-YFP.

PG Lipid	Fold change
β-Carotene	5.21
MGDG-18:3/16:3	3.25
Lutein	3.20
MGDG-18:3/18:3	2.06
Plastoquinone	1.96
Phylloquinone	1.44
Plastoquinol	1.06
Plastochromanol	1.06
α-Tocopherol-quinone	-1.02
DGDG-18:1/18:3	-1.23
MGDG-18:2/18:3	-1.44
α-Tocopherol	-1.50
δ-Tocopherol	-1.63
γ-Tocopherol	-1.81
FA 16:0	-2.26
FA 18:0	-2.49

3.5 Enhanced carotenoid degradation in 35S:CCD4

To assess the effects of increased *CCD4* expression on the degradation of carotenoids, we investigated the lipid contents in normal and senescent leaves of transgenic *A.thaliana* plants constitutively overexpressing *CCD4* by HPLC analysis. Senescence was induced in leaves of the two independent lines 35S:CCD4.2 and 35S:CCD4.4, as well as in WT, *ccd4-2* and *ccd4-4* (*n=5*). Untreated leaves were collected as well (*n=3*). Prenylquinones and carotenoids were subsequently extracted with an equal volume mixture of tetrahydrofuran and methanol. Lipid extracts were subjected to untargeted analysis with UHPLC-APCI-QTOFMS and to carotenoid-targeted analysis with UHPLC-DAD following two adapted protocols.

Data obtained from untargeted HPLC were used to detect statistical divergence with partial least squares-discriminant analyses (PLS-DA). Our findings underline an absence of statistical difference between WT and 35S:CCD4 under standard growth conditions (data not shown), whereas senescence resulted in genotype-clustering with the first component explaining 26.9% of the variability (Figure 3.9A). Under senescence conditions, the PLS-DA model was validated with a permutation test (*n= 200*; Q_2 = 0.0, -0.218). As expected, 35S:CCD4.2 and 35S:CCD4.4 displayed a similar lipid profile opposing the one of WT. The loading plot was investigated to point out the main compounds responsible for the discrimination between WT and 35S:CCD4. Outlying compounds were identified whenever possible (Figure 3.9B) and relative quantifications subjected to Student's T-test were assessed. In brief, WT accumulated significantly more lutein and β-carotene than 35S:CCD4. What is more, an unidentified compound at m/z 400.3339 (RT: 2.41 min) was 3 times higher in WT. Polar lipids such as MGDG 18:3/16:3, 18:3/18:3, DGDG 18:3/18:3 and PE 18:2/16:0 were more abundant in 35S:CCD4 suggesting a delayed degradation of galactolipids and phospholipids in the overexpressor. Potential cleavage products would be predicted to appear at the opposite of carotenoids in the lower left quadrant. Unfortunately, no outlying compounds were statistically significant except MGDG 18:3/18:3 in this quarter of the plot.

The carotenoid-targeted HPLC enabled an absolute and accurate quantification of carotenoids (Figure 3.10). On the whole, the total carotenoid levels in senescent leaves of 35S:CCD4 (63.7 $\mu g \cdot g^{-1}$ FW) were 1.8 times lower than those of the WT (113.57 $\mu g \cdot g^{-1}$ FW) and 2.3 times lower than those of *ccd4* (149.4 $\mu g \cdot g^{-1}$ FW). More precisely, the contents of β-carotene, lutein and violaxanthin were all significantly reduced in 35S:CCD4 while neoxanthin was not (Figure 3.10). Neoxanthin and violaxanthin contents were the least affected by the loss-of-function mutation (*ccd4*). Contrastingly, violaxanthin was reduced in 35S:CCD4 compared with WT (about 3 fold).

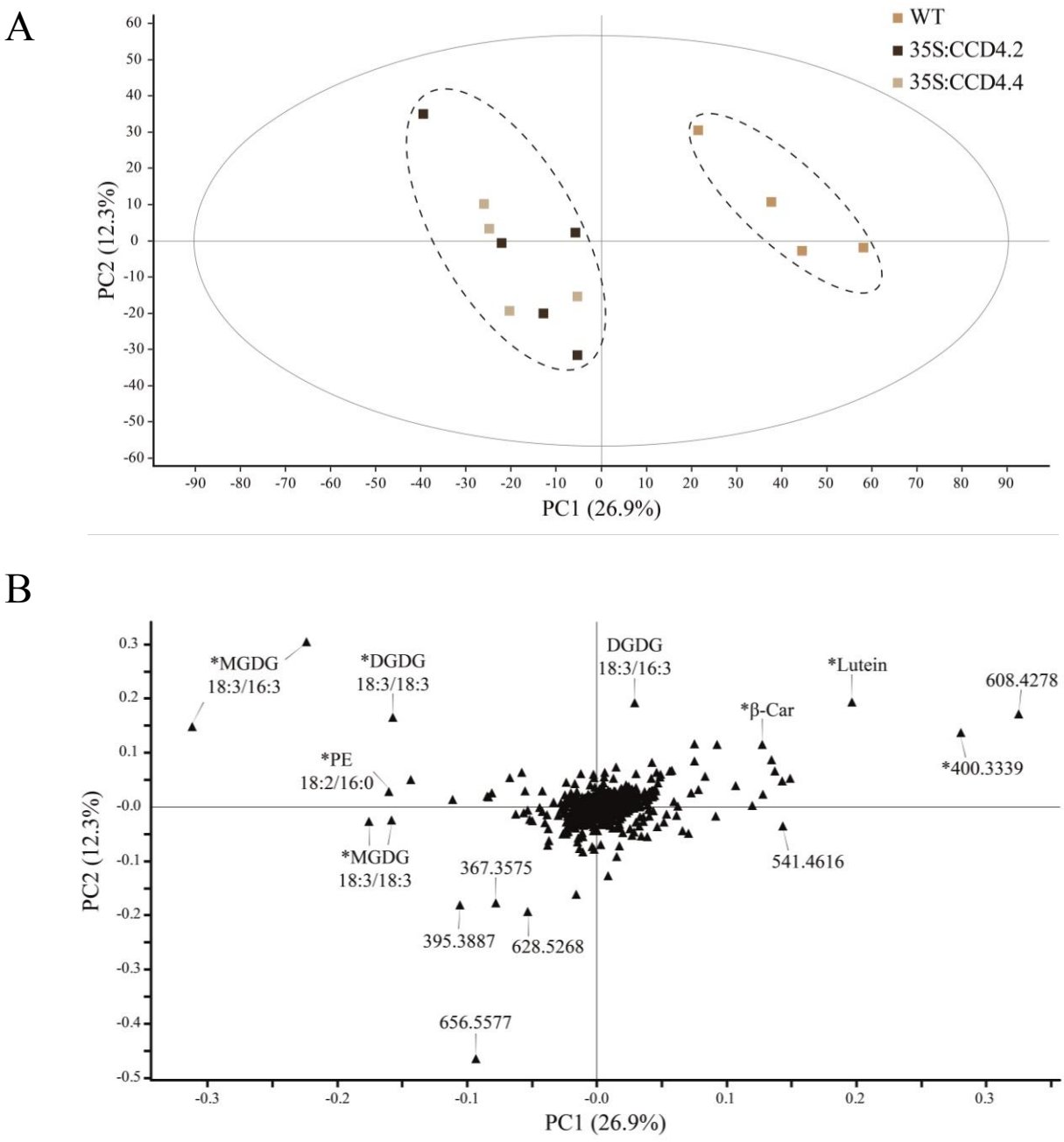

Figure 3.9 Constitutive expression of CCD4 resulted in a distinct lipid profile during dark-induced senescence in leaves when compared with WT.

Detached leaves were placed in darkness for 8 d prior to lipid extraction (*n=5*). Lipids were analyzed by UHPLC-APCI-QTOFMS.

(**A**) Discrimination was evaluated with a PLS-DA in which outlying samples were removed prior to data processing (one WT and one 35S:CCD4.4).

(**B**) Compounds responsible for the difference between 35S:CCD4 and WT are indicated on the loading plot. *Statistically significant according Student's T-test (unpaired heteroscedastic, two-tailed).

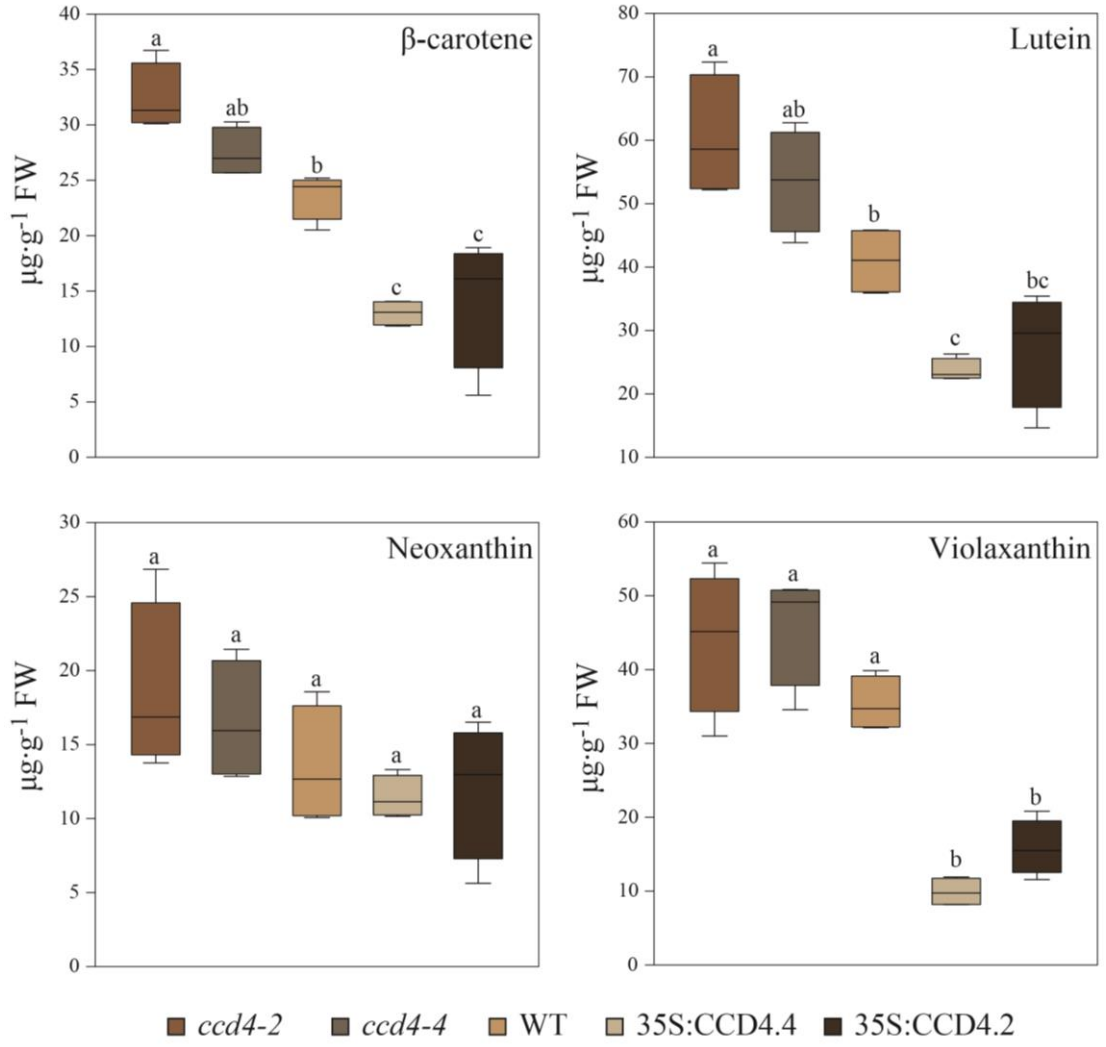

Figure 3.10 Reduced level of photosynthesis-related carotenoids during senescence in 35S:CCD4 as an "over-complemented" phenotype.
Detached leaves were placed in darkness for 8 d prior to lipid extraction (*n=5*). Lipids were separated on HPLC-DAD following the carotenoid-targeting protocol. Absolute quantification of carotenoids was calculated on the basis of calibration curves obtained with pure standards. Box plots created with SigmaPlot are shown. Statistical differences across genotypes were assessed with a one-way ANOVA. Pairwise multiple comparisons (Holm-Sidak method) revealed significant differences (letters are distributed accordingly, $P<0.05$).

3.6 Deciphering protein-protein interaction to understand regulatory pathway

CCD4 is a carotenoid cleavage dioxygenase that require a non-heme iron for its enzymatic activity. Four highly conserved histidine residues are believed to coordinate the iron in cooperation with three aspartate or glutamate residues. Whether CCD4 processes carotenoids alone or as a part of a protein complex, has not been investigated so far to our knowledge. To isolate candidate interaction partners, co-immunoprecipitation with CCD4-YFP-HA was attempted. Chloroplasts were isolated from the three following lines: 35S:CCD4-YFP, 35S:cYFP-HA (Ctrl1) and an unrelated control line expressing 35S:NAP13-YFP-HA (Ctrl2). After the solubilization of chloroplasts, co-immunoprecipitation with anti-HA microbeads was performed. Following protein in-gel tryptic digestion, qualitative (LTQ ion trap) and quantitative (Synapt Q-TOF) mass spectrometric identification of co-immunoprecipitated proteins were carried out to identify candidate interaction partners.

In the LTQ analysis (Table 3.3), three peptides (LTESGDIETIGR, TDPITGETFAFR, NGPNPQFLPR) were detected for CCD4 with a total of 49 peptide spectral matches (PSMs) (Coverage 5.71%), putting CCD4 at the second rank for PSM abundance after the common contamination chaperonin 60 beta (51 PSMs). Noteworthy, CCD4 was absent from our two controls suggesting that our purification procedure was successful. In addition, a small list of 24 *A. thaliana* proteins was obtained, from which eight proteins were not detected in the two controls. An interesting fact from the qualitative analysis was the presence of NCED5, from which two PSMs of the peptide VTDNGDLETIGR were recorded (Coverage 2.04%) with a medium confidence.

In the Synapt analysis (Table 3.4), CCD4 was the dominant protein in the three technical replicates with 27.555 fmol found on the column (1/20 of the sample injected). Together with CCD4, 53 *A. thaliana* proteins were identified and quantified whenever possible. A first attempt of short listing led us to normalize our data based on the bait quantification and to subsequently calculate the fold change between CCD4 and each control sample. Fold change calculations did not allow the short listing of significantly more concentrated proteins in CCD4 sample, thus data were filtered against unspecific matches by removing proteins found in both controls. After processing, quantitative data pointed out seven proteins which were exclusively found in CCD4 sample. Interestingly, the four most abundant proteins are involved in the NADH dehydrogenase-like complex, namely NdhN, PnsB1, PnsL1 and NdhU (Ifuku et al. 2011).

Both analyses showed a low overlapping rate, only 12 from 24 proteins of the LTQ were also identified by Synapt. What is more, among the short-listed proteins (9 in LTQ and 8 in Synapt), CCD4 was the sole shared protein. In other words, NCED5 and the four NDH-related proteins were pinpointed by only one of the two analyses, thus weakening our results. Being much more sensitive, the Synapt analysis was also supported by three technical replicates. From our point of view, the identification of four proteins related to the NDH complex was more reliable than the presence of NCED5.

Table 3.3 Qualitative mass spectrometric identification of co-immunoprecipitated proteins. The complete set of LTQ data is shown: #, peptide spectral matches; %, coverage.

1	2	AGI code	Description	CCD4			[a]Ctrl1			[a]Ctrl2		
				#	/	%	#	/	%	#	/	%
x	x	AT4G19170	Carotenoid cleavage dioxygenase 4, CCD4	49	/	5.71	0	/	0	0	/	0
		AT1G30100	Nine-cis-epoxycarotenoid dioxygenase 5, NCED5	2	/	2.04	0	/	0	0	/	0
		AT1G78340	Glutathione S-transferase TAU 22, GSTU22	1	/	5.5	0	/	0	0	/	0
		AT5G01420	Glutaredoxin family protein	1	/	3.99	0	/	0	0	/	0
		AT3G28690	Protein kinase superfamily protein	1	/	2.93	0	/	0	0	/	0
		AT1G10417	Uncharacterized protein	1	/	2.55	0	/	0	0	/	0
		AT1G27595	Symplekin C domain-containing protein, TANG1	1	/	1.25	0	/	0	0	/	0
		AT2G27090	Uncharacterized protein, DUF630 and DUF632	1	/	0.94	0	/	0	0	/	0
		AT4G16960	Disease resistance protein (TIR-NBS-LRR class) family	1	/	0.96	0	/	0	0	/	0
	x	AT1G55490	Chaperonin 60 beta, CPN60B, LEN1	51	/	11	0	/	0	64	/	11
	x	AT2G28000	Chaperonin 60 alpha, CPN60A, CH-CPN60A, SLP	34	/	12.29	0	/	0	72	/	14.51
		AT4G30640	RNI-like superfamily protein	3	/	2.99	0	/	0	3	/	2.99
	x	AT1G42970	Glyceraldehyde-3-phosphate dehydrogenase B subunit, GAPB	3	/	6.04	0	/	0	20	/	6.04
	x	AT3G05560	Ribosomal L22e protein family	1	/	10.48	3	/	9.68	0	/	0
		AT1G43980	Tetratricopeptide repeat (TPR)-like superfamily protein	1	/	1.29	0	/	0	1	/	1.29
	x	ATCG00490	Ribulose-bisphosphate carboxylases, RBCL	22	/	8.77	7	/	4.18	44	/	11.9
	x	ATCG00120	ATP synthase subunit alpha, ATPA	12	/	9.07	1	/	1.78	35	/	6.51
	x	ATCG00480	ATP synthase subunit beta, ATPB, PB	8	/	7.63	13	/	8.23	23	/	10.44
	x	AT1G05190	Ribosomal protein L6 family, EMB2394	6	/	4.93	15	/	4.93	6	/	4.93
	x	ATCG00280	Photosystem II reaction center protein, CPSBC	6	/	3.38	6	/	3.38	11	/	3.38
		AT2G24820	Translocon at the inner envelope membrane of chloroplasts 55-II , TIC55-II	4	/	1.86	1	/	1.86	6	/	1.86
x	x	AT4G27440	Protochlorophyllide oxidoreductase B, PORB	2	/	2.99	5	/	2.99	16	/	2.99
		AT5G16780	SART-1 family, DOT2, MDF	2	/	1.1	1	/	1.1	1	/	1.1
		AT3G47470	Light-harvesting chlorophyll-protein complex I subunit A4, LHCA4, CAB4	1	/	4.78	3	/	4.78	10	/	4.78
	x	AT4G20360	RAB GTPase homolog E1B, ATRAB8D, RABE1b	1	/	2.31	15	/	4.83	16	/	4.62

[a]Ctrl1 (cYFP-HA), Ctrl2 (NAP13-YFP-HA).
[1]Genes repressed by β-cyclocitral (Ramel et al. 2012), [2]Proteins found in Synapt analysis of CCD4 co-IP.

Table 3.4 Quantitative mass spectrometric identification of co-immunoprecipitated proteins. Filtered synapt data are shown and expressed in fmoles detected on the column.

1	2	3	AGI code	Loc	Description	CCD4	[a]Ctrl1	[a]Ctrl2
	x	x	AT4G19170	Plastid	Carotenoid cleavage dioxygenase 4, CCD4	27.555	0	0
			AT5G21430	Plastid	NADH dehydrogenase-like complex U, NdhU, CRRL	0.741	0	0
			AT2G39470	Plastid	Photosynthetic NDH subcomplex L1, PnsL1, PPL2	0.642	0	0
	x		AT5G58260	Plastid	NADH dehydrogenase-like complex N, NdhN	0.536	0	0
x			AT1G15980	Plastid	Photosynthetic NDH subcomplex B1, PnsB1, NDF1, NDH48	0.320	0	0
			AT3G52340	Cytosol	Sucrose-6F-phosphate phosphohydrolase 2 , SPP2	0.171	0	0
			ATCG00130	Plastid	ATPase F subunit, ATPF	0.145	0	0
			AT5G15510	-	TPX2 (targeting protein for Xklp2) protein family	0.117	0	0
			AT2G34420	Plastid	Photosystem II light harvesting complex gene B1B2, LHB1B2	2.470	0	2.727
			AT5G38420	Plastid	Rubisco small subunit 2B, RBCS2B	1.622	0	1.081
			AT2G39730	Plastid	Rubisco activase, RCA	1.302	0	4.296
			AT5G01530	Plastid	Light harvesting complex photosystem II, LHCB4.1	0.372	0	1.569
		x	AT3G05560	Cytosol	Ribosomal L22e protein family	0.368	1.091	0
			AT3G46740	Plastid	Translocon at the outer envelope membrane of chloroplasts 75-III, TOC75-III	0.159	0	0.804

[a]Ctrl1 (cYFP-HA), Ctrl2 (NAP13-YFP-HA).
[1]Genes coexpressing with CCD4 (ATTED II), [2]Genes repressed by β-cyclocitral (Ramel et al. 2012), [3]Proteins found in LTQ analysis of CCD4 co-IP.

4 Discussion

4.1 Plastoglobule proteomes revealed CCD4, a member of the carotenoid cleavage dioxygenase family

In the last decade, PGs have steadily become a subject of high interest regarding thylakoid lipid metabolism. First thought to be only lipid storage sites, many studies revealed that PGs actively participate in lipid synthesis and repair by hosting crucial enzymes. For instance, regeneration cycles of tocopherol and plastoquinone were largely resolved and turned out to occur at the PG interface. However, to date very little is known about the turnover of photosynthesis-related carotenoids. Interestingly, three proteomics studies revealed the presence of CCD4 in PGs (Vidi et al. 2006; Ytterberg et al. 2006; Lundquist et al. 2012b).

CCD4 belongs to the carotenoid cleavage dioxygenase family, which is composed of nine members in *A. thaliana*. Across the plant kingdom, CCD4 was shown to be a multifunctional enzyme that carries out a variety of related reactions depending on the timing and localization of gene expression. In *A. thaliana* the exact mechanism is still unsolved. Interestingly, the presence of AtCCD4 was correlated with the formation of C_{13}-apocarotenoid glycosides upon PSY overexpression (Lätari et al. 2015). As suggested by recent literature, CCD4 may preferentially cleave 7',8' double bonds in a large set of carotenoids releasing a colored apocarotenoid (e.g. β-citraurin, α-citraurin, β-apo-8'-carotenal) and a signaling molecule (β-cyclocitral as well as other volatiles) (Rodrigo et al. 2013). However, several cases reporting that CCD4 produced only achromatic compounds were studied.

For instance, in *Brassica napus* the interruption of *CCD4* by a CACTA-like transposon resulted in yellow flowers instead of white (Zhang et al. 2015). CCD4 was also reported to be responsible for white color formation in *Chrysanthemum* petals (Ohmiya et al. 2006).

Thus to test whether CCD4 is responsible for white color formation in *A. thaliana* flowers, we analyzed *ccd4* mutants under standard growth conditions. But, petal color did not change and no visible phenotype was observed suggesting that AtCCD4 does not degrade carotenoids in the chromoplast.

Not only functioning as pollinator attractants in flowers, carotenoids are antioxidants and major light harvesting pigments for photosynthesis. Consequently, rosettes of *ccd4* grown under standard conditions were subjected to lipidomic analysis. No significant difference in the carotenoid content was observed between *ccd4* and WT suggesting that CCD4 is not involved in carotenoid turnover under standard growth conditions. Nonetheless, we cannot exclude possible flux compensations through spontaneous carotenoid degradation and reduced carotenoid biosynthesis, thus masking the absence of CCD4. Measurements of carotenoids upon enhanced biosynthesis pathway flux (e.g. *PSY* overexpression) in *ccd4* background could clarify this question. In Lätari et al. (2015), PSY overexpressing lines were crossed with *ccd4* resulting in rapid cotyledon bleaching followed by death in the homozygous progeny. Unexpectedly, carotenoid content was reduced by about 40% in these homozygous seedlings compared to WT. Altogether these data suggest that spontaneous degradation of carotenoids, replacing the controlled degradation led by CCD4, released noxious compounds for the plant. Nevertheless, these noxious compounds seem well tolerated at natural pathway fluxes as *ccd4* mutants grew normally under standard growth conditions.

4.2 Plastoglobule localization of CCD4 and its significance

CCD4 was predicted to harbor a chloroplast transit peptide of 34 residues suggesting that CCD4 is targeted to chloroplast. In agreement with bioinformatics predictions, CCD4-6xHIS was successfully imported into isolated Pea chloroplasts *in vitro.* Noteworthy, the same conclusion, regarding CCD4 import into chloroplast, was reached in a previous study (Naested et al. 2004). What is more, we transiently expressed CCD4-YFP in tobacco protoplasts and observed a punctate fluorescent signal in chloroplasts. Similarly, Rubio et al. (2008) reported a spotty pattern for CsCCD4a-GFP in transgenic *A. thaliana* chloroplasts.

Considering the reported presence of CCD4 in PG proteomes (Vidi et al. 2006; Ytterberg et al. 2006; Lundquist et al. 2012b), we decided to demonstrate this physical interaction through two independent experiments. Using the 35S:CCD4-YFP-HA line, we transiently transformed protoplasts with the PG marker FBN1a-CFP to perform colocalization experiment by confocal microscopy. At the subcellular level, CCD4-YFP fluorescence was shown to overlap with FBN1a-CFP, strongly suggesting that CCD4 localized at PGs. Additionally, we fractionated chloroplast membranes of the 35S:CCD4-YFP-HA line onto a sucrose gradient. Immunodetection of CCD4-YFP-HA showed a typical PG distribution as observed with FBN1a. The fact that PG proteins were also detected in the densest thylakoid fraction has two explanations. Firstly, PG might be incompletely detached from the thylakoid membrane by the procedure. Secondly, as shown by Lundquist et al. (2012) some PG

proteins are partitioning between PG, thylakoid and stroma. Regarding CCD4, which represents 3.3 % of the PG proteome mass, they reported a PG relative enrichment of 18 fold compared with thylakoid. It means that CCD4 is found in PG and thylakoid, but more enriched in PG. However, this enrichment is not as high as observed for ABC1K9 (440 fold) for instance (Lundquist et al. 2012b).

The dual localization of CCD4 in PGs and thylakoid membranes raised the question whether carotenoids are degraded *in situ* in thylakoid or first delocalized to the PG core. Presumably, if the delocalization occurred, we would observe an anomalous accumulation of carotenoids in absence of CCD4. To resolve this question, we isolated PGs of naturally senescent *ccd4*. We noticed that PG fractions were distinctly more orange in *ccd4* than usually. Untargeted lipid analysis showed a clear correlation between this visible change in color and an increased carotenoid content. Indeed, PGs of *ccd4* contained 5- and 3-fold more β-carotene and lutein, respectively. In addition, PGs of *abc1k1abc1k3*, in which *CCD4* is downregulated, were previously reported to contain more carotenoids than WT (Lundquist et al. 2013), supporting a movement of carotenoids toward PGs for degradation. Provided that carotenoid catabolism really occurs at the PG, carotenoid derivatives will be detected too. Despite the fact that CCD4 cleavage products were unidentifiable in our study, a recent work reported the presence of carotenoid oxidation products in senescent PGs from barley (Springer et al. 2015). Moreover, it is interesting to note that PGs in senescent beech leaves were reported to contain carotenoid esters (Tevini and Steinmüller 1985). Thus, it is likely that carotenoids and their breakdown products are relocated to PGs and quickly further metabolized.

4.3 Two approaches to evaluate the implication of CCD4 in carotenoid breakdown during senescence

Knockout as well as overexpressing mutants are two valuable tools to study the function of a protein *in vivo*. Thus, to identify the physiological role of CCD4 in *A. thaliana*, abiotic (light) and biotic (*P. syringae* infection) stresses were applied to *ccd4* mutants. Considering the reported dark-induced accumulation of CCD4 in PGs (Ytterberg et al. 2006), we also subjected *ccd4* to dark-induced senescence. Lipid profiling and PCA revealed that *ccd4* and WT were indistinguishable under *P. syringae* infection and light stress. The absence of a distinctive phenotype under light stress was in agreement with a previous study in which CCD4 was shown to be down-regulated under high light (Ramel et al. 2012). Interestingly, a great difference between *ccd4* and WT, regarding phenotype and lipid profile, was detected under dark-induced senescence. Carotenoids (i.e. lutein, β-carotene, violaxanthin and neoxanthin) were the main compounds responsible for this discrimination and were accumulated in *ccd4*. Our results pointed out senescence as the most perturbed physiological state in *ccd4*. In the meantime, Gonzalez-Jorge et al. (2013) reported CCD4 as a major negative regulator of β-carotene in seeds and senescent leaves, in accordance with our observations. To bring novelty, we engineered plants constitutively expressing CCD4-YFP-HA in *ccd4* background (35S:CCD4).

As a starting point, WT, *ccd4* and 35S:CCD4 were analyzed under standard growth conditions showing no apparent phenotype and a similar carotenoid content. Under dark-induced senescence, we observed a rapid disappearance of carotenoid-like pigmentation in CCD4 overexpressing lines, what we called an "over-complemented" phenotype. Untargeted lipid analysis showed that WT accumulated significantly more lutein and β-carotene than 35S:CCD4. In addition, we observed that

other senescence-related processes are affected at random. For example, degradation of galactolipids and phospholipids were slowed down in 35S:CCD4. One major problem when working with senescence is the lack of consistency in the rates of senescence between individuals, leaves or even cells within the same leaf. Although the induction of artificial senescence by darkness/nutrient starvation synchronizes the senescence and allows minimizing the disparity between samples, an inconsistency was still observed. We should bear in mind that dark-induced senescence as well as methyl jasmonate-induced senescence are not a perfect mimic of natural senescence (Buchanan-Wollaston et al. 2005; Springer et al. 2015). Then, we focused our attention on carotenoids with a targeted analysis and observed a decrease in lutein, β-carotene and violaxanthin contents in 35S:CCD4 compared with WT.

Our study tends to support the idea of sequential cleavage reactions of carotenoid precursors (e.g. symmetrical cleavage or collaborative cleavage); preventing the accumulation of colored C_{30}-apocarotenoids in *A. thaliana* leaves. If, as suggested by Huang et al. (2009), CCD4 is predominantly able to cleave the colored apocarotenoid β-apo-8'-carotenal rather than β-carotene, another enzyme may be responsible for the cleavage step that enables the production of β-apo-8'-carotenal from β-carotene *in planta*. In that case, we should have observed an accumulation of this apocarotenoid concomitantly with the disappearance of β-carotene in *ccd4*. But actually β-carotene content was increased in *ccd4* and strongly reduced in 35S:CCD4 compared with WT, suggesting a defect at an earlier stage of the breakdown. In addition, the untargeted lipid analysis failed to reveal an accumulation of β-apo-8'-carotenal in *ccd4*. Together, our results provide evidence that the cleavage of the β-apo-8'-carotenal observed *in vitro* (Huang et al. 2009b) is probably not occurring *in vivo* in Arabidopsis. As observed for VvCCD1 (Lashbrooke et al. 2013), a divergence between the *in vitro* enzyme activity and the *in situ* activity is rather likely.

Based on the characterization of CCD4 loss-of-function mutants and complemented lines, we showed that an apparent phenotype, as well as an anomalous carotenoid content were exclusively occurring under senescence. Apart from pleiotropic effects that may occur, we identified lutein, β-carotene, violaxanthin and neoxanthin as the *in vivo* substrates of AtCCD4 in *ccd4* senescent leaves. Lutein, β-carotene, violaxanthin have been further confirmed as substrates using CCD4 overexpressing plants, while the effect on neoxanthin was not significant. Further stress and condition screening on *ccd4* and 35S:CCD4 should be performed to determine whether other conditions could perturb carotenoid content. In conclusion, together with previous reports our results suggest that AtCCD4 actively degrades carotenoids during the chloroplast to gerontoplast transition.

4.4 Potential interactions with NCED5 and the chloroplast NDH complex

Qualitative mass spectrometric analysis identified NCED5 co-immunoprecipitating specifically with CCD4. Both were previously reported to interact with VAR3/OZ1 in a yeast two-hybrid assay (Naested et al. 2004), NCED5 and CCD4 also shared a close localization at the thylakoid membrane and PG, respectively (Tan et al. 2003). Thus, their interaction is probable and suggests that sequential cleavage reactions may occur as observed for CCD7 and CCD8 (Schwartz et al. 2004). NCED5 is thought to catalyze the 11',12' cleavage of 9'-cis-neoxanthin and 9'-cis-violaxanthin to xanthoxin and a C_{25} aldehyde. Xanthoxin is known to be further metabolized to produce ABA,

whereas the fate of the C_{25} by-product is uncertain (Walter et al. 2010). Following *in vitro* enzyme assays, C_{25} apocarotenal was detected (Schwartz et al. 1997; Qin and Zeevaart 1999; Iuchi et al. 2000) but appeared to be rapidly metabolized *in planta* (Parry and Horgan 1991; Schwartz et al. 2003). Interestingly, AtCCD4 has been shown to cleave the β-apo-8'-carotenal *in vitro* (Huang et al. 2009b). Unfortunately, NCED5 was not confirmed in the quantitative proteomics experiment carried out on the Synapt instrument. Thus, whether NCED5 cooperates with CCD4 remains to be elucidated.

On the other hand, quantitative proteomics analysis revealed four proteins which are involved in the NADH dehydrogenase-like complex (also known as NDH), i.e. NdhN, PnsB1, PnsL1 and NdhU/CRRL (Ifuku et al. 2011). The NADH dehydrogenase-like complex is known to protect the photosynthetic apparatus against oxidative stress (Endo et al. 1999; Wang et al. 2006) by mediating the PSI-cyclic electron transport from reduced ferredoxin (Fd) to plastoquinone (PQ) (Peng et al. 2008). The electron donor of this cyclic electron transport was first thought to be NAD(P)H. However, the discovery of the CRR31 subunit, containing a Src homology 3 domain-like structure, pointed to Fd as electron donor (Yamamoto et al. 2011). Interestingly, the plant-type ferredoxins are iron-sulfur [2Fe-2S] proteins (Fukuyama 2004), in which the modification between electron acceptor and electron donor is operated by changing the oxidative state of the iron atom (+2, +3). As previously mentioned, CCD4 is a carotenoid cleavage dioxygenase that requires a non-heme iron (+2) for its enzymatic activity. The iron cofactor is coordinated by four histidine residues, thus leaving two free coordination sites on the iron for the catalysis, as observed with bacterial lignostilbene dioxygenases (LSD) (Tan et al. 1997; Han et al. 2002). Few detailed biochemical studies of these enzymes exist (Bugg and Ramaswamy 2008; Harrison and Bugg 2014). Harrison and Bugg (2014) reviewed the catalytic mechanism of CCD and proposed two possible mechanisms for the cleavage reaction, (1) Dioxetane formation (2) Criegee rearrangement, which are summarized in Figure 3.11. However, the exact mechanism behind the oxidative cleavage of carotenoids remains to be elucidated experimentally. As shown in Figure 3.11, the oxidative state of the iron cofactor should switch from +2 to +3 during the activation by molecular oxygen. In the light of our results and due to the shared iron between CCD4 and Fd, we hypothesized that one of the electron transfer occurring at the CCD4 iron level may be mediated by the NDH-like complex, which could accept or donate electrons.

5 Conclusion

In green leaf tissues the metabolic turnover of carotenoids such as lutein, β-carotene, violaxanthin and neoxanthin seems affected by neither the lack nor the overexpression of CCD4 as abundance comparable to WT was established by HPLC-MS. This suggests that the substrate accessibility is a factor governing carotenoid breakdown as previously suggested (Rodrigo et al. 2013). If no effects on carotenoid concentrations were observed in 35S:CCD4 plants under standard growth conditions, we should bear in mind that mechanisms such as *de novo* synthesis of carotenoids in healthy plants may compensate for degradation. However, this hypothesis is not supported by the mechanism proposed for the formation of white petal color in chrysanthemum (Ohmiya et al. 2006) where carotenoid biosynthesis continues to take place while CmCCD4a degrades carotenoids causing white

color. Whether carotenoid de novo biosynthesis masks the effect of CCD4 overexpression in healthy plants could be tested by using inhibitors of carotenoid synthesis, such as norflurazon and fluridone (Bartels and Watson 1978).

Interestingly, a significant difference in carotenoid contents was found during senescence which strongly correlates with the genotype (Figure 3.10). In a nutshell, major carotenoids were accumulated in *ccd4* whilst they were highly degraded in 35S:CCD4 compared to the wild type. These results suggest that carotenoids are subjected to a senescence-specific activity which enables CCD4 to degrade them. It is well known that carotenoids are associated with LHC proteins in the thylakoid membrane, thus during senescence they might be released into the lipid bilayer and possibly be transported to the PG where a large amount of CCD4 accumulates (Biswal 1995). To support this hypothesis, we isolated PGs from membranes of *ccd4* and Ctrl senescent plants onto a sucrose gradient and actually observed an increased accumulation of β-carotene and lutein in PGs of *ccd4*.

In conclusion, the spatio-temporal regulated gene expression, together with substrate availability through compartmentalization (Lashbrooke et al. 2013), as well as CCD4 ability to cleave a wide range of carotenoids and apocarotenoids are probably key factor in the regulation of carotenoid homeostasis in green leaves.

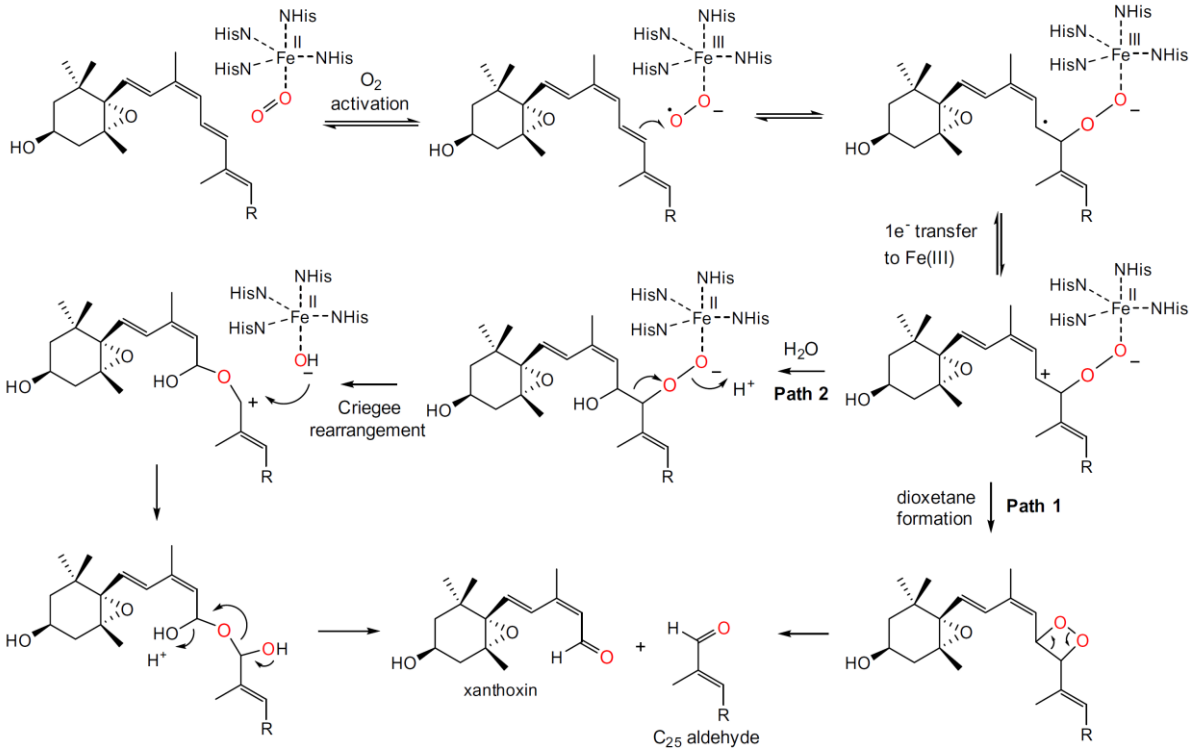

Figure 3.11 Two proposed mechanisms for the cleavage of carotenoids (here 9'-cis-neoxanthin) by CCD enzymes: (1) Formation of a dioxetane intermediate, (2) Criegee rearrangement. Figure from Harrison and Bugg 2014.

Chapter IV

Materials and methods

1 Materials

1.1 Biological material

Plants

Wild type (WT) refers to *Arabidopsis thaliana* var. Columbia 0, unless stated otherwise.

Arabidopsis T-DNA insertion mutants from the Salk Institute Genome Analysis Laboratory (Alonso et al. 2003) were obtained from the European Arabidopsis Stock Center (*http://arabidopsis.info/*, (Scholl et al. 2000)). Albino mutants (*pac*, *cla1* and *ppi2*) were kindly provided by Dr. Birgit Agne (Martin Luther University, Halle a. S., Germany).

Pisum sativum seeds were obtained from Bigler Samen AG (*www.biglersamen.ch*).

Bacteria

Escherichia coli DH5α and *ccdB* Survival™ cells were from Invitrogen. *E.coli* BL21 (DE3) cells were from Novagen.

Agrobacterium tumefaciens strain C58 was kindly originally provided by Dr. Roger Kuhn then at the Institute of Plant Sciences, ETH Zurich, Switzerland.

1.2 Oligonucleotides

Primers were synthesized at Microsynth GmbH (*http://www.microsynth.ch/*) and listed in Table 4.1.

Table 4.1 Oligonucleotide names, sequences and properties.

Primer ID	Nucleotide sequence 5'→3'	Length	$T_{melting}$
Cloning			
NAP13attB1	ACAAGTTTGTACAAAAAAGCAGGCTATGAATGGTCACTGTTTATTTGCA	49 bp	132°C
NAP13attB2	GGGGACCACTTTGTACAAGAAAGCTGGGTGAGAACCAATTTGATCAATGTA	51 bp	146°C
NAP14attB1	GGGGACAAGTTTGTACAAAAAAGCAGGCTATGGCAGTGTCGACGTTTTCGAGC	53 bp	158°C
NAP14attB2	GGGGACCACTTTGTACAAGAAAGCTGGGTGAAGTGGTGGACGTTCTGCAAC	51 bp	156°C
cSSUattB1	GGGGACAAGTTTGTACAAAAAAGCAGGCTATGGCTTCCTCTATGCTCTCC	50 bp	148°C
cSSUattB2	GGGGACCACTTTGTACAAGAAAGCTGGGTGCTTCTTTCCGATTGGTGGCCA	51 bp	156°C
CCD4TopoF	CACCATGGACTCTGTTTCTTCTTCTTCC	28 bp	82°C
CCD4TopoR	CCATGGAAGCTTATTAAGGTCACTTTCC	28 bp	80°C
Genotyping			
LBpROK2	TGGACTCTTGTTCCAAACTG	20 bp	58°C
nap13-LP	TGGAGCCAAGTCAACAAGATC	21 bp	62°C
nap13-RP	GCTTCTCCACAAAGACAGTGC	21 bp	64°C
nap14-LP	AAACTACCTTTTTGCCTTGGC	21 bp	60°C
nap14-RP	CCCAATTAAGGCCCATTCTAC	21 bp	62°C
ccd4-2LP	CTGTCACTTAACGGCGCTTAC	21 bp	64°C
ccd4-2RP	TTAGCGTCCATCACCAGAAAC	21 bp	62°C
ccd4-4LP	TATTCTCGATGACGTCTCCG	20 bp	60°C
ccd4-4RP	GTGTGCAACAACACTATGCG	20 bp	60°C
Sequencing			
nap13_seqF2	CAGAATCCTGATCATCAGGTAG	22 bp	64°C
nap13_seqR2	CCCATCTGGTCAGACTCATC	20 bp	62°C
nap14_seqF2	GCTTGATCTTTGGGAAGAGTG	21 bp	62°C
nap14_seqR2	AGCCTCCACTTAGTAACTGGG	21 bp	64°C
qRT-PCR			
CCD4-For	GGTTCTCCGGTTGGTACTGA	20 bp	62°C
CCD4-Rev	GCATGAACCAGATCCATCCT	20 bp	60°C
CCD1-For	TTGACATGGTCAGTGGGAAA	20 bp	58°C
CCD1-Rev	TCCGGTAACCTTTGCGATAC	20 bp	60°C
Actin-For	TGGAATCCACGAGACAACCTA	21 bp	62°C
Actin-Rev	TTCTGTGAACGATTCCTGGAC	21 bp	62°C
TAIL-PCR[1]			
LB1.1	TATTCAGTAATCTCGGCCAATATCCTAAATGTG	33 bp	90°C
LB2.1	TAAATGTGCGTGGCTTTATCTGTCTTTGTATTG	33 bp	90°C
LB3.1	TTCATCAATTCATGTAACGTTTGCTTTTCTTAT	33 bp	84°C
RB1.1	CGAACTAATAACGCTCACTGAAGGGAACTC	30 bp	88°C
RB2.1	GCATGGGTGAGATTCCTTGAAGTTGAGTAT	30 bp	86°C
RB3.1	CAAATGAAGTGCAGGTCAAACCTTGACAGT	30 bp	86°C
AD1 (12 µM)	NGTCGASWGANAWGAA	11 bp	-
AD2 (12 µM)	TGWGNAGSANCASAGA	11 bp	-
AD3 (12 µM)	AGWGNAGWANCAWAGG	11 bp	-
AD4 (16 µM)	STTGNTASTNCTNTGC	11 bp	-
AD5 (8 µM)	NTCGASTWTSGWGTT	10 bp	-
AD6 (16 µM)	WGTGNAGWANCANAGA	11 bp	-

The optimal melting temperature ($T_{melting}$) has been calculated as follow : $2 \cdot (A+T) + 4 \cdot (G+C)$.
[1]AD, arbitrary degenerate; S= G or C; W= A or T; N= A, C, G or T.

1.3 cDNA clones

cDNA clones were obtained from the Arabidopsis Biological Resource Center (*http://abrc.osu.edu/*; (Yamada et al. 2003)).

1.4 Antibodies

Antibodies specific to LHCBII and TIC40 were obtained from Agrisera AB (*http://www.agrisera.com*). The anti-HA-HRP antibody was purchased from Miltenyi Biotec (*http://www.miltenyibiotec.com*) and the anti-CBP was obtained from GenScript (*http://www.genscript.com/*). Antibodies specific to TOC75 and serum raised against FBN1a have been described (Hiltbrunner et al. 2001; Vidi et al. 2006).

1.5 Plasmids

Gateway-based vectors were used (Gateway® Technology, Invitrogen). Empty vectors contain *ccdB* gene inhibiting *E. coli* growth and were therefore propagated with *ccdB* Survival™ cells. pENTR D-TOPO and pDONR221 are entry vectors carrying attP1 and -P2 recombination sites, while p0GWA, pEarleyGate101 and pEarleyGate205 are destination vectors harboring attR1 and -R2 sites. The p0GWA vector (Busso et al. 2005), adapted for the expression in bacteria, results in a C-terminal 6xHIS fusion under the control of the T7 promoter. The two vectors specific for plant expression resulting in fusions under the control the CaMV 35S promoter, namely pEarleyGate101 and pEarleyGate205, were used for complementation in *A. thaliana* (Earley et al. 2006). The first fused a YFP-HA tag to the C-terminal of the protein of interest. The second is specifically designed for tandem affinity purification (TAP) resulting in C-terminal fusions composed of calmodulin binding peptide (CBP) and 2x IgG binding domains, the last part being removable by TEV protease cleavage.

The vector pCL62 carrying FBN1a in frame with the CFP was kindly engineered by Dr. P.A. Vidi during his thesis at the University of Neuchâtel, Switzerland (Vidi et al. 2006). The vector pEarleyGate101-CCD4 was previously engineered by Angélica Lima (Master 2008) under the guidance of Dr. C. Bréhélin (University of Bordeaux, Bordeaux, France).

1.6 Chemicals

Unless stated otherwise, the chemicals were purchased from Fluka Chemie GmbH.

2 Methods

2.1 Bioinformatics resources

Sequences were retrieved either from TAIR (*https://www.arabidopsis.org/*), NCBI (*http://www.ncbi.nlm.nih.gov/genbank/*), or from Phytozome version 10.3 (*http://phytozome.jgi.doe.gov/pz/portal.html#*). DNA microarray data were retrieved from public databases and analyzed using the Genevestigator toolbox (*https://genevestigator.com/gv/index.jsp*). Chloroplast transit peptides were predicted using ChloroP 1.1 server (*http://www.cbs.dtu.dk/services/ChloroP/*). Putative orthologues were identified using Phytozome platform version 10.3 (*http://phytozome.jgi.doe.gov/pz/portal.html*). Multiple sequence alignments were generated with ClustalW2 (*http://www.ebi.ac.uk/Tools/msa/clustalw2/*) using amino acid sequences. Alternatively, multiple protein sequence alignments were performed on the T-Coffee server using default settings (*tcoffee.crg.cat*; (Tommaso et al. 2011)). Alignments were formatted with the BoxShade version 3.21 server (*http://www.ch.embnet.org/software/BOX_form.html*) with a threshold fraction of residues set up at 0.5 (or 0.4, when mentioned). Phylogenetic analysis was performed on the Phylogeny.fr platform (*www.phylogeny.fr*; (Dereeper et al. 2008)) and comprised the following steps. Multiple alignments of amino acid sequences were produced with default settings of MUSCLE version 3.8.31 (Edgar 2004). The phylogenic tree was calculated with the maximum likelihood method using PhyML program version 3.0 and visualized with TreeDyn version 198.3 via the same Web site (Chevenet et al. 2006; Guindon et al. 2009).

2.2 Physiological methods

Growth of *A. thaliana* on Murashige and Skoog medium

Seeds were surface sterilized with [70% (v/v) EtOH, 0.05% (v/v) Triton X-100] according to (Kubis et al. 2008) and sowed on 0.5x Murashige-Skoog (MS; Duchefa) medium supplemented with 0.8% (w/v) PhytoAgar (Duchefa) and 1% (w/v) sucrose (AppliChem) (Murashige and Skoog 1962). Germination was synchronized by exposing the seeds for 2 days to 4°C in the dark. Seedlings were grown approximatively 3 weeks in a growth chamber (Percival, CLF Plant Climatics) under a light intensity of 150 $\mu mol \cdot m^{-2} \cdot s^{-1}$ with an 8 h photoperiod (short day). Selection of phosphinothricin-resistant plants was carried out on medium supplemented with 30 mg/L phosphinothricin (Glufosinate ammonium, Dr.Ehrenstorfer GmbH).

Growth of *A. thaliana* on soil

Seeds were sowed on soil (Top Dressing, Ricoter) soaked with Solbac (Andermatt Biocontrole AG). Germination was synchronized by exposing the seeds for 2 days to 4°C in the dark. Seedlings were grown for approximatively 3 weeks in a growth chamber (Percival, CLF Plant Climatics) under a light intensity of 150 $\mu mol \cdot m^{-2} \cdot s^{-1}$with an 8 h photoperiod (short day). Plants were then transferred to long-day conditions (150 $\mu mol \cdot m^{-2} \cdot s^{-1}$, 16 h light, 8 h dark, 22°C). To perform phosphinothricin selection on soil, 5-day-old seedlings were sprayed 3 times at 2-3-day intervals with 300 µM glufosinate ammonium.

Biotic stress by *P. syringae* infection

Pathogen infection was inoculated by dipping the rosette 3 seconds in a suspension of *Pseudomonas syringae* at $5 \cdot 10^7$ CFU/mL in [10mM $MgSO_4$, 0.03% (v/v) Silwet L77].

Oxidative stress by high light treatment

Light stress was applied by transferring plants for 3 d to continuous light with an intensity of 650 $\mu mol \cdot m^{-2} \cdot s^{-1}$.

Dark-induced senescence

Senescence was induced by detaching the whole rosette from roots and transferring it to darkness for 7 d on a slightly humidified (tap water) filter paper in a petri dish. Alternatively, single leaves were detached instead of the whole rosette.

Etiolated seedlings

Seeds sowed on ½ MS supplemented with 1% (w/v) sucrose were exposed to light for 1 h to induce germination. Plates were then kept vertically in darkness for 7 d. Deetiolation was induced by transferring seedlings to continuous light (150 $\mu mol \cdot m^{-2} \cdot s^{-1}$).

2.3 Methods for Gateway cloning

Coding sequences excluding the stop codon were amplified by PCR using attB1 and attB2 primers (see Table 4.1). PCR products were separated by agarose gel electrophoresis and purified using NucleoSpin® Extract II (Macherey-Nagel). Following manufacturer's instructions, purified PCR products were inserted in a donor vector using the BP Clonase® II Enzyme Mix (Invitrogen) and subsequently recombined in destination vectors using LR Clonase® II Enzyme Mix (Invitrogen). BP and LR reactions were used to transform competent *E.coli* DH5α following a heat-shock standard protocol. Cells were first grown on a solidified LB medium containing the appropriate antibiotics. Resistant colonies were used to inoculate a 4-mL liquid culture (LB + antibiotics). To multiply plasmids, cultures were incubated at 37°C overnight. Plasmids were isolated and purified using the GenElute ™ Plasmid Miniprep Kit (Sigma) according to the supplier's instructions. Plasmid integrity was assessed by restriction enzyme digestion (New England Biolabs). Finally, constructs were sequenced at Microsynth GmbH (Switzerland).

2.4 Agrobacterium-mediated transformation of *A.thaliana*

Plasmids, such as pEarleyGate101 and pEarleyGate205, carrying our constructs were introduced by electroporation into *Agrobacterium tumefaciens* strain C58. Flowering *A. thaliana* were stably transformed using the floral dip method as described (Clough and Bent 1998). Transgenic plants were selected on Murashige and Skoog medium containing phosphinothricin (30 mg/L). Segregation analyses were carried out to select heterozygous lines with a single insertion of the 35S transgene (= 75% of phosphinothricin resistant). Stable homozygous lines (= 100% of phosphinothricin resistant) were isolated from their progeny by another round of segregation analysis and genomic sequence

flanking insertion sites were identified when possible using the TAIL-PCR strategy originally adapted from (Liu et al. 1995) and published in (Weigel and Glazebrook 2002).

2.5 Diagnostic PCR on plants

Rapid genomic DNA extraction from leaves was performed essentially as described in (Edwards et al. 1991). Briefly, 1-2 leaves were ground in 400 µL of [0.2 M Tris-HCl pH 7.5, 0.25 M NaCl, 25 mM EDTA, 0.5% (w/v) SDS]. Cleared supernatant (5 min, 16'000×g) was supplemented with an equal volume of isopropanol and centrifuged 10 min at 16'000×g (4°C). DNA pellet was washed with 70% (v/v) EtOH and dried. Finally, DNA was resuspended in 50 µL [10 mM Tris pH 8] at 65°C.

Genotyping PCRs were carried out using 0.5 U GoTaq® DNA polymerase (Promega), 0.2 mM dNTPs (Promega), 0.2 µM of each primer and 2 µL DNA. The primer sets LP with RP were used to detect the WT allele, whereas LP or RP combined with LBpROK2 allowed the detection of the T-DNA insertion. Primers sequences are listed in Table 4.1. The PCR program was as follows: Initial denaturation (5 min, 94°C) followed by 30 cycles (30 s, 94°C; 30 s, 55°C; 1 min 30 s, 72°C), final extension (10 min, 72°C). PCR reactions were analyzed by agarose gel electrophoresis according to standard protocols (Sambrook and Russell 2001).

2.6 RNA extraction and qRT-PCR analysis

Total RNA was extracted from 100 mg of liquid nitrogen-ground leaves using the Plant RNA Extraction Kit (NucleoSpin RNA Plant, Macherey-Nagel). Possible DNA contaminations were removed by a DNase I treatment. From 1 µg of purified RNA, cDNAs were synthesized by reverse transcription PCR using the GoScript reverse transcriptase (Promega) and specific primers (Table 4.1). Levels of transcripts were analyzed by quantitative real-time PCR (qRT-PCR) with FastStart Green master (Roche). The primer sets CCD4-For and CCD4-Rev (Gonzalez-Jorge et al. 2013), CCD1-For and CCD1-Rev, Actin-For and Actin-Rev were used. Primer sequences are listed in Table 4.1. Reactions were carried out using a LightCycler 96 system (Roche Diagnostics). Relative gene expression levels were normalized based on the transcript level of *ACTIN2* (At3g18780). Specificity and efficiency of each primer set was verified prior to qRT-PCR analysis.

2.7 Protein extraction and Western blot analysis

Total protein was isolated from leaves of *A. thaliana* according to (Rensink et al. 1998). To avoid proteolytic degradation, 0.5% (v/v) protease inhibitor cocktail for plant cell extracts (Sigma) was added to the extraction buffer. Proteins were concentrated by chloroform-methanol precipitation (Wessel and Flugge 1984). Proteins were quantified according to the Bradford method (Bradford 1976) and resuspended at 5 µg/µL in sample buffer [50 mM Tris-HCl pH 6.8, 0.1 M DTT, 2% (w/v) SDS, 0.1% (w/v) bromophenol blue, 10% (v/v) glycerol]. 35 µg of protein were separated by SDS-PAGE and blotted onto nitrocellulose membrane (Whatman, PROTRAN, 0.45µm) for immunodetection. Proteins were stained with AmidoBlack and scanned. Membranes were incubated

in blocking buffer [PBS or TBS buffer, 5% (w/v) skim milk powder] for 30 min at least. The choice between PBS buffer [0.14 M NaCl, 2.7 mM KCl, 10 mM Na_2HPO_4, 2 mM KH_2PO_4] and TBS buffer [10 mM Tris-HCl pH 7.5, 150 mM NaCl] depends upon the needs of the following antibody. Primary antibodies were used as described in Table 4.2 and membranes were subsequently washed 3 times in PBS or TBS buffer, with or without 0.1% (v/v) Tween® 20 which increases the wash stringency.

Table 4.2 Antibody dilutions for immunoblotting. Incubation buffers and incubation times are indicated. ON, overnight.

Antibody	Dilution (v/v)	Buffer	Time
anti-HA-HRP	1/5000	PBS, 5% (w/v) skim milk	3 h
anti-LHCBII	1/3000	PBS, 5% (w/v) skim milk	2 h
anti-FBN1a	1/3000	PBS, 5% (w/v) skim milk	2 h
anti-TIC40	1/2500	PBS, 5% (w/v) skim milk	1 h
anti-TOC75	1/1000	TBS-T, 5% (w/v) skim milk	2 h
anti-CBP	1/2000	PBS, 5% (w/v) skim milk	ON

When necessary, primary antibodies were revealed by incubating the membrane 1 h with 1/3000 dilution of horseradish peroxidase-coupled goat anti-rabbit antibody (Millipore) in blocking buffer. After 3 washing steps, the membranes were incubated in [0.1 M Tris-HCl pH 8.5, 0.2 mM p-coumaric acid, 1.25 mM luminol, 0.009% (v/v) H_2O_2]. Enhanced chemiluminescence emission was detected by high performance chemiluminescence films (Amersham Biosciences). Exposure time was adapted to the strength of the signal.

2.8 Transmission electron microscopy

Leaf tissue was cut into 1-3 mm slices and fixed overnight at 4°C in phosphate buffer (0.1 M, pH 6.8) supplemented with 4% (w/v) formaldehyde and 5% (w/v) glutaraldehyde. Samples were washed three times in phosphate buffer for 20 min each and post-fixed at RT for 2 h in 1% (w/v) OsO_4 in phosphate buffer. After two washes in phosphate buffer and one in distilled water, samples were dehydrated in ethanol (30%, 50%, 70% and 90%) and acetone (90% and 2x100%) series; each incubation was for 15 min. Embedding in Spurr epoxy resin (Polyscience) required the following steps: 30 min in 66% acetone/33% Spurr, 1h in 33% acetone/66% Spurr, 2x30 min in 100% Spurr and 12h in 100% Spurr prior to polymerization overnight at 60°C. Semithin sections of 750 nm were cut on a Reichert-Jung Ultracut-E microtome with a glass knife, mounted on glass slides and stained with 7% toluidine blue. Leaf integrity and general cell organization was analyzed by light microscopy (Nikon Eclipse E800). Ultrathin sections of 80 nm were then cut using a diamond knife, mounted on copper grids and counterstained with uranyl acetate and Reynolds lead solution (Reynolds 1963). Sections were examined with a Philips CM100 electron microscope. Negatives were scanned using an Epson Expression 1640XL in the 1600 dpi resolution. The ImageJ software (*http://rsb.info.nih.gov/ij/)* was used to append scale bar on the micrographs.

2.9 Estimation of carotenoid contents by spectrophotometry

Carotenoids were extracted from leaves using dimethylformamide (DMF). First, leaves (50 mg FW) were finely ground in a microcentrifuge tube by using a metallic pestle with liquid nitrogen. Second, five volumes of DMF and 5-10 glass beads (Assistant, Sontheim, Germany) were added. Samples were homogenized for 3 min at 30 Hz in a tissue lyser (Retsch MM 300, Haan, Germany). Then, tubes were centrifuged 3 min at 16,000 × g. Finally, 2 µL of supernatant were analyzed with a Nanodrop 1000 Spectrophotometer (Thermo Fisher Scientific). Absorbance was recorded at the three following wavelengths: 480, 647 and 664 nm. To determine concentrations of total carotenoids, we applied published equations (Wellburn 1994).

From a sucrose-gradient loaded with a chlorophyll-equivalent of 30 mg of total chloroplast membranes (Vidi et al. 2006), 30 µl of the PG fraction (no.1-4) were mixed with 100 µl of ethyl acetate. After a short spin-down, 90µl of supernatant were collected and evaporated. The pellet was resuspended in 10 µl of ethyl acetate and the visible spectrum was measured using a Nanodrop 1000 Spectrophotometer (Thermo Fisher Scientific). A calibration curve was established in ethyl acetate using β-carotene as the standard. The carotenoid content was determined as the absorbance at 448 nm in ethyl acetate and is expressed as micrograms of β-carotene equivalent per total membranes loaded, which is expressed in milligrams of chlorophyll (µg Car /30 mg of chlorophyll).

2.10 Lipid extraction and HPLC analysis

Carotenoids

To protect carotenoids from oxidation, the following procedures were carried out in semi darkness. Leaves or rosette tissues (100 mg FW) were ground in a cold mortar in presence of liquid nitrogen and immediately transferred to a microcentrifuge tube. Five volumes of tetrahydrofuran-methanol (50:50, v/v) and 5-10 glass beads (Assistant, Sontheim, Germany) were added. Samples were further homogenized for 3 min at 30 Hz in a tissue lyser (Retsch MM 300, Haan, Germany). Tubes were centrifuged 5 min at 16,000 × g (Eppendorf Centrifuge 5415D) and 400 µL of supernatant was transferred to another 1.5 mL microcentrifuge tube. Centrifugation was repeated and 150 µL of supernatant was transferred to an amber glass vial (BGB, Boeckten, Switzerland) for HPLC analysis. Samples were either directly analyzed or conserved at -80°C for up to one week.

Carotenoid targeted quantification was achieved using UHPLC-DAD. The separation was carried out on a Waters Acquity BEH C18 column (50x2.1 mm, 1.7 µm particle size) thermostatted at 50°C at a flow rate of 0.7 mL/min. The following gradient program using water as solvent A and acetonitrile as solvent B was employed: 65-80% B in 5 min, 80-100% B in 1 min, holding at 100% B for 3.5 min, reequilibration at 65% B for 1 min. Total analysis time was 10.5 min. A volume of 2.5 µL was injected. For quantification, the UV trace at 450 nm was used. Calibration solutions were prepared as follows. Lutein, violaxanthin, neoxanthin and zeaxanthin were mixed and diluted at 20, 5, 2 and 0.5 µg/mL in tetrahydrofuran-methanol-water (42.5:42.5:15, v/v). Since β-carotene is highly apolar, it was separately prepared in tetrahydrofuran-water (85:15, v/v) at 20, 5, 2 and 0.5 µg/mL.

Prenyllipids

The extraction of prenyllipids from isolated PGs was carried out as described (Eugeni Piller et al. 2014; Kessler and Glauser 2014) with some modifications. To remove sucrose, 400 µL of fraction were partitioned 2 times against ethyl acetate (1:1). The upper phases were collected, combined and evaporated. Pellets of lipids were dissolved in 100 µL of tetrahydrofuran for HPLC analysis.

Specific prenyllipids were quantified absolutely using calibration curves established from dilutions of pure standards as mentioned in (Kessler and Glauser 2014).

Untargeted

For untargeted lipid profiling, pure tetrahydrofuran was used for the extraction instead of tetrahydrofuran-methanol. Lipid profiling was performed using a UHPLC-APCI-QTOFMS (Waters) as previously described (Martinis et al. 2011; Kessler and Glauser 2014). Raw data were processed using Markerlynx XS™ (Waters) for automatic peak detection. Principal component analysis (PCA) was applied on pareto-scaled variables.

2.11 Subcellular localization

In vitro translation and pea chloroplast import assay

Intact chloroplasts were isolated from 2-3-week-old pea plants (*Pisum sativum*) as described in (Smith et al. 2003) with minor modifications. *In vitro*-translated (IVT) proteins were produced with the TNT® Quick Coupled Transcription/Translation System (Promega) following the manufacturer's recommendations. The ^{35}S-radiolabeled proteins were then incubated with isolated import competent pea chloroplasts according to the protocol described in (Smith et al. 2003) with slight modifications.

Arabidopsis protoplast isolation and transformation

For single protein localization, protoplasts were rapidly isolated as described in (Fitzpatrick and Keegstra 2001) from transgenic or WT *A. thaliana*. In brief, leaves were harvested and finely sliced with a scalpel. Sliced leaves were washed in ice cold digestion buffer [400 mM sorbitol, 20 mM MES-KOH pH 5.2, 0.5 mM $CaCl_2$] prior to dark incubation at 20°C for 4 h with digestive enzyme solution [digestion buffer, 1.5% cellulose "onozuka R-10", 0.375% macerozyme R-10]. Protoplasts were released by gentle swirling on ice and subsequently filtered through 200 µm nylon mesh. A low-speed spin (110×g, 10 min, 4°C) was applied to collect protoplasts. Supernatant was carefully removed and protoplasts were resuspended in resuspension buffer [400 mM sorbitol, 20 mM MES-KOH pH 6, 0.5 mM $CaCl_2$]. Protoplasts were immediately observed with a confocal microscope.

For colocalization, the vector pCL62 carrying *FBN1a* in frame with *CFP* was used (Vidi et al. 2006). Protoplasts were isolated and transformed with the aforementioned vector as described (Jin et al. 2001). Prior to observations, protoplasts were incubated at RT for 30 h.

Fluorescence in protoplasts was monitored with a Leica TCS SP5 (Leica Microsystems) confocal microscope using the appropriate parameters for YFP, CFP and chlorophyll autofluorescence. The emission of YFP was excited by the 514-nm Argon laser line using a 525-600-nm detection window. CFP fluorescence was detected using 458-nm Argon laser line and 465-505-nm detection windows.

Settings were checked with untransformed protoplasts for one and both constructs to avoid unspecific background noise.

Chloroplast membrane fractionation on sucrose gradient

Intact chloroplasts from 10-week-old plants were isolated essentially as described (Hiltbrunner et al. 2001; Kessler and Glauser 2014). Membrane fractionation, verification by SDS-PAGE and immunoblotting were adapted from published protocols (Vidi et al. 2006; Besagni et al. 2011; Kessler and Glauser 2014). Lysed and homogenized chloroplasts were subjected to 1 h of ultracentrifugation (Optima XPN-80 Ultracentrifuge, Beckman Coulter) to separate the total membranes from the stroma. Subsequently, homogenized membranes (corresponding to 3 mg of chlorophyll) were separated with a miniaturized discontinuous sucrose gradient as follows. On the top of the 2 mL membrane-containing 45% sucrose, 805 µL of 38%, 805 µL of 20%, 540 µL of 15% and 845 µL of 5% sucrose were successively added in an Ultra-Clear™ Centrifuge Tube of 5 mL (13×51 mm, Beckman Coulter). Gradients were centrifuged at 100,000×g for 15 h in a SW55Ti swinging-bucket rotor (Beckman Coulter). Fractions of 200 µL were collected from the top (no.1) to the bottom of the gradient (no.25) with a micropipette. Each fraction was chloroform-methanol precipitated prior to the SDS-PAGE separation and transfer onto nitrocellulose membrane.

2.12 Solubilization assays

Plants were energetically homogenized with a cold mortar in hypotonic buffer [50 mM Tris-HCl pH 7.5, 100 mM NaCl, 1 mM PMSF, 5 mM NaF, 0.2% (v/v) plant protease inhibitor cocktail] supplemented with sand for 10 min. Ground material was filtered through 2 layers of Miracloth and centrifuged 2 times at 1’500×g to remove cell debris. Chlorophyll concentration of the supernatant was measured in 80% acetone at 652 nm (0.3 mg/ml). Proteins were then separated into soluble and insoluble fractions using ultracentrifugation (2 h at 100’000×g). Equal amounts of the insoluble fraction (corresponding to 1.5 mg of chlorophyll) were resuspended with a Dounce homogenizer in one of the following solubilization solutions: 1 M NaCl, 0.2 M Na_2CO_3, 0.1% Triton X-100, 0.5% Triton X-100 or 1% Triton X-100. After 30 min of incubation at 4°C, the experiments were separated into pellet and supernatant by centrifugation at 100’000×g for 1 h. Pellets were resuspended in the corresponding solubilization solution and equal amounts of protein were analyzed by immunoblotting.

Alternatively, plants were subjected to intact chloroplast isolation as described in (Fitzpatrick and Keegstra 2001). Chloroplasts were lysed in ice-cold hypotonic buffer with a glass-on-glass Dounce homogenizer (10 strokes). Soluble and insoluble protein fractions were separated at 100’000×g for 30 min (4°C) in a Beckman TLA-110 rotor. 6µg-chlorophyll equivalents of the insoluble fraction were then subjected to solubilization. Samples were incubated 30 min at 4 °C in one of the solubilization solutions described above and centrifuged at 100’000×g for 30 min to separate pellet and supernatant.

2.13 Co-immunoprecipitation and mass spectrometry

Intact chloroplasts from transgenic *A. thaliana* were prepared according to (Fitzpatrick and Keegstra 2001) with minor modifications. Chlorophyll concentration was measured spectroscopically in 80% (v/v) acetone at 652 nm. Chloroplasts, corresponding to 1 mg of chlorophyll (1 mg/mL), were solubilized for 30 min at 4°C with a solubilization buffer [100 mM NaCl, 50 mM Tris-HCl pH 7.5, 1 mM PMSF, 5 mM NaF, 0.2% (v/v) plant protease inhibitor cocktail, 1% (v/v) Triton X-100]. Non-solubilized material was pelleted for 5 min at 1'000×g in a refrigerated (4°C) bench centrifuge (Eppendorf Centrifuge, 5415 R). Supernatant was recovered and incubated with µMAC Anti-HA MicroBeads (Miltenyi Biotec) for 30 min at 4°C. Co-immunoprecipitation was performed with the µMAC™ Epitope Tag Protein Isolation Kit (Miltenyi Biotec) based on manufacturer's instructions with the following modifications. For column preparation, after the Lysis Buffer step we applied 200 µL of solubilization buffer (see above) to equilibrate the column. Once the chloroplast lysate had run through, the column was washed 4 times with 200 µL of solubilization buffer instead of the provided Wash Buffer 1. The final wash was performed with 200 µL of the provided Wash Buffer 2. A standard 2-step elution was carried out with 20 and 50 µL of hot Elution Buffer. Samples of 10 µL were collected at each step for subsequent SDS-PAGE analysis.

For proteomic analysis, elutions were loaded on a Mini-PROTEAN® TGX ™ Precast Gel (Bio-Rad). Using Tris/Glycine/SDS Buffer (Bio-Rad) proteins were allowed to migrate about 1 cm deep into the gel. Proteins were stained with SYPRO® Ruby Protein Gel Stain (Invitrogen) according to the Basic Protocol provided. Visible bands were excised and subjected to tryptic digestion using the In-Gel Tryptic Digestion Kit (Thermo Scientific) following the manufacturer's instructions. Tryptic peptides were lyophilized using the Freeze Dryer Modulyo (Edwards) and sent to Germany at Martin Luther University (Halle-Wittenberg) for protein identification by mass spectrometry. The samples were injected into a liquid chromatography system and were subsequently analyzed on an LTQ ion trap (Thermo Fisher) essentially as described (Motohashi et al. 2012). Moreover, quantitative analysis was carried out in three technical replicates where 1/20 of the sample was separated on an ACQUITY UPLC System (Waters). Mass spectra were acquired on a SYNAPT G2-S mass spectrometer (Waters) following peptide ionization with a nanoESI source. Raw data were processed as described (Helm et al. 2014).

Acknowledgements

In the first place, I would like to thank my thesis director *Felix Kessler* for giving me the opportunity to carry out this fascinating research in the Laboratory of Plant Physiology, where working conditions were so enjoyable. I appreciated his boundless enthusiasm which was so contagious and also his great support during these five years.

I would also like to acknowledge *Didier Schaefer*, *Markus Geisler* and *Enrico Martinoia* for accepting to serve in my mid-thesis and thesis committee. The discussion we had during my mid-thesis defense was highly stimulating.

I am grateful to former post-doc *Claire Bréhélin* and master student *Angélica Lima* for their preliminary work on CCD4 characterization in the Laboratory of Plant Physiology.

Special thanks go to my supervisor *Céline Besagni* for her help and encouragement throughout my Ph.D. thesis.

I am indebted to *Véronique Douet* for her invaluable technical support, to *Michèle Vlimant* for TEM, to *Gaétan Glauser* for lipidomics and to *Birgit Agne*, *Sacha Baginski* and *Stefan Helm* for proteomics experiments.

I am also grateful to apprentices, students and interns I have supervised during my thesis. Through them, I learned a lot and of course they helpfully contributed to the present research. So thank you *Mégane Boldini, Nicolas Picci, Hanna Wieser, Cindy Mettraux, Floriane Weber* and last but not least *Julie Devillers* for your friendship and estimable work.

Additional thanks go to *Romain Bessire* for his support on informatics, to *Gregory Roeder* regarding our GC-MS trial, to *Christiane Bobillier* for managing the Interuniversity Doctoral Program in Organismal Biology, and to all the members of the *Secretariat* and the *Library* of the Faculty of Science for their valuable assistance as well as to the *University of Neuchâtel* for providing funding.

Finally, a special acknowledgement goes also for my colleagues whose advices, help, inspiring discussions and friendship are priceless. Thank you *Cyrille Montandon, Shanmugabalaji Venkatasalam, Mónica Zufferey, Livia Spicher, Thibaut Pralon, Ashok Munusamy Lakshmanan, David Bornand, Axel Meyrat, Sophie Scheuner, Charles Andrès, Emilie Demarsy, Lucia Eugeni Piller, Rosa Pipitone, Sonia Accossato, Saskia Desmeules, Adrien Bottarelli* and *Bruno Cabete*.

References

Adami M, De Franceschi P, Brandi F, et al (2013) Identifying a Carotenoid Cleavage Dioxygenase (ccd4) Gene Controlling Yellow/White Fruit Flesh Color of Peach. Plant Mol Biol Report 31:1166–1175. doi: 10.1007/s11105-013-0628-6

Ahn CS, Lee JH, Pai H-S (2005) Silencing of NbNAP1 encoding a plastidic SufB-like protein affects chloroplast development in Nicotiana benthamiana. Mol Cells 20:112–118. doi: 884 [pii]

Ahrazem O, Trapero A, Gomez MD, et al (2010) Genomic analysis and gene structure of the plant carotenoid dioxygenase 4 family: A deeper study in Crocus sativus and its allies. Genomics 96:239–250. doi: 10.1016/j.ygeno.2010.07.003

Ajjawi I, Lu Y, Savage LJ, et al (2010) Large-Scale Reverse Genetics in Arabidopsis: Case Studies from the Chloroplast 2010 Project. Plant Physiol 152:529–540. doi: 10.1104/pp.109.148494

Alonso JM, Stepanova AN, Leisse TJ, et al (2003) Genome-wide insertional mutagenesis of Arabidopsis thaliana. Science 301:653–657. doi: 10.1126/science.1086391

Andersson MX, Kjellberg JM, Sandelius AS (2001) Chloroplast biogenesis. Regulation of lipid transport to the thylakoid in chloroplasts isolated from expanding and fully expanded leaves of pea. Plant Physiol 127:184–193. doi: 10.1104/Pp.127.1.184

Andersson MX, Stridh MH, Larsson KE, et al (2003) Phosphate-deficient oat replaces a major portion of the plasma membrane phospholipids with the galactolipid digalactosyldiacylglycerol. FEBS Lett 537:128–132. doi: 10.1016/S0014-5793(03)00109-1

Ariizumi T, Kishimoto S, Kakami R, et al (2014) Identification of the carotenoid modifying gene PALE YELLOW PETAL 1 as an essential factor in xanthophyll esterification and yellow flower pigmentation in tomato (Solanum lycopersicum). Plant J 79:453–465. doi: 10.1111/tpj.12570

Aronsson H, Schottler MA, Kelly AA, et al (2008) Monogalactosyldiacylglycerol deficiency in Arabidopsis affects pigment composition in the prolamellar body and impairs thylakoid membrane energization and photoprotection in leaves. Plant Physiol 148:580–592. doi: 10.1104/pp.108.123372

Asano T, Yoshioka Y, Machida Y (2004) A defect in atToc159 of Arabidopsis thaliana causes severe defects in leaf development. Genes Genet Syst 79:207–212. doi: 10.1266/ggs.79.207

Auldridge ME, Block A, Vogel JT, et al (2006a) Characterization of three members of the Arabidopsis carotenoid cleavage dioxygenase family demonstrates the divergent roles of this multifunctional enzyme family. Plant J 45:982–993. doi: 10.1111/j.1365-313X.2006.02666.x

Auldridge ME, McCarty DR, Klee HJ (2006b) Plant carotenoid cleavage oxygenases and their apocarotenoid products. Curr Opin Plant Biol 9:315–321. doi: 10.1016/j.pbi.2006.03.005

Austin II JR, Frost E, Vidi PA, et al (2006) Plastoglobules are lipoprotein subcompartments of the chloroplast that are permanently coupled to thylakoid membranes and contain biosynthetic enzymes. Plant Cell 18:1693–1703. doi: 10.1105/tpc.105.039859

Avalos J, Limón MC (2014) Biological roles of fungal carotenoids. Curr Genet. doi: 10.1007/s00294-014-0454-x

Avendano-Vazquez AO, Cordoba E, Llamas E, et al (2014) An Uncharacterized Apocarotenoid-Derived Signal Generated in zeta-Carotene Desaturase Mutants Regulates Leaf Development and the Expression of Chloroplast and Nuclear Genes in Arabidopsis. Plant Cell 26:2524–2537. doi: 10.1105/tpc.114.123349

Awai K, Marechal E, Block MA, et al (2001) Two types of MGDG synthase genes, found widely in both 16:3 and 18:3 plants, differentially mediate galactolipid syntheses in photosynthetic and nonphotosynthetic tissues in Arabidopsis thaliana. Proc Natl Acad Sci U S A 98:10960–10965. doi: 10.1073/pnas.181331498\r98/19/10960 [pii]

Awai K, Xu C, Tamot B, Benning C (2006) A phosphatidic acid-binding protein of the chloroplast inner envelope membrane involved in lipid trafficking. Proc Natl Acad Sci U S A 103:10817–10822. doi: 10.1073/pnas.0602754103

Bartels PG, Watson CW (1978) Inhibition of Carotenoid Synthesis by Fluridone and Norflurazon. Weed Sci 26:198–203.

Bauer J, Chen K, Hiltbunner A, et al (2000) The major protein import receptor of plastids is essential for chloroplast biogenesis. Nature 403:203–207. doi: 10.1038/35003214

Belal R, Tang R, Li Y, et al (2015) An ABC transporter complex encoded by Aluminum Sensitive 3 and NAP3 is required for phosphate deficiency responses in Arabidopsis. Biochem Biophys Res Commun 463:18–23. doi: 10.1016/j.bbrc.2015.05.009

Benning C (2009) Mechanisms of lipid transport involved in organelle biogenesis in plant cells. Annu Rev Cell Dev Biol 25:71–91. doi: 10.1146/annurev.cellbio.042308.113414

Ben-Shaul Y, Naftali Y (1969) The development and ultrastructure of lycopene bodies in chromoplasts of Lycopersicum esculentum. Protoplasma 67:333–344. doi: 10.1007/BF01254899

Besagni C, Kessler F (2013) A mechanism implicating plastoglobules in thylakoid disassembly during senescence and nitrogen starvation. Planta 237:463–470. doi: 10.1007/s00425-012-1813-9

Besagni C, Piller LE, Bréhélin C (2011) Preparation of plastoglobules from Arabidopsis plastids for proteomic analysis and other studies. Methods Mol Biol 775:223–239. doi: 10.1007/978-1-61779-237-3_12

Biswal B (1995) Carotenoid Catabolism during Leaf Senescence and Its Control by Light. J Photochem Photobiol B-Biology 30:3–13. doi: 10.1016/1011-1344(95)07197-A

Black CC (1973) Photosynthetic carbon fixation in relation to net CO2 uptake. Annu Rev Plant Physiol 24:253–286. doi: 10.1146/annurev.pp.24.060173.001345

Blomqvist LA, Ryberg M, Sundqvist C (2008) Proteomic analysis of highly purified prolamellar bodies reveals their significance in chloroplast development. Photosynth Res 96:37–50. doi: 10.1007/s11120-007-9281-y

Boudière L, Michaud M, Petroutsos D, et al (2014) Glycerolipids in photosynthesis: composition, synthesis and trafficking. Biochim Biophys Acta 1837:470–480. doi: 10.1016/j.bbabio.2013.09.007

Bradford MM (1976) A rapid and sensitive method for the quantitation of microgram quantities of protein utilizing the principle of protein-dye binding. Anal Biochem 72:248–254. doi: S0003269776699996 [pii]

Brandi F, Bar E, Mourgues F, et al (2011) Study of "Redhaven" peach and its white-fleshed mutant suggests a key role of CCD4 carotenoid dioxygenase in carotenoid and norisoprenoid volatile metabolism. BMC Plant Biol 11:24. doi: 10.1186/1471-2229-11-24

Bräutigam A, Hoffmann-Benning S, Weber APM (2008) Comparative Proteomics of Chloroplast Envelopes from C3 and C4 Plants Reveals Specific Adaptations of the Plastid Envelope to C4 Photosynthesis and Candidate Proteins Required for Maintaining C4 Metabolite Fluxes. Plant Physiol 148:568–579. doi: 10.1104/pp.108.121012

Bréhélin C, Kessler F (2008) The plastoglobule: a bag full of lipid biochemistry tricks. Photochem Photobiol 84:1388–1394. doi: 10.1111/j.1751-1097.2008.00459.x

Bréhélin C, Kessler F, van Wijk KJ (2007) Plastoglobules: versatile lipoprotein particles in plastids. Trends Plant Sci 12:260–266. doi: 10.1016/j.tplants.2007.04.003

Breithaupt DE, Bamedi A (2001) Carotenoid esters in vegetables and fruits: a screening with emphasis on beta-cryptoxanthin esters. J Agric Food Chem 49:2064–2070. doi: 10.1021/jf001276t

Buchanan-Wollaston V, Page T, Harrison E, et al (2005) Comparative transcriptome analysis reveals significant differences in gene expression and signalling pathways between developmental and dark/starvation-induced senescence in Arabidopsis. Plant J 42:567–585. doi: 10.1111/j.1365-313X.2005.02399.x

Bugg TD, Ramaswamy S (2008) Non-heme iron-dependent dioxygenases: unravelling catalytic mechanisms for complex enzymatic oxidations. Curr Opin Chem Biol 12:134–140. doi: 10.1016/j.cbpa.2007.12.007

Buseman CM, Tamura P, Sparks AA, et al (2006) Wounding stimulates the accumulation of glycerolipids containing oxophytodienoic acid and dinor-oxophytodienoic acid in Arabidopsis leaves. Plant Physiol 142:28–39. doi: 10.1104/pp.106.082115

Busso D, Delagoutte-Busso B, Moras D (2005) Construction of a set Gateway-based destination vectors for high-throughput cloning and expression screening in Escherichia coli. Anal Biochem 343:313–321. doi: 10.1016/j.ab.2005.05.015

Campbell R, Ducreux LJM, Morris WL, et al (2010) The Metabolic and Developmental Roles of Carotenoid Cleavage Dioxygenase4 from Potato. Plant Physiol 154:656–664. doi: 10.1104/pp.110.158733

Chatterjee M, Sparvoli S, Edmunds C, et al (1996) DAG, a gene required for chloroplast differentiation and palisade development in Antirrhinum majus. EMBO J 15:4194–207.

Chen W, Chi Y, Taylor NL, et al (2010) Disruption of ptLPD1 or ptLPD2, genes that encode isoforms of the plastidial lipoamide dehydrogenase, confers arsenate hypersensitivity in Arabidopsis. Plant Physiol 153:1385–1397. doi: 10.1104/pp.110.153452

Cheng Z, Sattler S, Maeda H, et al (2003) Highly divergent methyltransferases catalyze a conserved reaction in tocopherol and plastoquinone synthesis in cyanobacteria and photosynthetic eukaryotes. Plant Cell 15:2343–2356. doi: 10.1105/tpc.013656

Chevenet F, Brun C, Banuls AL, et al (2006) TreeDyn: towards dynamic graphics and annotations for analyses of trees. BMC Bioinformatics. doi: Artn 43910.1186/1471-2105-7-439

Chigri F, Fuchs M, Otters S, Vothknecht UC (2012) Thylakoid membrane formation: Vipp1 and more. Endocytobiosis Cell Res 23:6–10.

Clemens S, Palmgren MG, Kramer U (2002) A long way ahead: understanding and engineering plant metal accumulation. Trends Plant Sci 7:309–315. doi: 10.1016/S1360-1385(02)02295-1

Clough SJ, Bent AF (1998) Floral dip: A simplified method for Agrobacterium-mediated transformation of Arabidopsis thaliana. Plant J 16:735–743. doi: 10.1046/j.1365-313X.1998.00343.x

Crowell DN, Packard CE, Pierson CA, et al (2003) Identification of an allele of CLA1 associated with variegation in Arabidopsis thaliana. Physiol Plant 118:29–37. doi: 063 [pii]

Dalchau N, Hubbard KE, Robertson FC, et al (2010) Correct biological timing in Arabidopsis requires multiple light-signaling pathways. Proc Natl Acad Sci U S A 107:13171–13176. doi: 10.1073/pnas.1001429107

Dall'Osto L, Holt NE, Kaligotla S, et al (2012) Zeaxanthin protects plant photosynthesis by modulating chlorophyll triplet yield in specific light-harvesting antenna subunits. J Biol Chem 287:41820–41834. doi: 10.1074/jbc.M112.405498

Daniell H, Kumar S, Dufourmantel N (2005) Breakthrough in chloroplast genetic engineering of agronomically important crops. Trends Biotechnol 23:238–245. doi: 10.1016/j.tibtech.2005.03.008

Dassa E (2003) Phylogenetic and functional classification of ABC (ATP-binding cassette) systems. In: ABC proteins: From Bacteria to Man. Academic Press, pp 3–35

Dassa E (2011) Natural history of ABC systems: not only transporters. Essays Biochem 50:19–42. doi:

10.1042/bse0500019

Daum B, Kühlbrandt W (2011) Electron tomography of plant thylakoid membranes. J Exp Bot 62:2393–2402. doi: 10.1093/jxb/err034

Davidson AL, Dassa E, Orelle C, Chen J (2008) Structure, function, and evolution of bacterial ATP-binding cassette systems. Microbiol Mol Biol Rev 72:317–364. doi: 10.1128/MMBR.00031-07

Dean M, Allikmets R (1995) Evolution of ATP-binding cassette transporter genes. Curr Opin Genet Dev 5:779–785. doi: doi: 10.1016/0959-437X(95)80011-S

DellaPenna D (2005) A decade of progress in understanding vitamin E synthesis in plants. J Plant Physiol 162:729–737. doi: 10.1016/j.jplph.2005.04.004

Demmig-Adams B, Adams WW (1996) The role of xanthophyll cycle carotenoids in the protection of photosynthesis. Trends Plant Sci 1:21–26. doi: 10.1016/S1360-1385(96)80019-7

Dereeper A, Guignon V, Blanc G, et al (2008) Phylogeny.fr: robust phylogenetic analysis for the non-specialist. Nucleic Acids Res 36:W465–W469. doi: 10.1093/nar/gkn180

Deruère J, Römer S, d'Harlingue A, et al (1994) Fibril assembly and carotenoid overaccumulation in chromoplasts: a model for supramolecular lipoprotein structures. Plant Cell 6:119–133. doi: 10.1105/tpc.6.1.119

Dörmann P (2007) Galactolipids in plant membranes. Encycl. Life Sci.

Earley KW, Haag JR, Pontes O, et al (2006) Gateway-compatible vectors for plant functional genomics and proteomics. Plant J 45:616–629. doi: 10.1111/j.1365-313X.2005.02617.x

Edgar RC (2004) MUSCLE: multiple sequence alignment with high accuracy and high throughput. Nucleic Acids Res 32:1792–1797. doi: 10.1093/nar/gkh340

Edwards K, Johnstone C, Thompson C (1991) A simple and rapid method for the preparation of plant genomic DNA for PCR analysis. Nucleic Acids Res 19:1349. doi: 10.1093/nar/19.6.1349

Egea I, Barsan C, Bian W, et al (2010) Chromoplast differentiation: current status and perspectives. Plant Cell Physiol 51:1601–1611. doi: 10.1093/pcp/pcq136

Endo T, Shikanai T, Takabayashi A, et al (1999) The role of chloroplastic NAD(P)H dehydrogenase in photoprotection. FEBS Lett 457:5–8. doi: 10.1016/S0014-5793(99)00989-8

Estévez JM, Cantero A, Romero C, et al (2000) Analysis of the expression of CLA1, a gene that encodes the 1-deoxyxylulose 5-phosphate synthase of the 2-C-methyl-D-erythritol-4-phosphate pathway in Arabidopsis. Plant Physiol 124:95–104. doi: 10.1104/pp.124.1.95

Eugeni Piller L, Abraham M, Dörmann P, et al (2012) Plastid lipid droplets at the crossroads of prenylquinone metabolism. J Exp Bot 63:1609–1618. doi: 10.1093/jxb/ers016

Eugeni Piller L, Besagni C, Ksas B, et al (2011) Chloroplast lipid droplet type II NAD(P)H quinone oxidoreductase is essential for prenylquinone metabolism and vitamin K1 accumulation. Proc Natl Acad Sci U S A 108:14354–14359. doi: 10.1073/pnas.1104790108

Eugeni Piller L, Glauser G, Kessler F, Besagni C (2014) Role of plastoglobules in metabolite repair in the tocopherol redox cycle. Front Plant Sci 5:298. doi: 10.3389/fpls.2014.00298

Fagioni M, D'Amici GM, Timperio AM, Zolla L (2009) Proteomic analysis of multiprotein complexes in the thylakoid membrane upon cadmium treatment. J Proteome Res 8:310–326. doi: 10.1021/Pr800507x

Fatihi A, Latimer S, Schmollinger S, et al (2015) A dedicated type II NADPH dehydrogenase performs the penultimate step in the biosynthesis of vitamin K1 in Synechocystis and Arabidopsis. Plant Cell. doi: 10.1105/tpc.15.00103

Ferro M, Brugière S, Salvi D, et al (2010) AT_CHLORO, a comprehensive chloroplast proteome database with subplastidial localization and curated information on envelope proteins. Mol Cell Proteomics

9:1063–1084. doi: 10.1074/mcp.M900325-MCP200

Fetsch EE, Davidson AL (2002) Vanadate-catalyzed photocleavage of the signature motif of an ATP-binding cassette (ABC) transporter. Proc Natl Acad Sci U S A 99:9685–9690. doi: 10.1073/pnas.152204499

Fitzpatrick LM, Keegstra K (2001) A method for isolating a high yield of Arabidopsis chloroplasts capable of efficient import of precursor proteins. Plant J 27:59–65. doi: 10.1046/j.0960-7412.2001.01061.x

Floss DS, Walter MH (2009) Role of carotenoid cleavage dioxygenase 1 (CCD1) in apocarotenoid biogenesis revisited. Plant Signal Behav 4:172–175.

Flower DR (1994) The lipocalin protein family: a role in cell regulation. FEBS Lett 354:7–11. doi: 10.1016/0014-5793(94)01078-1

Flower DR (1996) The lipocalin protein family: structure and function. Biochem J 318 (Pt 1:1–14.

Flower DR, North a. CT, Sansom CE (2000) The lipocalin protein family: Structural and sequence overview. Biochim Biophys Acta - Protein Struct Mol Enzymol 1482:9–24. doi: 10.1016/S0167-4838(00)00148-5

Friso G, Majeran W, Huang M, et al (2010) Reconstruction of metabolic pathways, protein expression, and homeostasis machineries across maize bundle sheath and mesophyll chloroplasts: large-scale quantitative proteomics using the first maize genome assembly. Plant Physiol 152:1219–1250. doi: 10.1104/pp.109.152694

Froehlich JE, Wilkerson CG, Ray WK, et al (2003) Proteomic study of the Arabidopsis thaliana chloroplastic envelope membrane utilizing alternatives to traditional two-dimensional electrophoresis. J Proteome Res 2:413–425. doi: 10.1021/pr034025j

Fukamatsu Y, Tamura T, Hihara S, Oda K (2013) Mutations in the CCD4 carotenoid cleavage dioxygenase gene of yellow-flesh peaches. Biosci Biotechnol Biochem 77:2514–2516. doi: 10.1271/bbb.130626

Fukuyama K (2004) Structure and function of plant-type ferredoxins. Photosynth Res 81:289–301. doi: 10.1023/B:PRES.0000036882.19322.0a

Gámez-Arjona FM, de la Concepción JC, Raynaud S, Mérida A (2014) Arabidopsis thaliana plastoglobule-associated fibrillin 1a interacts with fibrillin 1b in vivo. FEBS Lett 588:2800–2804. doi: 10.1016/j.febslet.2014.06.024

Garcia O, Bouige P, Forestier C, Dassa E (2004) Inventory and comparative analysis of rice and Arabidopsis ATP-binding cassette (ABC) systems. J Mol Biol 343:249–65. doi: 10.1016/j.jmb.2004.07.093

Gaude N, Bréhélin C, Tischendorf G, et al (2007) Nitrogen deficiency in Arabidopsis affects galactolipid composition and gene expression and results in accumulation of fatty acid phytyl esters. Plant J 49:729–739. doi: 10.1111/j.1365-313X.2006.02992.x

Ghosh S, Hudak KA, Dumbroff EB, Thompson JE (1994) Release of photosynthetic protein catabolites by blebbing from thylakoids. Plant Physiol 106:1547–1553. doi: 10.1104/pp.106.4.1547

Ghosh S, Mahoney SR, Penterman JN, et al (2001) Ultrastructural and biochemical changes in chloroplasts during Brassica napus senescence. Plant Physiol Biochem 39:777–784. doi: 10.1016/S0981-9428(01)01296-7

Giacomelli L, Rudella A, van Wijk KJ (2006) High light response of the thylakoid proteome in arabidopsis wild type and the ascorbate-deficient mutant vtc2-2. A comparative proteomics study. Plant Physiol 141:685–701. doi: 10.1104/pp.106.080150

Giegé P, Grienenberger JM, Bonnard G (2008) Cytochrome c biogenesis in mitochondria. Mitochondrion 8:61–73. doi: 10.1016/j.mito.2007.10.001

Gillet B, Beyly A, Peltier G, Rey P (1998) Molecular characterization of CDSP 34, a chloroplastic protein induced by water deficit in Solanum tuberosum L. plants, and regulation of CDSP 34 expression by ABA and high illumination. Plant J 16:257–262. doi: 10.1046/j.1365-313x.1998.00292.x

Gomez-Roldan V, Fermas S, Brewer PB, et al (2008) Strigolactone inhibition of shoot branching. Nature 455:189–194. doi: 10.1038/nature07271

Gonzalez-Jorge S, Ha SH, Magallanes-Lundback M, et al (2013) Carotenoid cleavage dioxygenase 4 is a negative regulator of beta-carotene content in Arabidopsis seeds. Plant Cell 25:4812–4826. doi: 10.1105/tpc.113.119677

Greenwood AD, Leech RM, Williams JP (1963) The osmiophilic globules of chloroplasts: I. Osmiophilic globules as a normal component of chloroplasts and their isolation and composition in Vicia Faba L. Biochim Biophys Acta 78:148–162. doi: 10.1016/0006-3002(63)91620-2

Grennan AK (2008) Plastoglobule proteome. Plant Physiol 147:443–445. doi: 10.1104/pp.104.900261

Grevelding C, Suter-Crazzolara C, Von Menges A, et al (1996) Characterisation of a new allele of pale cress and its role in greening in Arabidopsis thaliana. Mol Gen Genet 251:532–541. doi: 10.1007/s004380050199

Gruszka J, Pawlak A, Kruk J (2008) Tocochromanols, plastoquinol, and other biological prenyllipids as singlet oxygen quenchers—determination of singlet oxygen quenching rate constants and oxidation products. Free Radic Biol Med 45:920–928. doi: 10.1016/j.freeradbiomed.2008.06.025

Grütter C, Alonso E, Chougnet A, Woggon WD (2006) A biomimetic chromanol cyclization leading to alpha-tocopherol. Angew Chemie 45:1126–1130. doi: 10.1002/anie.200503123

Grzyb JM, Solymosi K, Strzalka K, Mysliwa-Kurdziel B (2013) Visualization and characterization of prolamellar bodies with atomic force microscopy. J Plant Physiol 170:1217–1227. doi: 10.1016/j.jplph.2013.04.017

Guindon S, Dufayard JF, Hordijk W, et al (2009) PhyML: Fast and Accurate Phylogeny Reconstruction by Maximum Likelihood. Infect Genet Evol 9:384–385.

Gunning BE (2001) Membrane geometry of "open" prolamellar bodies. Protoplasma 215:4–15. doi: 10.1007/BF01280299

Hagemann R (2010) The foundation of extranuclear inheritance: plastid and mitochondrial genetics. Mol Genet Genomics 283:199–209. doi: 10.1007/s00438-010-0521-z

Han S, Inoue H, Terada T, et al (2002) Design and synthesis of lignostilbene-alpha,beta-dioxygenase inhibitors. Bioorg Med Chem Lett 12:1139–1142.

Harrison PJ, Bugg TDH (2014) Enzymology of the carotenoid cleavage dioxygenases: Reaction mechanisms, inhibition and biochemical roles. Arch Biochem Biophys 544:105–111. doi: 10.1016/j.abb.2013.10.005

Härtel H, Dörmann P, Benning C (2000) DGD1-independent biosynthesis of extraplastidic galactolipids after phosphate deprivation in Arabidopsis. Proc Natl Acad Sci U S A 97:10649–10654. doi: 10.1073/pnas.180320497

Havaux M (2014) Carotenoid oxidation products as stress signals in plants. Plant J 79:597–606. doi: 10.1111/tpj.12386

Havaux M, Dall'Osto L, Bassi R (2007) Zeaxanthin has enhanced antioxidant capacity with respect to all other xanthophylls in Arabidopsis leaves and functions independent of binding to PSII antennae. Plant Physiol 145:1506–1520. doi: 10.1104/pp.107.108480

Havaux M, Eymery F, Porfirova S, et al (2005) Vitamin E protects against photoinhibition and photooxidative stress in Arabidopsis thaliana. Plant Cell 17:3451–3469. doi: 10.1105/tpc.105.037036

Helm S, Dobritzsch D, Rodiger A, et al (2014) Protein identification and quantification by data-independent acquisition and multi-parallel collision-induced dissociation mass spectrometry (MSE) in the chloroplast stroma proteome. J Proteomics 98:79–89. doi: 10.1016/j.jprot.2013.12.007

Hiltbrunner A, Bauer J, Vidi PA, et al (2001) Targeting of an abundant cytosolic form of the protein import receptor at Toc159 to the outer chloroplast membrane. J Cell Biol 154:309–316. doi:

10.1083/jcb.200104022

Hirayama T, Shinozaki K (2007) Perception and transduction of abscisic acid signals: keys to the function of the versatile plant hormone ABA. Trends Plant Sci 12:343–351. doi: 10.1016/j.tplants.2007.06.013

Hjorth E, Hadfi K, Zauner S, Maier UG (2005) Unique genetic compartmentalization of the SUF system in cryptophytes and characterization of a SufD mutant in Arabidopsis thaliana. FEBS Lett 579:1129–1135. doi: 10.1016/j.febslet.2004.12.084

Holding DR, Springer PS, Coomber SA (2000) The chloroplast and leaf developmental mutant, pale cress, exhibits light-conditional severity and symptoms characteristic of its ABA deficiency. Ann Bot 86:953–962. doi: 10.1006/anbo.2000.1263

Hornero-Méndez D, Mínguez-Mosquera MI (2000) Xanthophyll esterification accompanying carotenoid overaccumulation in chromoplast of Capsicum annuum ripening fruits is a constitutive process and useful for ripeness index. J Agric Food Chem 48:1617–1622. doi: 10.1021/jf9912046

Hörtensteiner S, Feller U (2002) Nitrogen metabolism and remobilization during senescence. J Exp Bot 53:927–937. doi: 10.1093/jexbot/53.370.927

Huang CF, Yamaji N, Ma JF (2010) Knockout of a bacterial-type ATP-binding cassette transporter gene, AtSTAR1, results in increased aluminum sensitivity in Arabidopsis. Plant Physiol 153:1669–1677. doi: pp.110.155028 [pii] 10.1104/pp.110.155028

Huang CF, Yamaji N, Mitani N, et al (2009a) A bacterial-type ABC transporter is involved in aluminum tolerance in rice. Plant Cell 21:655–667. doi: 10.1105/tpc.108.064543

Huang FC, Molnar P, Schwab W (2009b) Cloning and functional characterization of carotenoid cleavage dioxygenase 4 genes. J Exp Bot 60:3011–3022. doi: 10.1093/jxb/erp137

Huang M, Friso G, Nishimura K, et al (2013) Construction of plastid reference proteomes for maize and arabidopsis and evaluation of their orthologous relationships; The concept of orthoproteomics. J Proteome Res 12:491–504. doi: 10.1021/pr300952g

Hurlock AK, Roston RL, Wang K, Benning C (2014) Lipid trafficking in plant cells. Traffic 15:915–932. doi: 10.1111/tra.12187

Ifuku K, Endo T, Shikanai T, Aro EM (2011) Structure of the Chloroplast NADH Dehydrogenase-Like Complex: Nomenclature for Nuclear-Encoded Subunits. Plant Cell Physiol 52:1560–1568. doi: 10.1093/pcp/pcr098

Imai A, Takahashi S, Nakayama K, Satoh H (2013) The promoter of the carotenoid cleavage dioxygenase 4a-5 gene of Chrysanthemum morifolium (CmCCD4a-5) drives petal-specific transcription of a conjugated gene in the developing flower. J Plant Physiol 170:1295–1299. doi: 10.1016/j.jplph.2013.04.001

Ischebeck T, Zbierzak AM, Kanwischer M, Dörmann P (2006) A salvage pathway for phytol metabolism in Arabidopsis. J Biol Chem 281:2470–2477. doi: 10.1074/jbc.M509222200

Iuchi S, Kobayashi M, Taji T, et al (2001) Regulation of drought tolerance by gene manipulation of 9-cis-epoxycarotenoid dioxygenase, a key enzyme in abscisic acid biosynthesis in Arabidopsis. Plant J 27:325–333. doi: 10.1046/j.1365-313x.2001.01096.x

Iuchi S, Kobayashi M, Yamaguchi-Shinozaki K, Shinozaki K (2000) A stress-inducible gene for 9-cis-epoxycarotenoid dioxygenase involved in abscisic acid biosynthesis under water stress in drought-tolerant cowpea. Plant Physiol 123:553–562.

Jahns P, Holzwarth AR (2012) The role of the xanthophyll cycle and of lutein in photoprotection of photosystem II. Biochim Biophys Acta 1817:182–193. doi: 10.1016/j.bbabio.2011.04.012

Jans F, Mignolet E, Houyoux PA, et al (2008) A type II NAD(P)H dehydrogenase mediates light-independent plastoquinone reduction in the chloroplast of Chlamydomonas. Proc Natl Acad Sci U S A 105:20546–20551. doi: 10.1073/pnas.0806896105

Jarvis P, Dörmann P, Peto CA, et al (2000) Galactolipid deficiency and abnormal chloroplast development in the Arabidopsis MGD synthase 1 mutant. Proc Natl Acad Sci 97:8175–8179.

Jasinski M, Sudre D, Schansker G, et al (2008) AtOSA1, a member of the Abc1-like family, as a new factor in cadmium and oxidative stress response. Plant Physiol 147:719–731. doi: 10.1104/pp.107.110247

Jensen RG, Bassham JA (1966) Photosynthesis by isolated chloroplasts. Proc Natl Acad Sci U S A 56:1095–1101. doi: 10.1073/pnas.56.4.1095

Jeong SY, Rose A, Meier I (2003) MFP1 is a thylakoid-associated, nucleoid-binding protein with a coiled-coil structure. Nucleic Acids Res 31:5175–5185. doi: 10.1093/nar/gkg693

Jia C, Zhang L, Liu L, et al (2013) Multiple phytohormone signalling pathways modulate susceptibility of tomato plants to Alternaria alternata f. sp. lycopersici. J Exp Bot 64:637–650. doi: 10.1093/jxb/ers360

Jin X, Yang X, Islam E, et al (2008) Effects of cadmium on ultrastructure and antioxidative defense system in hyperaccumulator and non-hyperaccumulator ecotypes of Sedum alfredii Hance. J Hazard Mater 156:387–397. doi: 10.1016/j.jhazmat.2007.12.064

Kang J, Park J, Choi H, et al (2011) Plant ABC Transporters. Arabidopsis Book 9:e0153. doi: 10.1199/tab.0153

Keddie JS, Carroll B, Jones JD, Gruissem W (1996) The DCL gene of tomato is required for chloroplast development and palisade cell morphogenesis in leaves. EMBO J 15:4208–17.

Keskitalo J, Bergquist G, Gardestrom P, Jansson S (2005) A cellular timetable of autumn senescence. Plant Physiol 139:1635–1648. doi: 10.1104/pp.105.066845

Kessler F, Glauser G (2014) Prenylquinone profiling in whole leaves and chloroplast subfractions. Methods Mol Biol 1153:213–226. doi: 10.1007/978-1-4939-0606-2_15

Kessler F, Schnell D, Blobel G (1999) Identification of proteins associated with plastoglobules isolated from pea (Pisum sativum L.) chloroplasts. Planta 208:107–113. doi: 10.1007/s004250050540

Kikuchi S, Bédard J, Hirano M, et al (2013) Uncovering the protein translocon at the chloroplast inner envelope membrane. Science 339:571–4. doi: 10.1126/science.1229262

Kim DY, Bovet L, Maeshima M, et al (2007) The ABC transporter AtPDR8 is a cadmium extrusion pump conferring heavy metal resistance. Plant J 50:207–218. doi: 10.1111/j.1365-313X.2007.03044.x

Kim HU, Wu SSH, Ratnayake C, Huang AHC (2001) Brassica rapa has three genes that encode proteins associated with different neutral lipids in plastids of specific tissues. Plant Physiol 126:330–341. doi: 10.1104/Pp.126.1.330

Kobayashi K, Kondo M, Fukuda H, et al (2007) Galactolipid synthesis in chloroplast inner envelope is essential for proper thylakoid biogenesis, photosynthesis, and embryogenesis. Proc Natl Acad Sci U S A 104:17216–17221. doi: 10.1073/pnas.0704680104

Kobayashi K, Narise T, Sonoike K, et al (2012) Role of galactolipid biosynthesis in coordinated development of photosynthetic complexes and thylakoid membranes during chloroplast biogenesis in Arabidopsis. Plant J 73:250–261. doi: 10.1111/tpj.12028

Kobayashi N, DellaPenna D (2008) Tocopherol metabolism, oxidation and recycling under high light stress in Arabidopsis. Plant J 55:607–618. doi: 10.1111/j.1365-313X.2008.03539.x

Kubis SE, Lilley KS, Jarvis P (2008) Isolation and preparation of chloroplasts from Arabidopsis thaliana plants. Methods Mol Biol 425:171–186. doi: 10.1007/978-1-60327-210-0_16

Larsen PB, Geisler MJB, Jones C a., et al (2005) ALS3 encodes a phloem-localized ABC transporter-like protein that is required for aluminum tolerance in Arabidopsis. Plant J 41:353–363. doi: 10.1111/j.1365-313X.2004.02306.x

Lashbrooke JG, Young PR, Dockrall SJ, et al (2013) Functional characterisation of three members of the Vitis

vinifera L. carotenoid cleavage dioxygenase gene family. BMC Plant Biol. doi: 10.1186/1471-2229-13-156

Lätari K, Wust F, Hubner M, et al (2015) Tissue-specific Apocarotenoid Glycosylation Contributes to Carotenoid Homeostasis in Arabidopsis Leaves. Plant Physiol. doi: 10.1104/pp.15.00243

Leggett Bailey J, Whyborn AG (1963) The osmiophilic globules of chloroplasts: II. Globules of the spinach-beet chloroplast. Biochim Biophys Acta 78:163–174. doi: 10.1016/0006-3002(63)91621-4

Leitner-Dagan Y, Ovadis M, Shklarman E, et al (2006) Expression and functional analyses of the plastid lipid-associated protein CHRC suggest its role in chromoplastogenesis and stress. Plant Physiol 142:233–244. doi: 10.1104/pp.106.082404

Leon P, Arroyo A, Mackenzie S (1998) Nuclear Control of Plastid and Mitochondrial Development in Higher Plants. Annu Rev Plant Physiol Plant Mol Biol 49:453–480. doi: 10.1146/annurev.arplant.49.1.453

Li L, Yuan H (2013) Chromoplast biogenesis and carotenoid accumulation. Arch Biochem Biophys 539:102–109. doi: 10.1016/j.abb.2013.07.002

Li-Beisson Y, Shorrosh B, Beisson F, et al (2013) Acyl-lipid metabolism. Arab B 11:e0161. doi: 10.1199/tab.0161

Li-Beisson Y, Shorrosh B, Beisson F, et al (2010) Acyl-lipid metabolism. Arab B 8:e0133. doi: 10.1199/tab.0133

Lichtenthaler HK (1968) Plastoglobuli and fine structure of plastids. Endeavour 27:144–149.

Lichtenthaler HK, Peveling E (1966) Plastoglobuli in verschiedenen differenzierungsstadien der plastiden bei Allium cepa L. Planta 72:1–13. doi: 10.1007/BF00388140

Lichtenthaler HK, Tevini M (1970) Distribution of pigments, plastidquinones and plastoglobuli in different particle fractions obtained from sonicated spinach chloroplasts. Zeitschrift Für Pflanzenphysiologie 62:33–50.

Lippold F, vom Dorp K, Abraham M, et al (2012) Fatty acid phytyl ester synthesis in chloroplasts of Arabidopsis. Plant Cell 24:2001–2014. doi: 10.1105/tpc.112.095588

Liu JQ, Chen JC, Wang CF, Qiu MH (2009) New cucurbitane triterpenoids and steroidal glycoside from Momordica charantia. Molecules 14:4804–4813. doi: 10.3390/molecules14124804

Liu JW, Rose RJ (1992) The spinach chloroplast chromosome is bound to the thylakoid membrane in the region of the inverted repeat. Biochem Biophys Res Commun 184:993–1000. doi: 10.1016/0006-291X(92)90689-I

Liu Y-G, Mitsukawa N, Oosumi T, Whittier RF (1995) Efficient isolation and mapping of Arabidopsis thaliana T-DNA insert junctions by thermal asymmetric interlaced PCR. Plant J 8:457–463. doi: 10.1046/j.1365-313X.1995.08030457.x

Lohmann A, Schottler MA, Bréhélin C, et al (2006) Deficiency in phylloquinone (vitamin K1) methylation affects prenyl quinone distribution, photosystem I abundance, and anthocyanin accumulation in the Arabidopsis AtmenG mutant. J Biol Chem 281:40461–40472. doi: 10.1074/jbc.M609412200

Lu B, Benning C (2009) A 25-amino acid sequence of the Arabidopsis TGD2 protein is sufficient for specific binding of phosphatidic acid. J Biol Chem 284:17420–17427. doi: 10.1074/jbc.M109.016014

Lu B, Xu C, Awai K, et al (2007) A small ATPase protein of Arabidopsis, TGD3, involved in chloroplast lipid import. J Biol Chem 282:35945–35953. doi: 10.1074/jbc.M704063200

Lundquist PK, Davis JI, van Wijk KJ (2012a) ABC1K atypical kinases in plants: filling the organellar kinase void. Trends Plant Sci 17:546–555. doi: 10.1016/j.tplants.2012.05.010

Lundquist PK, Poliakov A, Bhuiyan NH, et al (2012b) The functional network of the Arabidopsis plastoglobule proteome based on quantitative proteomics and genome-wide coexpression analysis. Plant

Physiol 158:1172–1192. doi: 10.1104/pp.111.193144

Lundquist PK, Poliakov A, Giacomelli L, et al (2013) Loss of plastoglobule kinases ABC1K1 and ABC1K3 causes conditional degreening, modified prenyl-lipids, and recruitment of the jasmonic acid pathway. Plant Cell 25:1818–1839. doi: 10.1105/tpc.113.111120

Lunn JE (2007) Compartmentation in plant metabolism. J Exp Bot 58:35–47. doi: 10.1093/jxb/erl134

Ma G, Zhang L, Matsuta A, et al (2013) Enzymatic formation of beta-citraurin from beta-cryptoxanthin and zeaxanthin by carotenoid cleavage dioxygenase4 in the flavedo of citrus fruit. Plant Physiol 163:682–695. doi: 10.1104/pp.113.223297

Majeran W, Friso G, Asakura Y, et al (2012) Nucleoid-enriched proteomes in developing plastids and chloroplasts from maize leaves: a new conceptual framework for nucleoid functions. Plant Physiol 158:156–189. doi: 10.1104/pp.111.188474

Mandel M a, Feldmann K a, Herrera-Estrella L, et al (1996) CLA1, a novel gene required for chloroplast development, is highly conserved in evolution. Plant J 9:649–658. doi: 10.1046/j.1365-313X.1996.9050649.x

Marchler-Bauer A, Derbyshire MK, Gonzales NR, et al (2015) CDD: NCBI's conserved domain database. Nucleic Acids Res 43:222–226. doi: 10.1093/nar/gku1221

Mariajancyrani J, Chandramohan G, Ravikumar R (2013) Isolation and identification of phytoconstituents from Delonix regia leaves. Int J Pharm Pharm Sci 5:671–674.

Marin E, Divol F, Bechtold N, et al (2006) Molecular characterization of three Arabidopsis soluble ABC proteins which expression is induced by sugars. Plant Sci 171:84–90. doi: 10.1016/j.plantsci.2006.02.014

Martinis J, Glauser G, Valimareanu S, et al (2014) ABC1K1/PGR6 kinase: a regulatory link between photosynthetic activity and chloroplast metabolism. Plant J 77:269–283. doi: 10.1111/tpj.12385

Martinis J, Glauser G, Valimareanu S, Kessler F (2013) A chloroplast ABC1-like kinase regulates vitamin E metabolism in Arabidopsis. Plant Physiol 162:652–662. doi: 10.1104/pp.113.218644

Martinis J, Kessler F, Glauser G (2011) A novel method for prenylquinone profiling in plant tissues by ultra-high pressure liquid chromatography-mass spectrometry. Plant Methods 7:23. doi: 10.1186/1746-4811-7-23

Martinoia E, Klein M, Geisler M, et al (2002) Multifunctionality of plant ABC transporters - more than just detoxifiers. Planta 214:345–355.

Mateo-Bonmati E, Casanova-Saez R, Candela H, Micol JL (2014) Rapid identification of angulata leaf mutations using next-generation sequencing. Planta 240:1113–1122. doi: 10.1007/s00425-014-2137-8

Matile P, Hörtensteiner S, Thomas H (1999) Chlorophyll degradation. Annu Rev Plant Physiol Plant Mol Biol 50:67–95. doi: 10.1146/annurev.arplant.50.1.67

Mehrshahi P, Johnny C, DellaPenna D (2014) Redefining the metabolic continuity of chloroplasts and ER. Trends Plant Sci 19:501–507. doi: 10.1016/j.tplants.2014.02.013

Mehrshahi P, Stefano G, Andaloro JM, et al (2013) Transorganellar complementation redefines the biochemical continuity of endoplasmic reticulum and chloroplasts. Proc Natl Acad Sci U S A 110:12126–12131. doi: 10.1073/pnas.1306331110

Mène-Saffrané L, DellaPenna D (2010) Biosynthesis, regulation and functions of tocochromanols in plants. Plant Physiol Biochem 48:301–309. doi: 10.1016/j.plaphy.2009.11.004

Meurer J, Grevelding C, Westhoff P, Reiss B (1998) The PAC protein affects the maturation of specific chloroplast mRNAs in Arabidopsis thaliana. Mol Gen Genet 258:342–351.

Millner PA, Barber J (1984) Plastoquinone as a mobile redox carrier in the photosynthetic membrane. FEBS

Lett 169:1–6. doi: 10.1016/0014-5793(84)80277-X

Moraga A, Nohales P, Perez J, Gomez-Gomez L (2004) Glucosylation of the saffron apocarotenoid crocetin by a glucosyltransferase isolated from Crocus sativus stigmas. Planta 219:955–966. doi: 10.1007/s00425-004-1299-1

Moraga AR, Ahrazem O, Rambla JL, et al (2013) Crocins with High Levels of Sugar Conjugation Contribute to the Yellow Colours of Early-Spring Flowering Crocus Tepals. PLoS One. doi: ARTN e7194610.1371/journal.pone.0071946

Motohashi R, Rodiger A, Agne B, et al (2012) Common and specific protein accumulation patterns in different albino/pale-green mutants reveals regulon organization at the proteome level. Plant Physiol 160:2189–2201. doi: 10.1104/pp.112.204032

Murashige T, Skoog F (1962) A Revised Medium for Rapid Growth and Bio Assays with Tobacco Tissue Cultures. Physiol Plant 15:473–&.

Murphy DJ (2012) The dynamic roles of intracellular lipid droplets: from archaea to mammals. Protoplasma 249:541–585. doi: 10.1007/s00709-011-0329-7

Mysliwa-Kurdziel B, Jemiola-Rzeminska M, Turek E, et al (2012) Variations in xanthophyll composition in etiolated seedlings of Arabidopsis thaliana correlate with protochlorophyllide accumulation. Acta Biochim Pol 59:57–60.

Nachin L, Loiseau L, Expert D, Barras F (2003) SufC: an unorthodox cytoplasmic ABC/ATPase required for [Fe-S] biogenesis under oxidative stress. EMBO J 22:427–437. doi: 10.1093/emboj/cdg061

Nacir H, Bréhélin C (2013) When proteomics reveals unsuspected roles: the plastoglobule example. Front Plant Sci 4:114. doi: 10.3389/fpls.2013.00114

Naested H, Holm A, Jenkins T, et al (2004) Arabidopsis VARIEGATED 3 encodes a chloroplast-targeted, zinc-finger protein required for chloroplast and palisade cell development. J Cell Sci 117:4807–4818. doi: 10.1242/jcs.01360

Nagane T, Tanaka A, Tanaka R (2010) Involvement of AtNAP1 in the regulation of chlorophyll degradation in Arabidopsis thaliana. Planta 231:939–949. doi: 10.1007/s00425-010-1099-8

Nakagami H, Sugiyama N, Mochida K, et al (2010) Large-scale comparative phosphoproteomics identifies conserved phosphorylation sites in plants. Plant Physiol 153:1161–1174. doi: 10.1104/pp.110.157347

Nakashima A, Iijima Y, Aoki K, et al (2011) Monogalactosyl diacylglycerol is a substrate for lipoxygenase: its implications for oxylipin formation directly from lipids. J Plant Interact 6:93–97. doi: 10.1080/17429145.2010.544767

Newell CA, Gray JC (2010) Binding of lac repressor-GFP fusion protein to lac operator sites inserted in the tobacco chloroplast genome examined by chromatin immunoprecipitation. Nucleic Acids Res 38:e145. doi: 10.1093/nar/gkq413

Ohmiya A (2009) Carotenoid cleavage dioxygenases and their apocarotenoid products in plants. Plant Biotechnol 26:351–358. doi: 10.5511/plantbiotechnology.26.351

Ohmiya A, Kishimoto S, Aida R, et al (2006) Carotenoid cleavage dioxygenase (CmCCD4a) contributes to white color formation in Chrysanthemum petals. Plant Physiol 142:1193–1201. doi: 10.1104/pp.106.087130

Ohmiya A, Toyoda T, Watanabe H, et al (2012) Mechanism behind Petal Color Mutation Induced by Heavy-Ion-Beam Irradiation of Recalcitrant Chrysanthemum Cultivar. J Japanese Soc Hortic Sci 81:269–274.

Olejnik D, Gogolewski M, Nogala-Kałucka M (1997) Isolation and some properties of plastochromanol-8. Food / Nahrung 41:101–104. doi: 10.1002/food.19970410209

Osterman A, Overbeek R (2003) Missing genes in metabolic pathways: A comparative genomics approach. Curr Opin Chem Biol 7:238–251. doi: 10.1016/S1367-5931(03)00027-9

Othman R, Mohd Zaifuddin FA, Hassan NM (2014) Carotenoid biosynthesis regulatory mechanisms in plants. J Oleo Sci 63:753–760. doi: 10.5650/jos.ess13183

Pang K, Li Y, Liu M, et al (2013) Inventory and general analysis of the ATP-binding cassette (ABC) gene superfamily in maize (Zea mays L.). Gene 526:411–428. doi: 10.1016/j.gene.2013.05.051

Parry AD, Horgan R (1991) Carotenoid Metabolism and the Biosynthesis of Abscisic-Acid. Phytochemistry 30:815–821. doi: 10.1016/0031-9422(91)85258-2

Peng L, Shimizu H, Shikanai T (2008) The chloroplast NAD(P)H dehydrogenase complex interacts with photosystem I in Arabidopsis. J Biol Chem 283:34873–34879. doi: M803207200 [pii] 10.1074/jbc.M803207200

Pfalz J, Pfannschmidt T (2012) Essential nucleoid proteins in early chloroplast development. Trends Plant Sci. doi: 10.1016/j.tplants.2012.11.003

Philippar K, Geis T, Ilkavets I, et al (2007) Chloroplast biogenesis: the use of mutants to study the etioplast-chloroplast transition. Proc Natl Acad Sci U S A 104:678–683. doi: 10.1073/pnas.0610062104

Poon WW, Davis DE, Ha HT, et al (2000) Identification of Escherichia coli ubiB, a gene required for the first monooxygenase step in ubiquinone biosynthesis. J Bacteriol 182:5139–5146. doi: 10.1128/JB.182.18.5139-5146.2000

Porfirova S, Bergmuller E, Tropf S, et al (2002) Isolation of an Arabidopsis mutant lacking vitamin E and identification of a cyclase essential for all tocopherol biosynthesis. Proc Natl Acad Sci U S A 99:12495–12500. doi: 10.1073/pnas.182330899

Pozueta-Romero J, Rafia F, Houlne G, et al (1997) A ubiquitous plant housekeeping gene, PAP, encodes a major protein component of bell pepper chromoplasts. Plant Physiol 115:1185–1194. doi: 10.1104/pp.115.3.1185

Qin XQ, Zeevaart JAD (1999) The 9-cis-epoxycarotenoid cleavage reaction is the key regulatory step of abscisic acid biosynthesis in water-stressed bean. Proc Natl Acad Sci U S A 96:15354–15361. doi: 10.1073/pnas.96.26.15354

Quirino BF, Noh YS, Himelblau E, Amasino RM (2000) Molecular aspects of leaf senescence. Trends Plant Sci 5:278–282. doi: 10.1016/S1360-1385(00)01655-1

Ramel F, Birtic S, Ginies C, et al (2012) Carotenoid oxidation products are stress signals that mediate gene responses to singlet oxygen in plants. Proc Natl Acad Sci U S A 109:5535–5540. doi: 10.1073/pnas.1115982109

Rayapuram N, Hagenmuller J, Grienenberger JM, et al (2007) AtCCMA interacts with AtCcmB to form a novel mitochondrial ABC transporter involved in cytochrome c maturation in Arabidopsis. J Biol Chem 282:21015–21023. doi: 10.1074/jbc.M704091200

Rea PA (2007) Plant ATP-Binding cassette transporters. Annu Rev Plant Biol 58:347–375. doi: 10.1146/annurev.arplant.57.032905.105406

Reboud X, Zeyl C (1994) Organelle inheritance in plants. Heredity (Edinb) 72:132–140. doi: 10.1038/Hdy.1994.19

Reiter RS, Coomber SA, Bourett TM, et al (1994) Control of leaf and chloroplast development by the Arabidopsis gene pale cress. Plant Cell 6:1253–1264. doi: 10.1105/tpc.6.9.1253 6/9/1253 [pii]

Rensink WA, Pilon M, Weisbeek P (1998) Domains of a transit sequence required for in vivo import in Arabidopsis chloroplasts. Plant Physiol 118:691–699.

Reverdatto S, Beilinson V, Nielsen NC (1999) A multisubunit acetyl coenzyme A carboxylase from soybean. Plant Physiol 119:961–978. doi: 10.1104/pp.119.3.961

Reyes-Prieto A, Weber APM, Bhattacharya D (2007) The origin and establishment of the plastid in algae and plants. Annu Rev Genet 41:147–168. doi: 10.1146/annurev.genet.41.110306.130134

Reynolds ES (1963) The use of lead citrate at high pH as an electron-opaque stain in electron microscopy. J Cell Biol 17:208–212.

Rodermel S (2001) Pathways of plastid-to-nucleus signaling. Trends Plant Sci 6:471–478. doi: 10.1016/S1360-1385(01)02085-4

Rodrigo MJ, Alquezar B, Alos E, et al (2013) A novel carotenoid cleavage activity involved in the biosynthesis of Citrus fruit-specific apocarotenoid pigments. J Exp Bot 64:4461–4478. doi: 10.1093/jxb/ert260

Roston R, Hurlock AK, Benning C (2014) Plastidic ABC Proteins. In: Plant ABC Transporter.

Roston RL, Gao J, Murcha MW, et al (2012) TGD1, -2, and -3 proteins involved in lipid trafficking form ATP-binding cassette (ABC) transporter with multiple substrate-binding proteins. J Biol Chem 287:21406–21415. doi: 10.1074/jbc.M112.370213

Rottet S, Besagni C, Kessler F (2015) The role of plastoglobules in thylakoid lipid remodeling during plant development. Biochim Biophys Acta-Bioenergetics 1847:889–899. doi: 10.1016/j.bbabio.2015.02.002

Rubio A, Rambla JL, Santaella M, et al (2008) Cytosolic and plastoglobule-targeted carotenoid dioxygenases from Crocus sativus are both involved in beta-ionone release. J Biol Chem 283:24816–24825. doi: 10.1074/jbc.M804000200

Rubio-Moraga A, Rambla JL, Fernandez-de-Carmen A, et al (2014) New target carotenoids for CCD4 enzymes are revealed with the characterization of a novel stress-induced carotenoid cleavage dioxygenase gene from Crocus sativus. Plant Mol Biol 86:555–569. doi: 10.1007/s11103-014-0250-5

Ruiz-Sola MA, Rodríguez-Concepción M (2012) Carotenoid biosynthesis in Arabidopsis: a colorful pathway. In: The Arabidopsis Book / American Society of Plant Biologists. p e0158

Rütgers M, Schroda M (2013) A role of VIPP1 as a dynamic structure within thylakoid centers as sites of photosystem biogenesis? Plant Signal Behav 8:e27037. doi: 10.4161/psb.27037

Sambrook J, Russell DW (2001) Molecular cloning: a laboratory manual. Cold Spring Harbor Laboratory Press, Cold Spring Harbor, New York

Sanchez-Fernandez R, Davies TG, Coleman JO, Rea PA (2001) The Arabidopsis thaliana ABC protein superfamily, a complete inventory. J Biol Chem 276:30231–30244. doi: 10.1074/jbc.M103104200M103104200 [pii]

Sandalio LM, Dalurzo HC, Gómez M, et al (2001) Cadmium-induced changes in the growth and oxidative metabolism of pea plants. J Exp Bot 52:2115–2126. doi: 10.1093/jexbot/52.364.2115

Schelbert S, Aubry S, Burla B, et al (2009) Pheophytin pheophorbide hydrolase (pheophytinase) is involved in chlorophyll breakdown during leaf senescence in Arabidopsis. Plant Cell 21:767–785. doi: 10.1105/tpc.108.064089

Scholl RL, May ST, Ware DH (2000) Seed and molecular resources for Arabidopsis. Plant Physiol 124:1477–1480.

Schwartz SH, Qin X, Loewen MC (2004) The biochemical characterization of two carotenoid cleavage enzymes from Arabidopsis indicates that a carotenoid-derived compound inhibits lateral branching. J Biol Chem 279:46940–46945. doi: 10.1074/jbc.M409004200

Schwartz SH, Qin X, Zeevaart JA (2003) Elucidation of the indirect pathway of abscisic acid biosynthesis by mutants, genes, and enzymes. Plant Physiol 131:1591–1601. doi: 10.1104/pp.102.017921

Schwartz SH, Tan BC, Gage DA, et al (1997) Specific oxidative cleavage of carotenoids by VP14 of maize. Science (80-) 276:1872–1874.

Schweiggert U, Kurz C, Schieber A, Carle R (2006) Effects of processing and storage on the stability of free and esterified carotenoids of red peppers (Capsicum annuum L.) and hot chilli peppers (Capsicum frutescens L.). Eur Food Res Technol 225:261–270. doi: 10.1007/s00217-006-0413-y

Seto Y, Sado A, Asami K, et al (2014) Carlactone is an endogenous biosynthetic precursor for strigolactones. Proc Natl Acad Sci U S A 111:1640–1645. doi: 10.1073/pnas.1314805111

Shanmugabalaji V, Besagni C, Eugeni Piller L, et al (2013) Dual targeting of a mature plastoglobulin/fibrillin fusion protein to chloroplast plastoglobules and thylakoids in transplastomic tobacco plants. Plant Mol Biol 81:13–25. doi: 10.1007/s11103-012-9977-z

Shimoni-Shor E, Hassidim M, Yuval-Naeh N, Keren N (2010) Disruption of Nap14, a plastid-localized non-intrinsic ABC protein in Arabidopsis thaliana results in the over-accumulation of transition metals and in aberrant chloroplast structures. Plant Cell Environ. doi: PCE2124 [pii] 10.1111/j.1365-3040.2010.02124.x

Simkin AJ, Gaffé J, Alcaraz JP, et al (2007) Fibrillin influence on plastid ultrastructure and pigment content in tomato fruit. Phytochemistry 68:1545–1556. doi: 10.1016/j.phytochem.2007.03.014

Simkin AJ, Schwartz SH, Auldridge M, et al (2004a) The tomato carotenoid cleavage dioxygenase 1 genes contribute to the formation of the flavor volatiles beta-ionone, pseudoionone, and geranylacetone. Plant J 40:882–892. doi: 10.1111/j.1365-313X.2004.02263.x

Simkin AJ, Underwood BA, Auldridge M, et al (2004b) Circadian regulation of the PhCCD1 carotenoid cleavage dioxygenase controls emission of beta-ionone, a fragrance volatile of petunia flowers. Plant Physiol 136:3504–3514. doi: 10.1104/pp.104.049718

Simm S, Papasotiriou DG, Ibrahim M, et al (2013) Defining the core proteome of the chloroplast envelope membranes. Front Plant Sci 4:11. doi: 10.3389/fpls.2013.00011

Singh DK, Laremore TN, Smith PB, et al (2012) Knockdown of FIBRILLIN4 gene expression in apple decreases plastoglobule plastoquinone content. PLoS One 7:e47547. doi: 10.1371/journal.pone.0047547

Singh DK, Maximova SN, Jensen PJ, et al (2010) FIBRILLIN4 is required for plastoglobule development and stress resistance in apple and Arabidopsis. Plant Physiol 154:1281–1293. doi: 10.1104/pp.110.164095

Singh DK, McNellis TW (2011) Fibrillin protein function: the tip of the iceberg? Trends Plant Sci 16:432–441. doi: 10.1016/j.tplants.2011.03.014

Smith MD, Schnell DJ, Fitzpatrick L, Keegstra K (2003) In vitro analysis of chloroplast protein import. Curr Protoc Cell Biol Chapter 11:Unit11 16. doi: 10.1002/0471143030.cb1116s17

Solfanelli C, Solfanelli C, Poggi A, et al (2006) Sucrose-Specific Induction of the Anthocyanin Biosynthetic Pathway in Arabidopsis. Plant Physiol 140:637–646. doi: 10.1104/pp.105.072579.the

Soll J, Schultz G, Joyard J, et al (1985) Localization and synthesis of prenylquinones in isolated outer and inner envelope membranes from spinach chloroplasts. Arch Biochem Biophys 238:290–299. doi: 10.1016/0003-9861(85)90167-5

Solymosi K, Schoefs B (2010) Etioplast and etio-chloroplast formation under natural conditions: the dark side of chlorophyll biosynthesis in angiosperms. Photosynth Res 105:143–166. doi: 10.1007/s11120-010-9568-2

Spicher L, Kessler F (2015) Unexpected roles of plastoglobules (plastid lipid droplets) in vitamin K1 and E metabolism. Curr Opin Plant Biol 25:123–129. doi: 10.1016/j.pbi.2015.05.005

Sprey B, Lichtenthaler HK (1966) Zur frage der beziehungen zwischen plastoglobuli und thylakoidgenese in gerstenkeimlingen. Zeitschrift Für Naturforsch Part B-Chemie Biochem Biophys Biol Und Verwandten Gebiete B 21:697–699.

Springer A, Acker G, Bartsch S, et al (2015) Differences in gene expression between natural and artificially induced leaf senescence in barley. J Plant Physiol 176:180–191. doi: 10.1016/j.jplph.2015.01.004

Steinmüller D, Tevini M (1985) Composition and function of plastoglobuli : I. Isolation and purification from chloroplasts and chromoplasts. Planta 163:201–207. doi: 10.1007/BF00393507

Szymańska R, Kruk J (2010) Plastoquinol is the main prenyllipid synthesized during acclimation to high light

conditions in Arabidopsis and is converted to plastochromanol by tocopherol cyclase. Plant Cell Physiol 51:537–545. doi: 10.1093/pcp/pcq017

Takahashi Y, Tokumoto U (2002) A third bacterial system for the assembly of iron-sulfur clusters with homologs in archaea and plastids. J Biol Chem 277:28380–28383. doi: 10.1074/jbc.C200365200 C200365200 [pii]

Tan BC, Joseph LM, Deng WT, et al (2003) Molecular characterization of the Arabidopsis 9-cis epoxycarotenoid dioxygenase gene family. Plant J 35:44–56. doi: 10.1046/j.1365-313X.2003.01786.x

Tan BC, Schwartz SH, Zeevaart JAD, McCarty DR (1997) Genetic control of abscisic acid biosynthesis in maize. Proc Natl Acad Sci U S A 94:12235–12240. doi: 10.1073/pnas.94.22.12235

Terasawa K, Sato N (2005) Visualization of plastid nucleoids in situ using the PEND-GFP fusion protein. Plant Cell Physiol 46:649–660. doi: 10.1093/pcp/pci070

Tevini M, Steinmüller D (1985) Composition and function of plastoglobuli : II. Lipid composition of leaves and plastoglobuli during beech leaf senescence. Planta 163:91–96. doi: 10.1007/BF00395902

Theodoulou FL (2000) Plant ABC transporters. Biochim Biophys Acta - Biomembr 1465:79–103. doi: 10.1016/S0005-2736(00)00132-2

Thomas H, Howarth CJ (2000) Five ways to stay green. J Exp Bot 51:329–337. doi: 10.1093/jexbot/51.suppl_1.329

Thomson WW, Whatley JM (1980) Development of non-green plastids. Annu Rev Plant Physiol Plant Mol Biol 31:375–394. doi: 10.1146/annurev.pp.31.060180.002111

Timmis JN, Ayliffe MA, Huang CY, Martin W (2004) Endosymbiotic gene transfer: Organelle genomes forge eukaryotic chromosomes. Nat Rev Genet 5:123–135. doi: 10.1038/Nrg1271

Tommaso P, Moretti S, Xenarios I, et al (2011) T-Coffee: a web server for the multiple sequence alignment of protein and RNA sequences using structural information and homology extension. Nucleic Acids Res 39:W13–W17. doi: 10.1093/nar/gkr245

Triantaphylidès C, Krischke M, Hoeberichts FA, et al (2008) Singlet oxygen is the major reactive oxygen species involved in photooxidative damage to plants. Plant Physiol 148:960–968. doi: 10.1104/pp.108.125690

Valentin HE, Lincoln K, Moshiri F, et al (2006) The Arabidopsis vitamin E pathway gene5-1 mutant reveals a critical role for phytol kinase in seed tocopherol biosynthesis. Plant Cell 18:212–224. doi: 10.1105/tpc.105.037077

Verrier PJ, Bird D, Buria B, et al (2008) Plant ABC proteins - a unified nomenclature and updated inventory. Trends Plant Sci 13:151–159. doi: 10.1016/j.tplants.2008.02.001

Vidi PA, Kanwischer M, Baginsky S, et al (2006) Tocopherol cyclase (VTE1) localization and vitamin E accumulation in chloroplast plastoglobule lipoprotein particles. J Biol Chem 281:11225–11234. doi: 10.1074/jbc.M511939200

Vidi PA, Kessler F, Bréhélin C (2007) Plastoglobules: a new address for targeting recombinant proteins in the chloroplast. BMC Biotechnol 7:-. doi: 10.1186/1472-6750-7-4

Villiers F, Ducruix C, Hugouvieux V, et al (2011) Investigating the plant response to cadmium exposure by proteomic and metabolomic approaches. Proteomics 11:1650–1663. doi: 10.1002/pmic.201000645

Vishnevetsky M, Ovadis M, Vainstein A (1999) Carotenoid sequestration in plants: the role of carotenoid-associated proteins. Trends Plant Sci 4:232–235. doi: 10.1016/S1360-1385(99)01414-4

Vothknecht UC, Otters S, Hennig R, Schneider D (2012) Vipp1: a very important protein in plastids?! J Exp Bot 63:1699–1712. doi: 10.1093/jxb/err357

Vothknecht UC, Westhoff P (2001) Biogenesis and origin of thylakoid membranes. Biochim Biophys Acta

1541:91–101. doi: S0167-4889(01)00153-7 [pii]

Vu HS, Tamura P, Galeva NA, et al (2012) Direct infusion mass spectrometry of oxylipin-containing Arabidopsis membrane lipids reveals varied patterns in different stress responses. Plant Physiol 158:324–339. doi: 10.1104/pp.111.190280

Walter MH, Floss DS, Strack D (2010) Apocarotenoids: hormones, mycorrhizal metabolites and aroma volatiles. Planta 232:1–17. doi: 10.1007/s00425-010-1156-3

Walther TC, Farese R V (2012) Lipid droplets and cellular lipid metabolism. Annu Rev Biochem 81:687–714. doi: 10.1146/annurev-biochem-061009-102430

Wang P, Duan W, Takabayashi A, et al (2006) Chloroplastic NAD(P)H Dehydrogenase in Tobacco Leaves Functions in Alleviation of Oxidative Damage Caused by Temperature Stress. Plant Physiol 141:465–474. doi: 10.1104/pp.105.070490.1

Wang Z, Xu C, Benning C (2012) TGD4 involved in endoplasmic reticulum-to-chloroplast lipid trafficking is a phosphatidic acid binding protein. Plant J 70:614–623. doi: 10.1111/j.1365-313X.2012.04900.x

Waters MT, Langdale JA (2009) The making of a chloroplast. EMBO J 28:2861–2873. doi: 10.1038/emboj.2009.264

Wei S, Hannoufa A, Soroka J, et al (2011) Enhanced beta-ionone emission in Arabidopsis over-expressing AtCCD1 reduces feeding damage in vivo by the crucifer flea beetle. Env Entomol 40:1622–1630. doi: 10.1603/EN11088

Weigel D, Glazebrook J (2002) Arabidopsis: a laboratory manual. Cold Spring Harbor Laboratory Press, Cold Spring Harbor, New York

Wellburn AR (1994) The Spectral Determination of Chlorophyll-a and Chlorophhyll-B, as Well as Total Carotenoids, Using Various Solvents with Spectrophotometers of Different Resolution. J Plant Physiol 144:307–313.

Wessel D, Flugge UI (1984) A method for the quantitative recovery of protein in dilute solution in the presence of detergents and lipids. Anal Biochem 138:141–143. doi: 0003-2697(84)90782-6 [pii]

Xie LX, Hsieh EJ, Watanabe S, et al (2011) Expression of the human atypical kinase ADCK3 rescues coenzyme Q biosynthesis and phosphorylation of Coq polypeptides in yeast coq8 mutants. Biochim Biophys Acta 1811:348–360. doi: 10.1016/j.bbalip.2011.01.009

Xu C, Fan J, Froehlich JE, et al (2005a) Mutation of the TGD1 chloroplast envelope protein affects phosphatidate metabolism in Arabidopsis. Plant Cell 17:3094–3110. doi: tpc.105.035592 [pii] 10.1105/tpc.105.035592

Xu C, Fan J, Riekhof W, et al (2003) A permease-like protein involved in ER to thylakoid lipid transfer in Arabidopsis. EMBO J 22:2370–2379. doi: 10.1093/emboj/cdg234

Xu XM, Adams S, Chua NH, Moller SG (2005b) AtNAP1 represents an atypical SufB protein in Arabidopsis plastids. J Biol Chem 280:6648–6654.

Xu XM, Moller SG (2006) AtSufE is an essential activator of plastidic and mitochondrial desulfurases in Arabidopsis. EMBO J 25:900–909. doi: 7600968 [pii] 10.1038/sj.emboj.7600968

Xu XM, Moller SG (2008) Iron-sulfur cluster biogenesis systems and their crosstalk. Chembiochem 9:2355–2362. doi: 10.1002/cbic.200800384

Yamada K, Lim J, Dale JM, et al (2003) Empirical analysis of transcriptional activity in the Arabidopsis genome. Science 302:842–846. doi: 10.1126/science.1088305

Yamamoto H, Peng LW, Fukao Y, Shikanai T (2011) An Src Homology 3 Domain-Like Fold Protein Forms a Ferredoxin Binding Site for the Chloroplast NADH Dehydrogenase-Like Complex in Arabidopsis. Plant Cell 23:1480–1493. doi: 10.1105/tpc.110.080291

Ye XD, Al-Babili S, Kloti A, et al (2000) Engineering the provitamin A (beta-carotene) biosynthetic pathway into (carotenoid-free) rice endosperm. Science (80-) 287:303–305. doi: 10.1126/science.287.5451.303

Yoshioka S, Aida R, Yamamizo C, et al (2012) The carotenoid cleavage dioxygenase 4 (CmCCD4a) gene family encodes a key regulator of petal color mutation in chrysanthemum. Euphytica 184:377–387. doi: 10.1007/s10681-011-0602-z

Youssef A, Laizet Y, Block MA, et al (2010) Plant lipid-associated fibrillin proteins condition jasmonate production under photosynthetic stress. Plant J 61:436–445. doi: 10.1111/j.1365-313X.2009.04067.x

Ytterberg AJ, Peltier JB, van Wijk KJ (2006) Protein profiling of plastoglobules in chloroplasts and chromoplasts. A surprising site for differential accumulation of metabolic enzymes. Plant Physiol 140:984–997. doi: 10.1104/pp.105.076083

Yu B, Xu C, Benning C (2002) Arabidopsis disrupted in SQD2 encoding sulfolipid synthase is impaired in phosphate-limited growth. Proc Natl Acad Sci U S A 99:5732–5737. doi: 10.1073/pnas.082696499

Zbierzak AM, Kanwischer M, Wille C, et al (2010) Intersection of the tocopherol and plastoquinol metabolic pathways at the plastoglobule. Biochem J 425:389–399. doi: 10.1042/BJ20090704

Zhang B, Liu C, Wang YQ, et al (2015) Disruption of a CAROTENOID CLEAVAGE DIOXYGENASE 4 gene converts flower colour from white to yellow in Brassica species. New Phytol 206:1513–1526. doi: 10.1111/nph.13335

Zhang W, Liu T, Ren G, et al (2014) Chlorophyll degradation: the tocopherol biosynthesis-related phytol hydrolase in Arabidopsis seeds is still missing. Plant Physiol 166:70–79. doi: 10.1104/pp.114.243709

Zhao Y, Wang H, Hammond RW, et al (2004) Predicted ATP-binding cassette systems in the phytopathogenic mollicute Spiroplasma kunkelii. Mol Genet Genomics 271:325–338. doi: 10.1007/s00438-004-0983-y

Zhu C, Bai C, Sanahuja G, et al (2010) The regulation of carotenoid pigmentation in flowers. Arch Biochem Biophys 504:132–141. doi: 10.1016/j.abb.2010.07.028

Zybailov B, Rutschow H, Friso G, et al (2008) Sorting signals, N-terminal modifications and abundance of the chloroplast proteome. PLoS One. doi: 10.1371/journal.pone.0001994